UILU-ENG 85-3607

Report No. 123

AN EVALUATION OF DAMAGE DEVELOPMENT DURING MULTIAXIAL FATIGUE OF SMOOTH AND NOTCHED SPECIMENS

by

James Walter Fash

Materials and Design Division
Department of Mechanical and Industrial Engineering

Sponsored by
National Science Foundation Grant MEA-81-11282
and
Society of Automotive Engineers Fatigue Design
and Evaluation Committee

A Report of the

MATERIALS ENGINEERING - MECHANICAL BEHAVIOR

College of Engineering, University of Illinois at Urbana-Champaign

August 1985

AN EVALUATION OF DAMAGE DEVELOPMENT DURING MULTIAXIAL FATIGUE OF SMOOTH AND NOTCHED SPECIMENS

James Walter Fash, Ph.D.
Department of Mechanical and Industrial Engineering
University of Illinois at Urbana-Champaign, 1985

ABSTRACT

Several theories have been proposed for multiaxial fatigue analysis, but a lack of consensus exists on the most appropriate for use in design. Five multiaxial fatigue theories are developed in the form of a strain parameter verses life relationship. Uniaxial, smooth specimen fatigue properties are employed to predict the results of two multiaxial fatigue test programs. Fatigue damage has been observed throughout both series of tests to relate the damage parameter for life analysis to the physical processes of fatigue.

Thin-wall tube specimens are tested in strain controlled, tension-torsion loading. A large volume of material is subjected to a uniform multiaxial strain state; hence, this geometry can be considered analogous to the smooth specimen for uniaxial fatigue. All five theoretical models result in good correlation of the thin-wall tube tests. A notched shaft designed to simulate a typical engineering component was tested under bending-torsion loading. Crack initiation occurs in a small volume of material in the vicinity of the notch, and subsequent growth is into a decreasing stress-strain field. Theoretical predictions and experimental results for the notch shaft program show considerably less correlation than that obtained for the thin-wall tube tests. Concepts of the local stress-strain fatigue analysis method suggest that if the local damage parameters for the smooth and notched specimen are equivalent, the fatigue lives will be equal. This

assumption of similitude also suggests that similar cracking characteristics should be observed in both specimens.

Crack behavior is observed using surface replicating techniques. Crack initiation in the thin-wall tube occurs on planes that experience the maximum range of shear strain. After a period of growth on this plane the crack changes direction and grows in a plane perpendicular to the maximum principal stress. For the 1045 steel considered, the crack size when this transition occurs is dependent on strain state and strain amplitude. Cracks in the notched shaft initiate in the notch plane rather than on planes of maximum shear for all tests except torsion. Growth to failure occurs on planes perpendicular to the maximum principal stress for low amplitude tests and in the notch plane for high amplitude tests. This behavior is reflected in the correlation of experimental results but is not accounted for in the theoretical models. The lack of similitude in damage development between the thin-wall tube and notched shaft is responsible for the poor correlation of the notched shaft test results.

The goal of labor is leisure.

paraphrase of Aristotle

ACKNOWLEDGMENTS

This study was conducted in the Materials Engineering Research Laboratory at the University of Illinois at Urbana-Champaign and was supported by National Science Foundation Grant MEA-81-11282 and the Society of Automotive Engineers Fatigue Design and Evaluation Committee.

Professor D. F. Socie, thesis advisor and friend, is gratefully acknowledge for many stimulating discussions and a broad range of experiences that have contributed to the author's personal and professional development. The author is grateful to Professor Jo Dean Morrow for sharing his philosophies on life, the university and materials. Dr. Peter Kurath and Dr. Nick Hurd are acknowledged for many worthwhile discussions. Professor F. A. Leckie, Professor F. V. Lawrence, and Dr. R. W. Landgraf are thanked for their advice. In addition, several members of the Society of Automotive Engineers have had a positive influence on the authors development. June Kempka, Tammy Lawhead, and Suzanne Palmer are thanked for their assistance and patience in the preparation of this manuscript.

A special thanks is expressed to the author's parents, Arthur and Lois Fash, and sister Sara, for their encouragement, understanding, and early example to venture beyond.

TABLE OF CONTENTS

NOMENCLATURE

A1,A2	Constants
a_s	Stage I crack length at transition to stage II growth
b	Fatigue strength experiment
BHN	Brinell hardness number
c	Fatigue ductility exponent
C	Constant
E	Modulus of elasticity
k	Constant
K	Strength coefficient
K_f	Fatigue notch factor
K_t	Elastic stress concentration factor
M_b	Bending moment
M_t	Torsion moment
N_{est}	Estimated life
N_f	Cycles to failure
N_i	Cycles to crack initiation
N_s	Life spent in Stage I crack development
%RA	Percent reduction in area
r_a	Average radius of thin-wall tube
S	Constant
t	Wall thickness of thin-wall tube
$\epsilon_1, \epsilon_2, \epsilon_3$	Ordered principal strain
$\Delta\epsilon_a$	Axial strain amplitude
$\Delta\epsilon/2$	Axial strain range
ϵ	Effective strain

ε_f	True fracture ductility
ε_f'	Fatigue ductility coefficient
ε_{ij}	Strain tensor
ε_n	Normal strain to γ_{max} plane
ε_n^*	Normal strain to γ^* plane
ε_{notch}	Normal strain to notch plane
$\varepsilon_x, \varepsilon_y, \varepsilon_z$	Direct strains
γ_a	Applied shear strain
γ_{max}	Maximum shear strain
γ^*	Maximum type B shear strain
γ_{notch}	Shear strain on notch plane
$\gamma_{xy}, \gamma_{xz}, \gamma_{yz}$	Shear strains
λ	Strain ratio (γ/ε)
σ_f	True fracture strength
σ_f'	Fatigue strength coefficient
σ_{uts}	Ultimate strength
σ_y	Yield strength
τ	Shear stress
ν	Poissons ratios
λ_{eff}	Effective Poissons ratio
ξ	Ratio of principal strains ($\varepsilon_1/\varepsilon_3$)

LIST OF TABLES

LIST OF FIGURES

1. INTRODUCTION

Advanced technology, the resulting liabilities, and economic considerations require the implementation of finite life design methods to ensure the safe and reliable operation of engineering structures and components. Current methodologies separate component fatigue life into two regimes: crack initiation and crack growth. Verification of these design methods to date has been primarily for situations that involve simple uniaxial stress-strain states in the critical location. However, many components are subjected to complex multiaxial stress-strain states.

Both crack initiation and crack growth life methodologies are based on materials characterization developed under uniaxial loading conditions. These test conditions impose primarily uniaxial stress-strain states in the critical location of the specimen. Analytical methods to account for multiaxial stress-strain states have been proposed and in some instances have shown good correlation with particular test results. In most cases, however, a strong relationship between the physical damage process and the correlating parameters has not been established.

Damage development during fatigue is assumed to be comprised of the initiation and growth of cracks. Stress-life and strain-life methods are employed to predict the formation of an "engineering size" crack (i.e. crack initiation). Bulk stress and strain values are employed in these analyses with little or no consideration of the stages of damage development leading to failure. Linear elastic fracture mechanics (LEFM) parameters, on the other hand, are formulated based on the physical crack behavior. Difficulties implementing LEFM arise as this

approach is not valid for physically small cracks, situations involving appreciable plasticity, and when multiple crack systems are present. Crack initiation methods overcome these weaknesses without directly dealing with crack behavior. However, current research suggests that the bulk parameters implemented in strain-life models should reflect the physical damage processes. An understanding of the influence of strain state, strain level and specimen geometry on microcrack behavior is required before appropriate models for multiaxial fatigue can be implemented with confidence.

1.1 Fatigue Mechanisms

Fatigue damage can be interpreted as the initiation and development of cracks that eventually result in failure. Damage processes have been separated into the crack initiation and crack growth portions of fatigue life (Fig. 1) primarily for the convenience of engineering analysis. For ductile metals, both processes involve slip mechanisms; however, the macroscopic loading parameters that model these processes differ.

Crack initiation (Fig. 2) is a result of reversed plastic slip [1,2,3] on crystallographic slip planes within single grains favorably oriented with the maximum applied shear stress. Reversed slip during cyclic loading results in the development of discrete regions called persistent slip bands. These regions coarsen, and material is displaced, resulting in the development of intrusions and extrusions. At some point in the process decohesion occurs, and these regions become crack-like. Failure of a component results from the growth of this initial crack to a size that prevents further use or results in catastrophic fracture.

Forsyth [4] has suggested a two stage model for crack growth. Stage I is a period of crystallographically oriented growth usually following initiation. Crack dimensions are typically small, and microstructural features can influence the crack behavior. Both shear stresses and normal stresses acting on the crack plane are important during stage I growth. Cracks will sometimes change direction from stage I planes to grow in stage II.

Stage II is a period of continuum crack growth occurring macroscopically in the plane perpendicular to the maximum principal stress (i.e., mode I direction). Crack growth models for stage II propagation are based on the behavior of the crack tip zone. For ductile metals the mechanism of stage II crack extension shown in Fig. 3 has been proposed [5,6]. Growth increments occur by local shear processes at the crack tip. Slip acts on two intersecting slip planes at the crack tip. Unloading or compressive loading (Fig. 3-2) relaxes the stress (dislocations) on the active slip planes. This process continues with an increment of crack extension on each load cycle that can be directly related to the formation of fatigue striations in some materials [7]. This model suggests that macroscopic crack growth will occur in the plane perpendicular to the maximum principal stress. Herein lies some of the difficulty in classifying crack growth, as it can be argued whether this is a shear strain controlled process (local growth) or a principal strain/stress controlled process (macroscopic growth).

1.2 Local Strain-Life Concepts

Many fatigue problems, particularly in the ground vehicle industry, have been analyzed by the local stress-strain approach [8,9,10]. This analytical tool (Fig. 4) incorporates material selection, component geometry, and service loading conditions to model the local stress-strain response and predict the crack initiation life. Although this is called a crack initiation analysis, it often accounts for initiation and some or all of stage I growth. A portion of stage II growth may also be accounted for depending on the crack behavior and the definition of failure for the baseline tests used to develop the analysis.

Component fatigue problems usually arise in an area of stress concentration. This is often a result of the component geometry and is therefore unavoidable. The elastic stress concentration factor, K_t, characterizes the elevation of stress due to geometry. It is usually observed that the effect of stress concentrations during fatigue loading is less than for the static loading case and is characterized by the empirical fatigue notch factor, K_f. This parameter is determined from the ratio of stresses of unnotched and notched specimens of the same material tested at the fatigue limit (usually taken at 10^7 cycles to failure). However, a physical significance of K_f has not been established.

Microcrack development has been shown to occupy a significant portion of the life of smooth specimens for some materials [11,12] during uniaxial loading. Similar results have been observed in crack development during multiaxial loading [13], but detailed characterization of crack behavior was not reported. Although the methodology in

Fig. 4 does not directly address the development of fatigue cracks, assumptions made in applying these concepts account for microcrack development. Assumptions of similitude (Fig. 5a) between the smooth specimen used to characterize the fatigue behavior and the local region of a notched component are implied when applying this analysis. Equal fatigue lives are expected when the stress-strain excursions are equivalent. This also implies that the development and type of fatigue damage (microcracking) is similar.

Extending these concepts to multiaxial fatigue requires the assumptions of similitude shown in Fig. 5b. The thin-wall tube geometry may be considered the "smooth specimen" for multiaxial fatigue research since a relatively uniform multiaxial stress-strain state can be developed over a large volume of material. Arguments of similitude (Fig. 5b) suggest that this should be characteristic of the local behavior in the critical area of a component subjected to similar multiaxial stress-strain states. If these assumptions are valid and the applied stress-strain states are similar, the fatigue lives and microcrack development should be similar.

In the classical application of strain-life fatigue concepts, the damage parameter used to characterize fatigue is the applied uniaxial strain amplitude, $\Delta\varepsilon/2$. For multiaxial fatigue analysis an equivalent correlating parameter that relates any stress-strain state to the uniaxial case is desired. This would allow reliable life estimates to be made based on uniaxial smooth specimen fatigue properties and eliminate the need for extensive multiaxial fatigue testing.

1.3 Theoretical Fatigue Models

Several thorough reviews [14,15,16,17] of multiaxial fatigue have been presented. Their findings will not be repeated here. However, important developments leading to current theoretical models are discussed briefly.

Early research on multiaxial fatigue was based upon infinite life design concepts. The first theories proposed were stress based extensions of static yield criteria. Various formulations of the von Mises, Tresca, and maximum principal stress criteria have been suggested. In general, these methods are unable to consolidate experimental results [14,17]. Strain based criteria have developed in parallel with finite life design concepts and an understanding of the role of plastic deformation in the fatigue process. Various modifications of static yield theories have been written in terms of strain parameters and proposed for the correlation of multiaxial fatigue data with results similar to those obtained by the stress based parameters [14,17,18,19]. Recent research has lead to the development of multi-parameter models.

An important concept, that of a critical plane and the stresses (or strains) acting on that plane, seems to have been first introduced by Mohr [20]. Findley [21] alluded to two types of crack growth and suggested that for one case the crack growth is dependent on two parameters: the maximum shear stress and the normal stress acting on the plane of maximum shear. Stullen and Cummings [22] developed a criteria incorporating these parameters from arguments based on Goodman diagram concepts.

Brown and Miller [23] first presented a similar two parameter formulation written in strain terms as

$$\gamma_{max} = f(\varepsilon_n). \qquad (1)$$

They proposed that the maximum shear strain is the primary driving force in crack initiation and that the strain normal to the plane of maximum shear, ε_n, has a modifying influence. Experimental data were presented as contours of constant life on plots of maximum shear strain versus the strain normal to the plane of maximum shear (r planes). Observations [24] of fatigue crack development support the use of these parameters for some materials (however most tests reported by Miller, et al. are very short life, $< 10^4$ cycles to failure). In addition, two types of shear strain, termed type A and type B, have been identified (Fig. 6). The difference between these shear strains is the direction in which they act in relation to the specimen surface and, hence, how they drive crack development. Type A shear strains drive the crack along the surface of the specimen or component. Type B shear strains act into the depth of the specimen. For combined tension-torsion and torsion loading of a thin-wall tube, type A shear strains are larger in magnitude than type B. Tension loading results in equal magnitude of type A and B shear strain, and biaxial tension results in only type B shear. Other component geometries and loading conditions can result in different combinations of type A and B shear.

Another critical plane theory has been proposed by Lohr and Ellison [25] to resolve the differences in type A and B shear behavior. They

argue that only a crack being driven into the specimen (i.e. type B shear strain) would result in catastrophic failure. Their formulation was presented in the form

$$\gamma^* + k\ \varepsilon_n^* = C. \qquad (2)$$

Data were presented as contours of constant life on plots of γ^* versus ε_n^* (Γ^* plane).

As proposed, implementation of Eqs. (1) or (2) in a design analysis is difficult. Socie, et al. [26] combined these expressions with the Coffin-Manson equation for plastic strain versus life relationships. Fash, et al. [27] have developed total strain-fatigue life relationships in terms of both these critical plane theories and three classical approaches. Materials properties determined from smooth specimens tested in uniaxial fatigue were used to predict the lives of multiaxial fatigue tests, and good correlation of thin-wall tube fatigue test data was obtained. Test results of a notched geometry deviated considerably from the predicted values. Although most component fatigue failures originate at geometric stress concentrations, very few studies have investigated the influence of geometry on multiaxial fatigue behavior.

Acceptance of a single unifying theory for multiaxial fatigue has not occurred. Nishihara, et al. [28] suggested the use of different theories depending on the material. Difficulties are encountered when interpreting the results of multiaxial fatigue research. These include different specimen geometries, failure criteria, and crack growth behavior. Additionally, materials behave differently for a given strain

state and life regime. These factors cause confusion when considering the correlation of experimental results with theoretical models.

1.4 Crack Behavior

The idea of a critical orientation for damage accumulation emphasizes the importance of the relationship between crack behavior and the theoretical models used to estimate fatigue lives. Crack development reported in the literature varies with materials, loading conditions, and specimen geometry.

Nishihara, et al. [28] reported the behavior for solid specimens (12 to 15 mm in diameter) of several materials under combined bending and torsion loading. Cracking was reported on planes of maximum principal stress for three grades of steel at the endurance limit. At higher stress ranges in torsion, growth was observed on maximum shear planes. Findley [21] reported initiation on maximum shear planes in solid aluminum specimens (7 mm in diameter) subjected to bending and torsion. A transition to growth on the plane of maximum principal stress was observed for long life tests. Both investigations suggest that the mode of crack growth (stage I or stage II) is dependent on the stress level.

Thin-wall cylinders (1.5 mm wall thickness) of mild steel were investigated by Yokobori, et al. [19]. Under uniaxial loading, only stage II crack growth was noted. Crack initiation and growth to failure for short life torsion tests occurred entirely on shear planes (stage I), but at long life ($>10^4$ cycles), shear cracks branched to grow as stage II cracks. Taira, et al. [29] tested hollow cylindrical specimens

of mild steel and found results similar to those of Yokobori, et al. at room temperature. At elevated temperature (450°C), only stage II growth was reported [30]. These studies suggest that the type of crack growth that can be expected is strain state as well as strain level dependent and is also influenced by environmental conditions.

Pascoe and deVilliers [31] tested a mild steel and a heat treated steel in low cycle fatigue (LCF) using cruciform specimens. Cracks initiated on planes of maximum shear (stage I). Of note are results obtained by varying the angle between the material rolling direction and the maximum shear plane. For the same strain state (torsion), lives differed by a factor of two to three. Shorter lives were obtained when the shear plane corresponded with the rolling direction. For a similar specimen geometry, Parsons and Pascoe [32] discussed shear initiation and the transition to stage II growth for a heat treated steel and a stainless steel. At high strain levels, multiple crack systems were reported, and linking of these cracks caused final failure.

Observations of crack behavior in an alloy steel have been reported by Kanazawa, et al. [33] for both in-phase and out-of-phase tension-torsion loading of thin-wall tube specimens (3.0 mm wall thickness). Stage I cracks formed on or near the maximum shear strain plane that experienced the largest normal strain during the loading cycle. All tests reported resulted in lives of less than 2.0×10^4 cycles to failure.

Crack behavior during tension-torsion loading of thin-wall tube specimens of Inconel 718 (2.0 mm wall thickness) has been reported by Socie and co-workers [26,34]. Stage I growth was observed for all tests

[35]. Crack profiles were semi-ellyptical for all loading conditions [36]. These results show that a modification of the critical plane theory proposed by Brown and Miller can account for mean stress effects during multiaxial fatigue.

Brown and Miller [24] have discussed the influence of strain state on crack development. An elastic fracture mechanics analysis was used to determine the critical strain state for the transition from stage I to stage II growth. Their analysis suggests that crack length and stress level do not influence this transition but, rather, that it is influenced only by the strain ratio, λ. This conflicts with the observation of several of the studies discussed above. Brown and Millers' [24] experimental results were all in the LCF regime, but a transition in behavior may occur with strain state or strain amplitude.

Development of damage during multiaxial fatigue of the 1045 steel used in this study was reported by Hua and Socie [13,37]. Differences were reported between the high cycle fatigue (HCF) and the LCF regimes. In HCF, a single crack initiated and grew to failure. In LCF, multiple crack systems developed, and failure resulted by rapid linking of the multiple damage regions. Damage accumulation was non-linear with life and strain level. Cumulative damage theories were evaluated to model these differences in damage rate for two level tests [37]. Fatigue life estimates and the character of the crack development were not discussed. These subjects are covered in detail in the following chapters.

In summary, many engineering parameters have been proposed for multiaxial fatigue. Critical plane approaches have directed attention to the details of crack behavior. It is not sufficient that life prediction models only correlate experimental lives in simple tests. They must also reflect the physical damage processes so that they can be applied with confidence to more complex situations. It is clear that the material, strain state, and strain level affect the crack behavior and in particular, the transition from stage I to stage II cracking. Further research is required to identify the critical bulk stress-strain parameters affecting crack behavior for various life regimes, strain states and materials.

1.5 Purpose and Scope

The intent of the present study was to investigate the application of crack initiation (crack nucleation and early growth) methodologies to multiaxial fatigue analysis. In particular, crack initiation models are evaluated based on their ability to correlate fatigue test results and the physical damage processes observed for several multiaxial stress-strain states. Fatigue damage is interpreted to be the formation and growth of cracks. Microcrack growth has been observed to determine the influence of strain state, strain level, and specimen geometry on the process of damage development. These observations assist in the appropriate formulation of life methodologies for both crack initiation and crack growth approaches.

Two specimen geometries were chosen for the purpose of this study. Thin-wall tube specimens were tested under completely reversed,

strain controlled, combined tension-torsion loading. This geometry is considered to be the smooth specimen for multiaxial fatigue, since crack initiation and early growth occur in a uniform stress-strain field. The extent of damage development and the direction of crack growth have been observed using surface replicating techniques. A fillet notched shaft specimen designed to represent a typical engineering component was tested under completely reversed combinations of torsion and bending [38]. Stress gradients were present in the local notch area due to the specimen geometry and loading conditions. Again, surface crack development was observed using replicating techniques.

Application of crack initiation life models to the analysis of notched components assumes that similitude exists between the baseline tests used to characterize the fatigue performance of the material and the behavior in the local notch region (Fig. 5). This assumption is evaluated based on the observed cracking behavior in the two test programs. Five multiaxial fatigue theories developed in a previous paper [12], are evaluated for their ability to relate to the physical damage process over a range of lives and strain states as well as their ability to correlate fatigue results. Smooth specimen uniaxial fatigue results provide all the baseline materials data required for these life prediction models.

All test specimens were machined from normalized SAE 1045 steel provided as hot rolled bar stock. All tests were conducted under constant amplitude, completely reversed, in-phase loading conditions.

2. EXPERIMENTAL PROGRAM

Details of the material, baseline fatigue tests, and both multiaxial test programs are described in this chapter. It is important when applying the initiation life prediction models to have representative baseline data, and when comparing results of different test series to have a consistent definition of failure. Four sets of uniaxial smooth specimen test data are reported, with the most representative data set being selected for use in the life predictions. Development of a 1.0 mm surface crack has been chosen as the definition for crack initiation. Although this does not correspond to the number of cycles when a crack first formed, it is a typical definition of initiation for engineering calculations. The growth of cracks before achieving this dimension has been observed and is discussed in relation to the parameters implemented in the life relationships.

2.1 Material

The material used in all tests reported in this investigation was a normalized SAE-1045 steel furnished as 63.5 mm diameter, hot rolled bar stock. All of the material was poured from the same heat and was processed in a similar manner [38] for use in a round robin test program sponsored by the Society of Automotive Engineers Fatigue Design and Evaluation Committee. Microstructural features are shown in Figs. 7 and 8. The grain size was ASTM size 6.5 (approximately 40 μm). Magnesium sulfide inclusions approximately 0.1 mm in length (Fig. 8) are present in the longitudinal direction. Chemical composition and characterization of the microstructure are given in Table 1. Monotonic properties are reported in Table 2.

2.2 Uniaxial Smooth Specimen Results and Data

Fatigue tests were performed on smooth cylindrical specimens in completely reversed, uniaxial strain control to determine low cycle fatigue constants. In order to assess anisotropy, specimens were taken from the bar stock in both the longitudinal and tangential directions. Orientation of the specimens and the specimen geometry employed in these tests are shown in Fig. 9. A 2.5 mm diameter gage section was chosen for the smooth specimens to correspond to the wall thickness of the tube specimens.

Results of the uniaxial tests are shown in Fig. 10. The material displays anisotropy in terms of fatigue life that can be attributed to the notch effect of the magnesium sulfide inclusions. In the tangential specimen, the inclusions are perpendicular to the applied load. Fatigue lives are between a factor of two to three shorter than the results of the longitudinal test series in which the inclusions are parallel to the applied load and have minimal influence. This influence on life is similar to that reported by Parsons and deVilliers [31] for torsion loading with and without the rolling direction aligned with the shear planes. Fatigue constants are given in Table 3 for both series of tests.

Constant amplitude tests have also been reported for this material using specimens with 5.0 mm (Ford Motor Company) [39] and 6.0 mm (Deere and Company) [40] diameter gage sections taken from the longitudinal direction. All four sets of smooth specimen data are presented in Fig. 11 and Table 3. Results of the 5.0 mm specimens show slightly

longer lives (approximately a factor of two to three) than the 2.5 mm longitudinal specimens. The Deere data are another factor of two to three longer in life than the Ford specimens. Hua and Socie [13] have reported the presence and growth of cracks during most of the life of smooth specimens of this material. The difference between the lives of 2.5 mm and 5.0 mm diameter specimens is attributed to the difference in the amount of crack growth possible due to the difference in specimen size. The difference in life between the Ford (5.0 mm) and Deere (6.0 mm) data cannot be fully attributed to crack growth but may in part be a result of slight differences in testing technique.

2.3 Thin-Wall Tube Test Program

Tension, torsion, and combined tension-torsion tests were performed on the thin-wall tube geometry shown in Fig. 12. All test results reported here are for in-phase, constant amplitude, completely reversed, strain controlled loading at room temperature. Tests were performed on an MTS model 809 tension-torsion machine interfaced to a PDP 11/23 computer with an MTS model 463 processor/interface to perform test control, data acquisition, and data reduction. An internal extensometer [26] was designed to measure axial strains independent of torsional strains and to allow easy access to the outer surface of the specimen for observing fatigue damage. Coupling between the two measurements was less than 1 percent.

Strain levels selected for these tests were based upon equivalent von Mises strain amplitudes of 0.15, 0.22, 0.43, and 1.0 percent. Strain ratios (λ = shear strain/axial strain) of 0.0 (axial), 0.5, 1.0,

2.0, and ∞ (torsion) were employed. Two torsion tests were also performed at an effective strain amplitude of 0.13 percent. Stabilized stress-strain values and fatigue lives are reported in Table 4. Life predictions and crack observations are presented in Chapter 3.

Life estimates were developed to predict the formation of a 1.0 mm (engineering size) surface crack. Thin-wall tube tests were terminated when a 10 percent load drop from the stabilized axial load value occurred for all test conditions except $\lambda = \infty$. A torsional load drop of 10 percent was the criterion for $\lambda = \infty$. Cracks of a few millimeters (5-20) in length were present when a 10 percent load drop occurred. Replica observations [37] have shown that growth from 1.0 mm to the length at 10 percent load drop occupies only a small percentage of the life. Consequently, the life at 10 percent load drop is used as the crack initiation life in this study.

A choice of baseline data was required to implement the five multiaxial fatigue theories investigated. Thin-wall tube specimens tested in axial loading ($\lambda = 0.0$) are compared with the four sets of baseline data in Fig. 13. The Ford data (5.0 mm) best correlates the axial results, and therefore were used as the baseline data in correlating the results of other strain states. It should be noted that in the application of the local strain approach, it is the assumption of similitude (Fig. 5) that allows component life predictions to be based on smooth uniaxial specimen properties.

Observations of crack initiation and growth phenomena have been accomplished using standard acetyl tape replicating methods. Tests were stopped intermittently and replicas of the surface taken. Observations

of crack behavior were made from the replicas after the test was completed using transmitted light optical microscopy. Details of the replicating procedure can be found in Ref. [41]. This procedure provided a series of surface observations from which crack initiation and growth behavior were inferred.

2.4 Notched Shaft Test Program

The geometry of the notched shaft specimen is shown in Fig. 14. A test frame, designed by Galliart and Downing [42], was fabricated in the Materials Engineering Research Laboratory at the University of Illinois for this test program. Two linear servo-hydraulic actuators were used to apply the loads to the specimen through a yolk and collet arrangement (Fig. 15). Tests were performed under load control resulting in constant amplitude bending and torsion moments in the notch root. Test results are reported here and discussed for constant amplitude, completely reversed, in-phase bending, torsion and combined bending and torsion loading.

Test amplitudes were selected to result in fatigue lives of approximately 10^4, 10^5, and 10^6 cycles. The distortion energy criteria employing elastically calculated stresses and elastic notch stress concentration factors was implemented to determine load levels that resulted in equivalent notch stresses. Tests were performed for the conditions shown in Fig. 16 and will be referred to in the text as bending (BR), XR, YR, ZR, and torsion (TR) loading conditions. These conditions have a ratio of torsion moment to bending moment (M_t/M_b) of approximately 0.0, 1.4, 0.6, 2.3, and ∞, respectively. A few tests were

also performed at test conditions with smaller bending moments but the same torsion moment as these conditions. Test results are reported in Table 5.

In some instances, initiation lives were either uncertain or missed entirely, and only the life to failure was reported. Data in Table 5 have been scrutinized to detect these cases, and initiation lives have been estimated based on the percentage of failure life spent in initiation for tests employing similar loading conditions in which initiation was reliably detected. These estimated initiation lives are also reported in Table 5 and were used in the correlation of the life prediction methods. Strains in the notch region are required for the fatigue life estimates and have been determined using an elastic plastic finite element model. Details of this analysis are presented in a subsequent chapter and results are tabulated in Table 6. Life predictions and crack observations are presented in Chapter 4.

Crack initiation was determined using ultrasonic surface wave techniques for the tests performed at Deere and Company and the University of Illinois. A crack size of approximately 1.0 mm surface length was determined employing this method, with the life at this crack size being reported as the initiation life. This is consistent with the failure criteria for the thin-wall tubes. Although this method is very sensitive to the presence of cracks, the calibration of the ultrasonic transducer signal to a particular crack size is not precise. The device was roughly calibrated by electrodischarge machining semi-elliptical cracks of 0.1, 0.25, 0.5, and 1.0 mm surface length in the notch plane of a calibration specimen. The 12.5 mm wide transducer gave an average

reading over this dimension in the notch. Consequently, a signal representing 1.0 mm could be due to the presence of a single crack or of multiple cracks which together produce the amplitude of signal determined on the calibration specimen.

Crack observations in the critical area of the shaft were made using surface replica techniques. Acetyl film replicas could not be used because of the complex curvature of the notch. Therefore, a silicone based two component polymer* was implemented. Replicas of the notch region were mounted on aluminum stands and sputtered with a thin film (~100Å) of 50 percent platinum, 50 percent gold. This provided a conducting surface for observation with a scanning electron microscope. This technique allows cracks on the order of 10 μm to be easily observed. Close observation from replicas demonstrated good correlation between the ultrasonic signal output suggesting a 1.0 mm crack and the presence of a crack(s) of that size.

The surface finish in the notched shaft was the result of a low stress surface grinding operation. This surface was smoother than is often found in real components. However, the surface finish made replica observations of very small cracks difficult. In some tests, the notch area was polished to allow more reliable observations of crack behavior. For the material used in this investigation, these modifications of surface finish would not be expected to have any appreciable influence on the crack behavior. In the experimental program, polishing was not observed to change crack behavior or to significantly influence the cyclic life for a given loading condition or amplitude.

* The replicating material was XANTOPREN. It is a dental molding compound supplied by Unitek, 2724 South Peck Road, Monrovia, CA 91016.

3. ANALYSIS

Five multiaxial forms of the strain-life equation and stress analysis for use in the life predictions were developed [27] and are reviewed in this chapter. Expected cracking behavior is discussed in relation to the multiaxial fatigue models and the strain states imposed. Details of the stress-strain analysis are described for determining the values needed in the life analysis and intepretation of crack observations.

3.1 Development of Multiaxial Life Prediction Models

Basic elements of the local strain approach for fatigue crack initiation analysis have been shown in Fig. 4. Local strain fatigue analysis has developed from an understanding of plastic deformation in the fatigue process. Coffin [43] and Manson [44] introduced the well known power law relation between plastic strain amplitude and fatigue life. Morrow [45] offered Eq. (3) along with definitions of the fatigue constants for use in finite life fatigue analysis.

$$\frac{\Delta\varepsilon}{2} = \frac{\sigma_f'}{E} (2N_f)^b + \varepsilon_f' (2N_f)^c \qquad (3)$$

This equation assumes that the strain range, $\Delta\varepsilon$, serves as a measure of damage for uniaxial fatigue.

The multiaxial fatigue theories implemented in this study are: the maximum principal strain, effective strain [von Mises], maximum shear strain [Tresca], Brown and Miller, and Lohr Ellison theories. Expected cracking behavior based on the physical interpretation of the particular damage parameter is discussed for each approach.

3.1.1 Maximum Principal Strain Parameter

The maximum principal strain approach is analogous to the traditional use of the applied strain amplitude in uniaxial analysis. For the geometries and loadings used in this study, principal strains (ε_1, ε_2, ε_3) are determined by an appropriate transformation of the measured or applied strains (ε_{ij}). For correlating multiaxial fatigue tests the range of maximum principal strain on the plane that experiences the maximum principal strain range is considered the dominant parameter to describe damage, and is implemented in the strain life equation as

$$\frac{\Delta\varepsilon_1}{2} = \frac{\sigma_f'}{E} (2N_f)^b + \varepsilon_f' (2N_f)^c. \qquad (4)$$

Since the maximum principal strain is the applied strain in the uniaxial test, the direct application of Eq. (4) is appropriate. Relating this theory to crack behavior would suggest that fatigue damage accumulates on planes perpendicular to the maximum principal strain direction.

3.1.2 Effective Strain Parameter (von Mises)

Effective strain parameters have often been suggested and are frequently employed by design engineers. The effective strain parameter takes the form of a von Mises yield formulation or the octahedral shear strain. Normalized to the axial case, the effective strain can be determined from the principal strain values by

$$\Delta\varepsilon_{eff} = \frac{\sqrt{2}}{2(1+\nu_{eff})} \frac{\Delta}{2} [(\varepsilon_1-\varepsilon_2)^2 + (\varepsilon_2-\varepsilon_3)^2 + (\varepsilon_1-\varepsilon_3)^2]^{1/2}. \quad (5)$$

The Δ is taken as the range of principal strains over a given loading cycle. Poisson's ratio, ν_{eff}, is taken to be 0.3 for elastic deformation and 0.5 for plastic deformation (assuming constancy of volume). For intermediate strains, an effective Poisson's ratio can be implemented as

$$\nu_{eff} = (\nu_e \varepsilon_e + \nu_p \varepsilon_p)/\varepsilon_t. \quad (6)$$

This simple expression is only valid for completely reversed proportional loading. For other situations, elastic and plastic strains must be considered separately. Elastic and plastic strain components are determined from the measured stress-strain values for each thin-wall tube test. A value of $\nu_{eff} = 0.5$ was used in the formation of this parameter for the notched shaft. Tipton [17] showed that the assumption of Poisson's ratio did not affect the accuracy of the analysis. A life relation can then be written as

$$\frac{\Delta\varepsilon_{eff}}{2} = \frac{\sigma_f'}{E} (2N_f)^b + \varepsilon_f' (2N_f)^c. \quad (7)$$

Effective strain is often considered a scalar quantity which would suggest that there is no geometric relationship between the parameter and the physical damage observed during fatigue [46]. An alternate interpretation based on octahedral shear would lead one to expect damage to be observed on octahedral shear planes.

3.1.3 Maximum Shear Strain Parameter (Tresca)

An extension of the Tresca yield theory relates the applied multiaxial strain state to fatigue life by the range of the maximum shear strain. Previous observations of the fatigue process and slip theories are consistent with the assumption that fatigue mechanisms are related to shear processes. The maximum shear strain amplitude is determined from the principal strain values as

$$\frac{\Delta\gamma_{max}}{2} = \Delta(\varepsilon_1 - \varepsilon_3). \qquad (8)$$

By relating the applied uniaxial loading conditions to the resolved values of shear strain and applying the appropriate Poisson's ratio for elastic and plastic components of strain the following shear strain-life relation can be developed:

$$\frac{\Delta\gamma_{max}}{2} = 1.3\,\frac{\sigma_f'}{E}\,(2N_f)^b + 1.5\,\varepsilon_f'\,(2N_f)^c. \qquad (9)$$

This model suggests that damage development should be observed on planes that experience the maximum cyclic shear strain amplitude.

3.1.4 Brown and Miller Parameter

Brown and Miller [23] have been proponents of critical plane theories for multiaxial fatigue and have proposed that the maximum shear parameter (Eq. (8)) is the dominant factor in initiation. They argue that the strain normal to the plane of maximum shear has a secondary influence. The normal strain term is determined by

$$\frac{\Delta\varepsilon_n}{2} = \left(\frac{\varepsilon_1 + \varepsilon_3}{4}\right). \tag{10}$$

Kandil, et al. [47] suggested a form of Eq. (1) that can be developed into a life relation by relating the axial test to the maximum shear and normal strain values, assuming appropriate values of Poisson's ratio for elastic and plastic strain components. The life relation can then be represented as

$$\left(\frac{\Delta\gamma_{max}}{2} + S\,\frac{\Delta\varepsilon_n}{2}\right) = A1\,\frac{\sigma_f'}{E}\,(2N_f)^b + A2\,\varepsilon_f'\,(2N)^c$$
$$A1 = (1 + \nu_e) + S(1 - \nu_e)/2.0 = 1.65 \tag{11}$$
$$A2 = (1 + \nu_p) + S(1 - \nu_p)/2.0 = 1.75$$

The material parameter, S, is taken as unity. Damage development should be observed on planes that experience the maximum cyclic shear strain amplitude.

3.1.5 Lohr and Ellison Parameter

Lohr and Ellison [25] have proposed that the shear strain that drives the crack into the specimen is the controlling parameter for fatigue failure (Eq. (2)), as the crack must grow into the depth of a component in order to be catastrophic. This would always be a type B shear strain (Fig. 6). $\Delta\gamma^*/2$ is given by Eq. (8) when the minimum principal strain is primarily normal to the surface (type B shear strain). If the second principal strain is most nearly normal to the surface (type A shear strain) the value is given by

$$\frac{\Delta\gamma^*}{2} = \Delta(\varepsilon_1 - \varepsilon_2). \qquad (12)$$

As in the Brown and Miller approach, the normal strain to the plane of shear is thought to have a modifying influence. The normal strain term is determined by Eq. (10) when the third principal strain is normal to the surface, or when the second principal is nearly normal to the surface by

$$\frac{\Delta\varepsilon_n^*}{2} = \frac{(\varepsilon_1 - \varepsilon_2)}{4} . \qquad (13)$$

A life relationship based on these parameters can be developed from Eq. (2) and the unaxial case as

$$\left(\frac{\Delta\gamma^*}{2} + k\,\frac{\Delta\varepsilon_n^*}{2}\right) = 1.44\,\frac{\sigma_f'}{E}\,(2N_f)^b + 1.60\,\varepsilon_f'\,(2N_f)^c \qquad (14)$$

with k = 0.4. The constants are dependent on k, similar to the dependence of A1 and A2 on S in Eq. (11). Crack observations should show initiation on planes of type B shear strain which drive the crack into the specimen.

Uniaxial strain-life fatigue constants that are employed in the five life relations (Eqs. (4), (7), (9), (11), (14)) are presented in Table 3. These five theories will be used to evaluate the experimental results of both test series to determine their ability to correlate multiaxial test results from uniaxial data. Crack observations will be related to the physical interpretation of these models to assess the relation between the damage parameter and the actual physical damage.

3.2 Stress-Strain Analysis

Stress-strain analysis to determine the appropriate strain parameters for the life prediction models is developed in this section. This is a simple matter for the thin-wall tube, since the applied loads and strains are measured and recorded during testing. For the notched shaft, an elastic-plastic FEM was developed to determine the relation between applied loading and the local stress-strain state. This was chosen as the most accurate method for determining the local multiaxial strain state in the notch. Other approximate methods are available, such as the use of elastic (K_t) and fatigue (K_f) notch factors and Neubers rule. These approaches have been addressed in Ref. [17] and will not be discussed in this study.

3.2.1 Thin-Wall Tube

Principal strain values and directions are determined from simple analysis and consideration of Mohr's circle in strain space (Fig. 17). Conditions of plane stress are assumed, resulting in $\varepsilon_y = \varepsilon_a$ being the applied axial strain amplitude, and ε_x and ε_z are the Poission's contractions equal to $-\nu\varepsilon_y$ in the x- and z-directions. Shear strains of $\gamma_{xy} = \gamma_a$ are also applied strains. Values for Poisson's ratio vary from approximately 0.3 for elastic straining to 0.5 for fully plastic strains.

In the experimental program, strains were controlled to the desired value on the inside surface of the wall using the internal extensometer. During torsional loading there is a slight gradient (18 percent)

from the inside surface to the outside surface of the wall. Strains reported in Table 4 are values at the mid-thickness of the wall of the specimen. Surface stress-strain values were calculated from those measured during the test. The strain gradient was assumed linear through the wall thickness and, hence, surface strains were approximately 9 percent higher than the average values. The average or mid-thickness torsional stress was calculated by:

$$\tau = \frac{M_t}{(2\pi r_a^2 t)}. \tag{15}$$

Surface values were then determined by extrapolating along the torsional cyclic stress-strain curve represented by a Ramberg-Osgood relationship [40].

In calculating the principal strains a weighted value of Poission's ratio given previously in Eq. (6) was employed. The maximum shear strain amplitude for plane stress conditions was then calculated as

$$\frac{\Delta\gamma_{max}}{2} = \frac{1}{2}\left\{\left[\left(\frac{\Delta\varepsilon_a}{2}\right)(1 + \nu_{eff})\right]^2 + \left(\frac{\Delta\gamma_a}{2}\right)^2\right\}^{1/2}. \tag{16}$$

The normal strain to the plane of maximum shear was:

$$\frac{\Delta\varepsilon_n}{2} = \frac{\Delta\varepsilon_a}{2}\frac{(1 - \nu_{eff})}{2}. \tag{17}$$

Principal strains were calculated using Eqs. (16) and (17) as:

$$\varepsilon_1 = \frac{\Delta\varepsilon_n}{2} + \frac{\Delta\gamma_{max}}{4}, \tag{18a}$$

$$\varepsilon_2 = -\nu_{eff}\,\frac{\Delta\varepsilon_a}{2}, \tag{18b}$$

$$\varepsilon_3 = \frac{\Delta\varepsilon_n}{2} - \frac{\Delta\gamma_{max}}{4}\,. \tag{18c}$$

The principal strains were then used in the formulation of the five parameters to estimate the life of the thin-wall tube tests.

3.2.2 Notched Shaft

Local stress-strain response in the critical region of the notched shaft is a key factor in the life prediction methodology. Approximate methods based on elastic stress concentration factors and fatigue notch factors often employed in engineering analysis have been considered for the determination of notch root strains during bending of the SAE notched shaft in Ref. [17]. No solutions are available for combined loading. In this study, local response to the remote loading has been analyzed in two ways. First, an elastic-plastic FEM [48] was developed for all loading conditions. Secondly, experimental strain gage measurements have been made and compared with the FEM results for a number of test conditions. Details of the FEM are given in APPENDIX A and results are presented below.

Results of the FEM are tabulated in Table 6 for most of the loading conditions applied in the test program. These are presented as the strain tensor, ε_{ij}, relative to the notch, with a right handed coordinate system defined as follows: the z-axis is the primary bending

axis, the y-axis is perpendicular to the notch, and the x-axis being tangent to the surface (see APPENDIX A). Principal strains and directions have been determined using standard tensor operations.

Examples of the strain tensor, ε_{ij}, and the resolved principal strains and maximum shear directions are given in Fig. 18a-e for bending, YR, XR, ZR, and torsion loading conditions. In these figures, the notch FEM strains are shown on the faces of an elemental cube of material in the left schematic of each figure. The arrows indicate the values given in Table 6 and the length of the arrows are scaled in proportion to the maximum principal strain. The center schematic shows the principal strain values on a unit cube of material rotated to the principal directions. The schematic on the right indicates the directions that the planes of the maximum shear strain and the plane of the maximum principal stress intersect the surface in the notch. The dotted lines represent the maximum shear strain. Note that since all loading conditions are applied in-phase, the maximum principal stress and strain are in the same direction. For bending and the YR condition (Figs. 18a and b) the third principal strain acts primarily in the y-direction (normal to the specimen surface). On the notch surface the maximum shear strain and maximum principal strain are nearly coincident. Hence for these conditions the maximum shear strain ($\varepsilon_1 - \varepsilon_3$) is nearly a type B shear acting into the surface. For the XR, ZR and torsion conditions (Figs. 18c-e), the third principal strain acts primarily in the x-direction and the maximum shear strain is primarily a type A shear acting along the surface.

Notch geometries often provide constraint on the lateral Poisson's contractions which result during deformation. For the notched shaft geometry, flow requirements during deformation result in larger strains perpendicular to the notch surface (ε_{yy}) than might be expected and smaller strains parallel to the notch (ε_{xx}). The ratio of the transverse strains to the principal bending strain, ($\varepsilon_{xx}/\varepsilon_{zz}$) and ($\varepsilon_{yy}/\varepsilon_{zz}$), gives an indication of the notch constraint on deformation. For the plane stress situation assumed in the analysis of the thin-wall tube, these ratios are equal to Poisson's ratio. Results of the elastic FEM for bending give values of ($\varepsilon_{xx}/\varepsilon_{zz}$) = -0.13 and ($\varepsilon_{yy}/\varepsilon_{zz}$) = -0.36. These values are in good agreement with the measured values reported in Ref. [17]. For elastic-plastic analysis at 2600 Nm bending, the ratios become ($\varepsilon_{xx}/\varepsilon_{zz}$) = -0.15 and ($\varepsilon_{yy}/\varepsilon_{zz}$) = -0.56. The minimum principal strain, ε_3, is nearly perpendicular to the notch plane (see Fig. 18a). For this principal strain orientation, it should be noted that surface strain gage measurements would not determine this strain value and would underestimate the magnitude of the maximum shear strain.

Principal strain values are plotted against applied moments in Figs. 19a-c for bending, XR, and torsion load cases. In Figs. 20a-c principal stress gradients are plotted in the longitudinal, circumferential and radial directions for both elastic and elastic-plastic solutions. The diagram in the upper left indicates the gradient along the length of the shaft. This indicates that the peak stress occurs at the tangent point of the radius and gage section. It has been shown [17,49] that the maximum stress actually occurs slightly up the radius. In bending, the principal strains can be as much as 14 percent

greater than at the tangency point. The finite element results reported here indicate the tangency point as the highest stress because of the elements used in the model and the method used to extrapolate to the nodal stress-strain values. The elastic stress concentration factor in bending (K_t = 1.62) agrees very well with that given by Peterson [50]. This value also agrees with that measured up the notch [17] and, consequently, is felt to represent the maximum bending strains. As the proportion of torsional loading increases, the point of maximum stress approaches the tangency point. The figure on the lower left indicates the radial gradient which decreases to zero at the central axis of the specimen. This gradient is analogus to the gradient away from the notch usually considered in uniaxial notch problems. The diagram in the upper right of Figs. 20a-c is the gradient around the circumference.

Figures 21a-c also show the concentration in the notch in terms of maximum shear stress contours from the FEM. By comparing the end view on the right and the side view on the left, the critically stressed volume in the notch area is found to be a small fraction of the material in the notch root. This volume increases with an increasing proportion of torsional loading. This will be discussed further in relation to the crack observations given in the next chapter.

FEM strain results are compared with a number of strain gage measurements in Figs. 22a and b for bending and torsion loadings. Reasonable agreement is obtained, with measured values being within 20 percent of the computed values. Further study of the strain versus moment relation for torsion loading [51] has shown that at the high amplitude torsion condition (M_t = 3000 Nm) gross specimen yielding

results. Strains at this level are not stable. Consequently FEM strain values at this level are somewhat suspect, since the applied strain levels become a function of test frequency.

4. RESULTS AND OBSERVATIONS

Correlation of both multiaxial test series with the five multiaxial strain-life models is presented in this chapter. The 5.0 mm diameter Ford uniaxial data (Table 3) were shown to best represent the thin-wall tube axial tests and have been used in the life prediction models. The definition of the crack initiation life was described in the experimental program to be the formation of a 1.0 mm crack. Detailed observations of the development of damage are also presented here.

4.1 Life Predictions

It should be noted that all of the biaxial models are normalized to the axial case; consequently, all will show similar correlation of the axial thin-wall tube results. Of particular interest is the ability to reduce the results for other strain states to a single line, and also whether the experimental data falls parallel to the theoretical life line over the complete life range. If the data are parallel to the theoretical predictions but are not coincident with the predictions, the choice of a different set of baseline data from Fig. 11 may shift predictions to coincide with the data. If, on the other hand, the data are skew to the predictions a different choice of baseline data (Fig. 11) will not improve the correlation.

4.1.1 Thin-Wall Tube

Correlation of the life prediction models and experimental results is shown in Figs. 23a-e for the maximum principal strain, effective strain, maximum shear strain, Brown-Miller, and Lohr-Ellison theories, respectively.

As expected, axial results fall about the line of perfect correlation for all predictive methods. Combined loading tests fall on the conservative side of the axial tests and tend to become more conservative with increasing strain ratio (λ = 0.5, 1.0, 2.0). When predicted with the same baseline data, torsion results fall within the scatter of the other strain states, becoming more conservative at long lives for the effective strain, maximum shear strain, Brown-Miller, and Lohr-Ellison parameters. The maximum principal strain parameter shows non-conservative predictions for torsion at short lives but excellent correlation for the two longest life tests. If the material anisotropy were to be considered for only the torsion tests, the predictions would be a factor of two to three shorter in life. Consequently, the correlation would follow the trend of the other strain states being more conservative with increasing strain state. This would result in extremely conservative predictions (about a factor of 10) for the long life tests.

All five methods result in similar correlation for the thin-wall tube test results. The critical plane theory of Brown and Miller shows the least scatter and can be fine tuned by adjusting the constant, S (Eq. 11), in front of the normal strain term. If fatigue life is dependent only on the local strain state, similar correlation of the notched shaft tests should be observed.

4.1.2 Notched Shaft

Predictions and experimental results for the notched shaft are compared in Figs. 24a-e for the maximum principal strain, effective strain, maximum shear strain, Brown-Miller, and Lohr-Ellison theories respectively.

All five methods correlate the bending tests within plus or minus a factor of three in life except for a long life test that did not fail. All of the parameters are conservative at long lives becoming nonconservative at shorter lives. Some results are skewed to the 45° line of perfect correlation. Lack of correlation for a given loading condition increases as the proportion of torsion moment to bending moment (M_t/M_b) increases. Bending results are only slightly skew. The torsion results deviate the most from the 45° slope of perfect correlation. This suggests that the influence of the notch on crack initiation and early growth increases as the torsional component of loading increases.

Scatter in experimental lives is much greater than in the thin-wall tube tests for several reasons. Differences in testing technique between laboratories reporting data for the SAE program may result in some scatter. At least one test was performed for almost all test conditions at the University of Illinois. These points should not be affected by differences in test technique, yet the trends of these data show the lack of correlation discussed above.

Difficulties and inaccuracies in the finite element modeling and experimental strain measurements could result in inaccurate local strain values for the life predictions. Although finite element results and measured strain gage results show reasonable correlation, further work [50] suggests that for some of the larger loading levels in torsion, stabilized strains under static loading are not achieved because of gross plasticity. The notch strains may be overestimated by as much as 25 percent at the high load levels (Fig. 22). In the LCF life regime, this would result in a factor of 1.6 in predicted life. Methods based

on experimental strain gage measurements [17] do not adequately assess the notch constraint on transverse strains and lead to inaccurate strain values.

Difficulty in detecting a 1.0 mm crack could also lead to scatter. As pointed out in Section 2.4, this has been accounted for, in part, by comparing the life fractions spent initiating a crack and adjusting those lifes where crack detection was obviously missed. Nonetheless, the ultrasonic crack detection method is an averaging technique over a portion of the notch. Errors in the detection of a crack can arise when multiple cracks are present, or when the crack(s) are not in the notch plane. This will be discussed further in relation to the crack observations presented below.

Lack of similutide in the damage process between the thin-wall tube and the notched shaft might result from specimen geometry effects. Differences in the damage process would suggest different damage rates, and may lead to inaccuracies in the life estimates. Observations of cracking behavior are presented in the next section.

4.2 Crack Observations

Details of the development of fatigue damage are important from a phenomenological viewpoint. Two factors must be taken into account when comparing the crack behavior. First is the orientation of the plane or planes on which cracks initiate and grow. This orientation is indicative of the phase (initiation, stage I or stage II development). Second is the extent of damage over the critical area (crack density), and how this influences the failure process. If assumptions of

similitude between smooth and notched specimens are valid, similar crack behavior should be observed for the two geometries.

4.2.1 Thin-Wall Tube

Differences have been identified [13,37] in the damage process when comparing long life (HCF) and short life (LCF) tests. Crack behavior in the thin-wall tube tests will be separated into observations of HCF and observations of LCF crack systems. HCF damage is characterized by the formation and development of a single dominant crack resulting in failure. LCF damage is characterized by the formation of multiple crack systems and interaction of these crack systems at failure.

HCF Type Damage

Figure 25 shows typical crack initiation and macrogrowth for axial loading (λ = 0.0) at a low strain amplitude ($\bar{\varepsilon}$ = 0.22%). Planes of maximum shear strain intersect the surface at any angle within ±45° of the circumferential direction [3], assuming plane stress conditions. A crack of about 50 μm surface length, shown at 80,000 cycles, appears on the surface perpendicular to the specimen axis. The arrows provide a common reference mark in all of the photos. In other axial tests at this strain level, cracks initiated at angles different than that shown in Fig. 25 but always within ±45° of the circumferential direction. Sectioning of cracks to determine the early growth direction into the specimen (Fig. 17, Ref. [37]) was inconclusive. Growth to failure occurs perpendicular to the maximum principal stress. This is stage II

growth (mode I in fracture mechanics terminology). Crack sectioning observations of longer cracks made in Ref. [37] indicate that the crack does grow in the stage II plane. Microscopic observations indicate that the local crack tip extension often occurs at 45° to the circumferential direction. This is consistent with the crack growth mechanism (Fig. 3) discussed previously.

Type B shear strain, or the principal stress, is the driving force for the formation of a horizontal crack (Fig. 25). Peterson [3] suggested that, for uniaxial loading, initiation would be more likely to occur by a type B rather than a type A shear strain, because slip out of the surface (type B) is unconstrained. Slip due to type A shear is constrained by grain boundaries at both ends of the slip band. Although Fig. 25 shows initiation by a type B shear strain when other axial tests were observed, no preference was found for initiation on A or B shear strain planes. For uniaxial loading, it was impossible to precisely determine the transition from stage I to stage II growth from surface observations. Combined loading, however, resulted in a unique strain state allowing conclusions to be drawn from surface observations.

Crack observations for λ = 0.5 and 1.0 are shown in Fig. 26 and 27, respectively. Initiation and early growth are in a direction alligned with one of the maximum shear planes in specimens where shear processes rather than material imperfections dominate (failure was observed to initiate from a material "defect" in only one test). Initial formation of the crack that eventually resulted in failure was detected at less than 20 percent of the failure life. After approximately half the life spent in stage I growth, the cracks changed direction to grow perpen-

dicular to the maximum principal stress. This change in growth direction corresponds to the transition from stage I to stage II growth suggested by Forsyth [4]. After the transition, microscopic growth deviated from the plane of maximum principal stress in local areas; however, the macroscopic growth direction is perpendicular to the maximum principal stress. Again, this is consistent with the crack growth model described in Fig. 3.

Figure 28 shows crack development for $\lambda = 2.0$. Similarly, crack initiation occurs on planes of maximum shear strain. At approximately the half life (~ 50,000 cycles), the crack had developed to approximately 100 μm by stage I growth. At 70,000 cycles, the stage I-stage II transition is clearly observed. Overall growth to failure is approximately perpendicular to the maximum principal stress, but the crack changes direction often, and the extent of growth on planes other than the plane of maximum principal stress is larger than for $\lambda = 0.0$, 0.5, or 1.0. Again, on the microscale, the local crack extension is often on maximum shear planes. This is primarily HCF damage, but the final crack development includes some crack linking, which is characteristic of LCF damage.

In torsion, crack development occurs exclusively on maximum shear planes in the longitudinal direction (Fig. 29) for all strain levels resulting in lives of 10^6 cycles or less. Cracks appear to initiate very early in life from the magnesium sulphide inclusions. Many cracks can be found over the entire surface. Growth occurs on stage I planes. Previous research [19,28,29] suggests that in torsion, cracks would be expected to show a stage I to stage II transition similar to

that found under mixed loading conditions. In an attempt to get stage II growth in torsion, two tests were performed at a strain level of $\Delta\gamma/2 = 0.0022$ ($\bar{\varepsilon} = 0.13\%$). Specimen 4582 was cycled to 7.5×10^6 cycles without the development of a major crack. This strain level is below the fatigue limit of the material. The amplitude was then increased 15 percent and failure occurred in approximately 10^6 additional cycles. The failure crack was primarily on a longitudinal shear plane but showed some deviation.

Specimen 4587 was also a torsion test at $\Delta\gamma/2 = 0.0022$. After a few initial cycles, a large torsional overload was applied. It is well known that overloads can eliminate the fatigue limit in mild steels [52]. After the overload, the stress-strain response showed a slight torsional mean stress. Failure occurred after 3.1×10^6 cycles. Figure 30 shows the failure crack. Initiation and early growth again occurred on the maximum shear plane before the crack branched to grow perpendicular to the maximum principal stress. The two branches at each end of the shear crack have grown at different rates, indicating the influence of the torsional mean stress. A torsional mean stress results in a tensile mean stress on one of the principal stress planes and a compressive mean stress on the other. After a period of stage II growth the crack then switched back to grow on stage I planes.

LCF Type Damage

LCF damage occurs in high amplitude tests for all strain states and is characterized by the initiation of multiple crack systems. Surface damage just prior to failure is shown in Fig. 31 for all test conditions

except torsion at a strain level of $\bar{\varepsilon}$ = 1.0 percent. LCF damage in torsion is shown in Fig. 29.

An axial test is shown in the upper left of Fig. 31. Damage occurs primarily at angles between ±45° to the horizontal. For all other strain states (λ = 0.5, 1.0, 2.0, and ∞), the damage develops on or very close to the planes of maximum shear strain. This can be considered stage I growth. Damage is distributed over the entire surface, and the density of damage increases [37] with applied cycles prior to the final failure process. Damage sites which initiate early in life tend to coarsen and become more clearly visible, rather than extending in surface length. The average length is roughly 50 μm, (approximately the grain size of this material).

Final failure results from rapid crack development by linking of the many damage sites. This process occurs in a very few number of cycles and is quite different than that observed at long lives. Failure cracks are shown in Fig. 32 for λ = 0.0 and λ = 1.0. Growth tends to align with the plane perpendicular to the maximum principal stress; however, the growth direction changes often as the crack seeks the easiest path through the specimen. It can best be described as a "weakest link" process, as the crack follows the most damaged path through the material.

4.2.2 Notched Shaft

Cracking behavior in the critical area of the notched shaft has been observed for several of the loading conditions shown in Fig. 16. Medium life conditions (approximately 10^5 cycles to failure)

for bending, XR, ZR, and torsion loading conditions have been observed to determine if the crack initiation and early growth behavior is influenced by a change in direction of the plane of maximum shear. Differences in damage development, similar to the LCF-HCF damage processes in the thin-wall tube, are interpreted by comparing short life (approximately 10^4 cycles to failure) and medium life tests. Characteristic behavior in torsion is reported for long and short life tests.

Bending

Crack development for a medium amplitude (1730 Nm) bending test is shown in Fig. 33. The stress-strain state is shown in the specimen diagram and indicates that the intersection of the maximum shear strain plane and maximum principal stress plane are both in the circumferential direction on the surface of the notch. This results because the maximum shear is type B. A crack of 250 μm was found at 49,200 cycles in the circumferential direction parallel to the finish grinding marks. The cross marks on this picture at 45° are not cracks but are imperfections in the sputtered coating applied to the replica. At 67,000 cycles, a surface crack length of approximately 3.0 mm was present. Two major cracks just prior to linking up are shown at 102,925 cycles. The three cross marks on this photo are locating marks placed on the specimen prior to testing to aid determination of specimen location during observation of the replicas. The arrows indicate the same point in all the photographs, but it is not known if this was the exact site of crack initiation.

At an amplitude of 1730 Nm bending, a small number (3) of cracks initiated and eventually linked to form a single dominant crack. At lower stress levels, fewer cracks initiated until, at very long lives, a single crack initiated and grew to failure. At higher stress levels many cracks initiated at various points in the critical area. After a period of growth, these cracks linked to cause failure. This is illustrated by the macroscopic fracture surfaces in Fig. 34. For the test at 1875 Nm, several cracks are identified (see arrows) that eventually contributed to the failure crack. For the test at 1475 Nm, however, a single site can be identified as the initial crack.

XR Loading

A medium amplitude test for the XR loading condition is shown in Fig. 35. This specimen was polished so that only traces of the surface grinding operation remained in the critical area. Typical crack initiation, shown at 100,000 cycles, occurred in the circumferential direction. This crack had grown to approximately 350 μm in surface length prior to a change in growth direction. Cracks that initiated in the circumferential direction branched to grow perpendicular to the maximum principal stress (stage II). At 130,000 cycles, three cracks which displayed this behavior were observed in the notch root. Another fatigue crack that formed in the vicinity of those in Fig. 35 is shown in Fig. 36. The two features shown at 20,000 cycles are thought to be a particularly severe group of longitudinal inclusions and were observed on the first replica taken at 5,000 cycles. At 100,000 cycles, the inclusions had linked. A brief period (<100 μm) of growth in the

circumferential direction preceded branching to stage II growth perpendicular to the maximum principal stress. Although this growth process differed from the cracks shown in Fig. 35, the failure life was not dominated by either process. Instead, final failure occurred by stage II growth of the three major cracks that developed. It should be noted, once the tips of the stage II cracks overlapped, growth occurred primarily at the crack tips at the extreme ends of the multiple crack system.

Behavior in a high amplitude XR loading condition is shown in Fig. 37 to be quite different. More cracks initiate and develop in comparison with the lower amplitude test. The critical area for initiation is much larger, extending further around the circumference and along the length direction in the radius (Figs. 20 and 21). Again, initiation was in the circumferential direction rather than in the direction of maximum shear strain or maximum principal stress. At 4,000 cycles, one of the cracks shown had reached a size greater than 1.0 mm. At 5,000 cycles, this crack had linked with another along the longitudinal direction. Others that were not identifiable at 4,000 cycles had also developed. At 6,000 cycles, many cracks on different but parallel planes had linked up to form a main crack system in the circumferential direction. (The rotation of the crack in this photo is a result of the photography, the crack was in fact parallel to the notch root.)

Macroscopic failure surfaces for the medium and high amplitude XR tests are shown in Fig. 38. Failure in the medium amplitude test is perpendicular to the maximum principal stress, consistent with stage II growth concepts. In the high amplitude test, however, failure is in the

notch plane. This is a result of the extensive damage and crack linking which constrains the final failure to the notch plane.

ZR Loading

Similar behavior was found under the ZR loading conditions. Figure 39 shows a small portion of the critical area of a high amplitude ZR test. Cracks are observed in the circumferential and longitudinal directions as well as at angles in between. Extensive damage of this nature was visible over several millimeters in the notch. Macroscopic failure, shown in Fig. 40, illustrates similar characteristics between the XR and ZR conditions (Figs. 35,37,38). Again, for the medium amplitude test at the top of Fig. 40, a few cracks initiated in the circumferential direction. These cracks then branched to grow perpendicular to the maximum principal stress. In the high amplitude test shown at the bottom of Fig. 40, extensive cracking was observed in the circumferential direction and linking of these crack systems resulted in the failure being constrained to the notch plane.

Torsion

Long life torsion behavior is shown in Fig. 41. A few cracks initiate around the circumference on longitudinal shear planes. As these cracks develop, they grow into a decreasing stress field. Branching to stage II growth planes occurs in tests lasting more than 10^6 cycles and final failure is by linking of the 45° cracks. The macroscopic failure surface exhibits the classical "star" pattern often reported.

Higher amplitude torsion tests exhibit different behavior (Fig. 42). Cracks not only initiate in the notch region but also in the parallel gage section. Growth occurs by stage I extension on longitudinal shear planes. Many cracks are observed to develop over the entire length of the 40 mm diameter section of the shaft. Final failure in many of these tests was a result of increased torsional compliance of the specimen rather than separation into two pieces. The cracks in Fig. 42 have been highlighted using magnetic particle techniques [51].

5. DISCUSSION

Current crack initiation fatigue life methodologies assume that similitude (Fig. 5) exists in the damage process occurring in the specimen used for determining the baseline fatigue properties, and the damage process in the specimen or component being analyzed. The validity of this assumption for multiaxial fatigue has been investigated by comparing the damage development in two specimen geometries. A discussion of these assumptions, the crack observations, and the application of the five crack initiation life methods for multiaxial fatigue follow.

5.1 Thin-Wall Tube

The thin-wall tube geometry is considered to be the smooth specimen for multiaxial fatigue. It is desirable that the multiaxial life prediction methodologies implement only smooth specimen uniaxial fatigue constants to predict the life of other strain states. Implementation of a multiaxial fatigue theory suggests that equal fatigue lives will result for specimens tested at equal values of the equivalent damage (strain) parameter. This implies similitude in the damage process. Initiation and early growth stages for uniaxial tests should be identical for the smooth cylindrical specimen and the thin-wall tube, since both experience a state of uniform, plane stress over a large gage section. Differences in crack growth to final failure result from the larger size of the tube specimen. This is not a significant factor in the comparison of these tests, since most of the life is spent in the growth of cracks much smaller than the specimen dimensions (see Fig. 12 Ref. [37]).

It is necessary to consider the similarities and differences in damage development for other strain states in the thin-wall tube tests compared with those observed in the uniaxial tests. Two damage processes, LCF and HCF, have been identified [37] from surface crack observations of the thin-wall tube. Observation of a wider range of test conditions in this study shows (Fig. 43) that the dominant damage process is strain state, strain level, and material [26] dependent. The abscissa in Fig. 43 shows the number of cycles required to form a 1.0 mm crack and may be interpreted to be a function of strain level. The ordinate is given in terms of strain state and has been plotted as the ratio of the principal strains, $\xi = \varepsilon_1/\varepsilon_3$. This strain state representation has been adopted so that torsion data could be included in the plot. Strain states in terms of λ have been included for reference. Test conditions that fall to the right of the shaded region exhibit HCF damage, and those that fall to the left exhibit LCF damage. Conditions which fall within the shaded region exhibit mixed behavior.

It is difficult, if not impossible, to identify from surface observations the end of the initiation stage and the start of stage I growth. Indeed, for this material, there is little reason to make a distinction other than to say that crack initiation and early growth occur on maximum shear planes. In the ensuing discussion, stage I crack development will refer to both the initiation and early shear growth processes. Stage II behavior will refer to the crack development on planes perpendicular to the maximum principal stress.

HCF damage is characterized by the formation and development of a single dominant crack system. From the observations reported in Section 4.2 (see Figs. 25-28, and 30), this process follows the classic stages of fatigue development. Crack initiation occurs on a plane of maximum shear strain amplitude. Stage I growth proceeds in the same plane as the initiation process. The crack then changes direction, and stage II growth to failure continues in a plane perpendicular to the maximum principal stress. Combined loading cases $\lambda = 0.5$ and $\lambda = 1.0$ (Figs. 26 and 27) display this behavior most clearly. For the combined loading case, $\lambda = 2.0$ (Fig. 28), a larger number of crack systems were nucleated over the gage section, and final failure showed some crack linking, indicating mixed HCF and LCF behavior.

Interpretation of the crack behavior for uniaxial loading is complicated by the general nature of the strain state. During axial loading the second and third principal strains are equal. Consequently, the maximum shear strain can intersect the surface at any angle between $\pm$ 45° from the circumferential direction [3]. In other words, the type A and type B shear strains are equal in magnitude. When a crack forms as a result of a type B shear strain, such as that shown in Fig. 25, it appears on the surface in the same direction that stage II growth is expected. Identification of stage I and stage II cracking, therefore, is somewhat ambiguous.

Torsional cracking behavior is influenced by the presence of the magnesium sulphide inclusions. Fatigue cracks grow in the longitudinal shear plane from the inclusions, which are approximately 100 μm in length. This is larger than the length of stage I shear growth observed

for some mixed loading conditions which exhibited HCF damage. HCF behavior was observed for torsional loading only at lives near or in excess of the fatigue limit. At higher strain levels, only LCF damage and stage I cracking were observed. Difficulties encountered in analyzing the torsional cracking have been discussed further in Ref. [37].

Stage I cracking is most stable in torsional loading, but the tests at a strain level of $\Delta\gamma/2 = 0.0022$ support the observations [19] that stage II crack growth will occur in torsion at long lives. It appears that torsional overloads have a similar effect as overloads in uniaxial loading, resulting in failures at stress levels below the fatigue limit. It is not clear that torsional mean stresses affect stage I crack behavior, but Fig. 30 clearly indicates the influence on stage II crack development. In the absence of mean stress, equal growth would be expected on both 45° tensile planes (Fig. 41). In Fig. 30 the crack favors the plane of tensile mean stress. The contributions of the inclusions to torsional crack behavior is incompletely understood at this time. The fact that there is not an opening strain (ε_n) across the stage I crack may be a factor in the stability of stage I growth in torsion.

Transition from stage I to stage II growth for HCF damage is thought to be influenced by the magnitude of the normal strain, ε_n, to the plane of maximum shear strain. The surface length of the stage I crack when the transition to stage II growth occurred has been determined for the test conditions that experience HCF damage. This crack length, a_s, is plotted against strain ratio in Fig. 44 (see also

Table 7) for strain levels of $\bar{\varepsilon}$ = 0.22% and $\tilde{\varepsilon}$ = 0.15%. Torsion was not included in this figure because of the complications arising from the presence of the inclusions. Figure 44 shows that the length of the stage I crack increases with strain ratio, λ. This corresponds to a decreasing value of the normal strain. A decrease in the extent of stage I growth is also observed as the strain level decreases. Brown and Miller [24] applied a linear elastic fracture mechanics analysis to predict the stable cracking behavior. Their analysis suggests that the transition is independent of strain level or crack length, and is only a function of strain ratio (i.e., normal strain). This conclusion conflicts with the trends shown in Fig. 43 which suggest the transition in crack behavior is related to the micro-mechanics of crack growth in addition to metallurgical factors. Fig. 44 shows a strong dependence of stage I crack development on effective strain amplitude. Linear elastic fracture mechanics analysis, however, is inadequate to describe the behavior. This should not be surprising since, for these stage I crack sizes, assumptions of LEFM are violated. These observations are important from the mechanistic viewpoint but are not accounted for in the application of any of the life prediction methods.

LCF damage occurs in tests which fall to the left of the shaded region in Fig. 43. This damage process is characterized by the formation and development of multiple crack systems (Fig. 31). For all test conditions, stage I cracking occurred on or near the planes of maximum shear strain. Multiple initiation was observed and is expected at higher strain levels, since a larger number of grains within the material are subjected to a critical level of shear stress [53].

Failure is the result of a linking process, as the failure crack progresses rapidly through the damaged material. This occurs in a plane approximately perpendicular to the maximum principal stress, but the crack changes direction often as it follows the "weakest link" path.

Hua and Socie [13] implemented a crack density approach to describe the development of LCF damage and noted that once damage sites formed they did not immediately grow in length, but instead became coarser and better defined. An attempt in Fig. 45 (see also Table 7) was made to correlate the length of the stage I, LCF damage prior to extensive crack linking in a similar format as was performed for HCF damage. The length of the stage I damage sites, were measured at approximately 90 percent of the failure life. This is plotted against strain ratio (ξ and λ) in Fig. 45. In contrast to the HCF damage, the length of stage I damage development for LCF damage is not dependent on strain state. The average length of the stage I damage sites was approximately 50 μm for the four strain ratios. This is on the order of the grain size for this material. Although not confirmed, it is suspected that the growth of the damage prior to failure is limited by microstructural factors, and that once the shear processes extend beyond a grain or two crack growth by linking of these sites becomes dominant.

Differences in stage I crack development in the LCF and HCF regime may be related to the monotonic and cyclic stress strain behavior. At low strains (< 0.5 percent) the material cyclically softens. Once a slip band has formed the slipped region becomes weaker (cyclic softening) than the surrounding material. Slip remains concentrated in the local region, and the slip band does not coarsen. This band grows

as a discrete stage I crack. At cyclic strains above 0.5 percent, once a slip band has formed, cyclic hardening occurs. This results in coarsening and broadening of the slip band as the surrounding weaker material experiences slip.

Current multiaxial fatigue models, such as the Brown-Miller and Lohr-Ellison theories, are based on the desire for the models to physically relate to the actual damage processes [23,25,33,34]. For the thin-wall tube tests the fraction of life spent in stage I and stage II crack development is plotted in Fig. 46 for strain levels of $\bar{\varepsilon}$ = 0.15% and 0.22% and in Fig. 47 for $\bar{\varepsilon}$ = 1.0%. The tests at $\bar{\varepsilon}$ = 0.15% and $\bar{\varepsilon}$ = 0.22% exhibit primarily HCF damage development, and the tests at $\bar{\varepsilon}$ = 1.0% exhibit LCF damage. Stage I development is indicated by the cross-hatched areas. For $\bar{\varepsilon}$ = 0.15%, λ = 0.5 and 1.0, less than 20% of the life is spent in stage I crack development. At $\bar{\varepsilon}$ = 0.22%, between 18% and 50% of the life for all the strain ratios tested except torsion is stage I crack development. Consequently, most of the life of a 1.0 mm crack is spent in growth perpendicular to the maximum principal direction. The fraction of life spent in stage I development tends to increase with strain ratio, which is consistent with the test condition becoming closer to the LCF-HCF transition region shown in Fig. 43. At $\bar{\varepsilon}$ = 1.0% (Fig. 47), more than 95% of the life is spent in stage I development. The LCF damage development precludes a large portion of stage II growth because the failure crack forms by a linking process. These results indicate that a parameter based on the maximum shear strain best relates to the LCF damage process, and that the maximum principal strain is representative of the major portion of life in the

HCF damage where stage II growth occupies more than 50 percent of the life.

Analysis of the damage development in terms of a damage curve approach [13,37] has shown that a two-phase damage law is required in the HCF region, and a single phase damage law predicts the LCF damage development. In these studies [13,37], crack behavior was interpreted to be entirely stage I development. The transition from the first phase to the second phase for the HCF damage curve (Fig. 16 Ref. [37]) corresponds (both in terms of life fraction and crack length) very closely with the transition from stage I to stage II crack behavior identified in the current investigation. This indicates that the stage I crack growth rate is much lower than the stage II growth rate. The LCF damage curve has only a single phase [37] because the LCF life consisted almost entirely of stage I damage development.

The character of damage development in the thin-wall tube for the range of multiaxial conditions tested varies with strain state and strain level. This violates the assumption of similitude in damage development between the uniaxial condition and other strain states. Despite the lack of similitude the ability of the five theories to estimate the lives of the thin-wall tube test results is good. This is due in part to an averaging effect, since the failure definition employed (1.0mm surface crack) incorporates both stage I and II development.

In addition, since all tests were completely reversed constant amplitude loading, the differences in HCF and LCF damage and the fact that the stage I crack length varies with strain state did not interact

in any given test. Variable loading conditions, both in terms of strain state and strain amplitude, may result in the interaction of these damage conditions and influence the process of damage development.

Recall, that the test amplitudes for the thin-wall tube were determined to give a constant effective strain for the various strain states tested. Also, for a given effective strain level, the fatigue lives tend to increase with increasing strain ratio (see Fig. 23 and Table 4). For a constant effective strain, the influence of strain state on the other four parameters investigated is shown in Fig. 48. This figure has been prepared for $\bar{\varepsilon}$ = 1.0% and Poissions' ratio equal to 0.3. The trends are relatively insensitive to the values chosen. Maximum principal strain and effective strain are nearly equal up to a strain ratio value of ξ = -1.6. As the proportion of torsional loading increases from this value the principal strain value decreases. Coupled with the fact that the maximum shear strain value continually increases from axial to torsional loading, this may explain the stability of stage I cracking during torsional loading. The Brown-Miller parameter varies approximately 10% from a minimum at the axial condition to a maximum at about ξ = -1.6 whence it decreases to a value equal to the maximum shear strain for torsion. This parameter, like the effective strain parameter, is a weighed average of the maximum shear strain and the principal strain, and similar correlations are observed (Fig. 23b and d) since they follow the same trends over the strain states considered (Fig. 48). Considering the increasing life with increasing strain state (given $\bar{\varepsilon}$ constant), the Lohr-Ellison parameter shows the proper trends to correlate the data. The decreasing value of the parameter with

increasing strain state should better correlate the results but, since Eqn. 14 is normalized to the axial test, correlation similar to the other parameters is obtained.

All five predictive methods show good correlation of the test results. When LCF type damage is dominant, the maximum shear strain and the Brown-Miller parameter are most appropriate, since most of the life is stage I crack development. For HCF type damage, the maximum principal strain parameter best relates to the physical damage, since most of the life is spent in growth on planes of maximum principal stress. Although the effective strain and Lohr-Ellison parameters result in good life predictions, the damage observations do not support the use of these models.

5.2 Notched Shaft

Application of the local stress-strain approach to notched multiaxial fatigue problems requires the assumptions of similitude shown in Fig. 5. Damage that occurs in the thin-wall tube is assumed to be representative of damage in the critical location of the notched shaft. In fact, the observations of microcracking show that some stages of the initiation and growth processes exhibit similitude, and some do not. Microcracking behavior and, hence, similitude arguments are dependent on strain state and strain amplitude.

Crack initiation in the notched shaft was found to be constrained to the notch plane for all loading conditions except torsion. During bending tests, the maximum shear plane and the maximum principal stress plane intersect the surface of the notch in the circumferential

direction (Fig. 18a). As the load amplitude increases, the number of cracks that form and interact in the failure process also increases (Fig. 34). Surface observations (Fig. 33) do not clearly identify the transition from initiation and stage I shear behavior to stage II growth, since both occur in the same direction. It is not clear from observations in bending if similitude exists between the thin-wall tube and the shaft.

For combined loading, initiation and early growth are constrained to the circumferential direction rather than occurring on maximum shear planes as would be expected from the behavior observed in the thin-wall tube tests. Figures 35, 37, and 39 display this behavior for high and medium amplitude test conditions for different ratios of torsion and bending (XR and ZR). Growth to failure is a stage II process for medium and low amplitude tests, but for high amplitude tests, failure cracks develop in the plane of the notch (Figs. 38 and 40). Again, as the load amplitudes are increased, the number of cracks that initiate and grow also increase. Similitude in crack initiation and early growth does not exist.

During torsional loading, cracks initiate on longitudinal shear planes (stage I). In tests lasting less than 10^6 cycles for failure, macrogrowth also proceeds on shear planes as stage I cracks (Fig. 42). At longer lives (Fig. 41), the cracks which initiate on shear planes in the area of stress concentration branch to grow as stage II cracks as they grow out of the geometric stress concentration. Torsional crack behavior is similar for the thin-wall tube and notched shaft.

Similitude in the failure process must also be considered. Growth to failure in the notched shaft exhibits behavior similar to the LCF-HCF failure conditions shown in Fig. 43 for the thin-wall tube. After early growth in the circumferential direction, cracks in the medium and long life tests change direction to grow perpendicular to the maximum principal stress. This is analogous to the behavior observed in the HCF damage in the thin-wall tube. Growth is constrained to the notch only in the high amplitude short life test condition. In this case, the initiation damage in the notch is so extensive that failures occur by a rapid linking of the many cracks that have initiated in the notch plane. This is similar to the LCF damage condition reported in the thin-wall tubes.

In the notched shaft tests, as in the thin-wall tube tests, two different damage processes occur that are amplitude and strain state dependent (Fig. 49). Strain state is presented as the ratio of torsional moment to bending moment (M_t/M_b). In test conditions that fall to the right of the division in Fig. 49, a few cracks initiate in the notch and then change direction to grow in stage II (mode I). To the left of the division, many cracks form in the notch, and the extensive damage results in final failure by linking of the many cracks. Similitude between the thin-wall tube and notched shaft specimens does not exist for the initiation and early growth process. Similarities do exist in the failure processes, i.e. stage I growth at long lives and crack linking as result of extensive damage at short lives.

Several factors may influence the lack of similitude between the two specimens. The surface finish of the notch shaft differs from that

of the thin-wall tube and may affect crack behavior. The notched shaft has been prepared to represent a typical component [38]. A low stress surface grinding operation was the final surface preparation on the shafts. This resulted in fine grinding marks in the circumferential direction. Relatively low strength ductile metals, like the 1045 steel of this study, are not expected to be particularly sensitive to such surface finish. Initial observations showing crack development in the circumferential direction (Fig. 39) were performed on the as ground shafts. Several shafts were then polished using techniques similar to those used for the thin-wall tube. These tests still resulted in crack initiation and early growth in the circumferential direction rather than on the maximum shear planes. Surface finish has been shown to influence the development of cracks in other materials [54,55], but the effect remains unquantified. The extent of residual stresses and deformation from the machining operation is not known. Even at long lives (10^6 cycles to failure) some plasticity is present that should act to relax residual stresses. In fact, in tests to study the effect of mean stress in the thin-wall tube specimen the mean stresses always relaxed out [56], indicating that residual stresses from the machining operations should not have a significant effect.

Another difference for combined loading is that the maximum shear strain in the thin-wall tube is always a type A shear strain acting along the surface, whereas for the notched shaft it is mixed type A and type B depending on loading conditions. For axial loading of the thin-wall tube, type A and B shear strains are equal, and in observations of a number of tests initiation was found to occur by either showing no

preference toward one or the other. In the same sense, the difference in type A or B shear strains would not be expected to force crack initiation from the maximum shear plane in the notched shaft.

Another factor to consider is the stress gradients present in the notched shaft that may influence the crack behavior. In the thin-wall tube, cracks develop in a uniform stress-strain field. In the notched shaft, however, the stress-strain field decreases rapidly in magnitude away from the notch both toward the center of the shaft and along the length of the shaft. Typical stress-strain gradients are shown in Figs. 20 and 21. Gradients in the radial direction are analogous to the gradients away from the notch root usually considered in axial fatigue of notched plates. Gradients along the length of the specimen may constrain the crack behavior to the notch plane while the crack is small. Stage I growth in the maximum shear plane would require crack extension into a decreasing stress-strain field. To some extent this limits growth to the notch plane until the crack has developed sufficiently to grow independent of the notch concentration. A discussion of how the gradients during uniaxial loading influence the similitude shown in Fig. 5a and how the multiaxial case differs is given in APPENDIX C.

If the stress gradient along the length of the shaft is the dominant factor in the constraint of crack behavior, a specimen that does not show large gradients in the longitudinal direction would be expected to result in crack initiation and early growth on the maximum shear planes. A few tests have been performed on an unnotched shaft specimen subjected to torsion-bending loads (Fig. 50) to observe the cracking behavior. Stress-strain analysis has been performed using the

elastic plastic FEM described in APPENDIX A and results are given in Table 8. Stress-strain fields for a combined test are shown in Fig. 51. A stress gradient into the specimen is still present, but the gradient along the length of the shaft is much smaller than in the notched shaft.

Crack behavior for a combined loading test of the unnotched specimen is shown in Fig. 52. Fig. 52a is for a well polished specimen and Fig. 52b is for a specimen tested in the as ground condition. Both are for a test amplitude of 1330Nm bending and 1800 Nm torsion. The angle of the cracks to the notch plane are equal and opposite since, one test cracked on the top and the other cracked on the bottom of the specimen. Initiation and early growth of the crack, indicated by the arrows, are in the maximum shear direction. The majority of the growth is stage II, perpendicular to the maximum principal stress. This loading condition is similar to the XR condition for the notched shaft and should be compared with Fig. 20b. Similitude in the damage development exists for the thin-wall tube and this test condition of the unnotched shaft. In the notched shaft, the constraint caused by the gradient along the length of the shaft is in part responsible for the lack of similitude in the early crack development. However, Fig. 52b indicates that portions of crack growth also occurs in the notch plane. These cracks are associated with the grinding marks. This is unexpected for this material but indicates the sensitivity of the initiation and early growth process to surface finish. Baseline data is generated on smooth polished specimens, and the influence of the final finishing operation on component behavior is not often considered in design analysis.

None of the five life prediction models has a strong relationship between the damage parameter and the observed physical damage processes for combined loading cases of the notched shaft. All methods are normalized to the axial case and show the best correlation for the bending results. This is expected, since for bending the physical damage coincides with the damage parameters. The maximum principal strain, effective strain and maximum shear strain (Fig. 24 a, b, and c) predictions all show similar amounts of scatter in the correlation of the shaft data. The Brown-Miller parameter (Fig. 24d) shows slightly less scatter. If the constant S, in Eq. (11), is taken as 0.0 this parameter is equivalent to the maximum shear strain parameter. If the constant S is taken as 2.0, Eq. (11) is equivalent to the maximum principal strain theory. Consequently, the Brown-Miller parameter is an intermediate or averaged strain parameter. Although the conceptual formulation is based upon γ_{max} and ε_n, arguments based on the actual crack development in the notched shaft would suggest that γ_{notch} and ε_{notch} would be more appropriate parameters for the prediction of initiation and early growth. Predictions based on these damage parameters fitted to Eq. (11) did not improve the correlation. At longer lives, an improvement would not be expected because the cracking is dominated by the principal stress or strain. For short lives, the slope of the strain-life curve results in only small changes in life for small changes in strain. At long lives, only the principal strain correctly accesses the damage development. The Lohr-Ellison parameter shows the most scatter and non-conservative predictions.

In general, all five life prediction methods (Fig. 24a-e) show a tendency for non-conservative predictions at short lives and conservative predictions at long lives. These trends arise as a result of the cracking behavior and the relationship to the damage parameters used in the analysis. Development of a 1.0 mm crack occurs more quickly at short lives than predicted. In part, this is a result of the extensive damage nucleation and the interaction of damage sites to give a 1.0 mm crack. Stress gradients at high amplitude test conditions are less severe because of plasticity. Consequently, the crack growth driving force does not decrease very rapidly as the crack grows into the specimen. At long lives, fewer cracks are nucleated, and the interaction of crack systems in the failure process is negligible.

At low amplitudes (small plastic strains) the radial stress gradient near the surface is very severe and will influence crack growth into the specimen. Slower growth than expected from the baseline tests can result from the radial stress gradient, and can lead to the conservative trend in the predictions at long lives. In the baseline tests cracks do not experience the same decreasing stress field as they grow into the depth of the specimen.

Possible errors in the determination of the local strains can certainly influence the life predictions. At low amplitudes there is good agreement between the measured strains and the FEM results. The FEM results are taken at the point of tangency of the gage section and radius. Tipton [17] has shown that, for bending, maximum strains actually occur up the notch slightly and for the elastic case are approximately 14 percent higher. This is not felt to be a factor,

because the results of the FEM used in this analysis agree well with the maximum concentration reported [17,50]. If higher strains slightly up the notch were considered, though, the predicted lives would be even more conservative at long lives. At high load levels the FEM results overpredict bending strains (Fig. 22a) by 20 percent. This could result because measured strains are averaged over the gage area and do not reflect the true maximum strain. Considering that the actual strain values are lower than those determined by the FEM would result in more non-conservative predictions at short lives. Consequently, possible errors in the strain analysis have resulted in better correlation and do not explain the trends of the data.

Results of the five life prediction methods (Figs. 24a-e) also show an increasing lack of correlation with an increasing amount of torsional loading for the notched shaft tests. Crack initiation and early growth occur in the notch plane and, consequently, for a given test condition the shear strains in the crack (notch) plane decrease as the loading ratio (M_t/M_b) increases. A smaller driving force for crack initiation for a given strain level in the notch results in longer lives. This accounts in part for the increasingly skew correlation of the test conditions with increasing, M_t.

6. CLOSURE

Detailed observations of the development of fatigue damage have been reported for two specimen geometries subjected to multiaxial fatigue. The stages and extent of damage are dependent on strain amplitude, strain state, and material. In the notched specimen, stress concentration and surface finish that result from specimen preparation significantly influence crack development. These are important factors in the micromechanics of damage development. Life methods based upon the micromechanics of crack development will result in improved life estimates and greater confidence in the application of both initiation and propagation methodologies.

Another element in the prediction of component fatigue life that must be considered in light of the current results is the cumulative damage algorithm. In conventional analysis, Miner's linear damage hypothesis is used to sum variable amplitude loading cycles and predict failure. The shear parameters (maximum shear strain, Brown-Miller, and Lohr-Ellison) have been shown to best represent the damage development at short lives. At longer lives, damage accumulates for a greater percentage of the life on planes of maximum principal strain. Because of this dependence on amplitude it is important in a service load analysis to identify the primary life limiting loading cycles. If the cycles are predominantly large amplitude, a shear based parameter should be implemented into the cumulative damage scheme. If, as is often the case, the service loading history comprises mainly small cycles with a few large amplitude events, the damage parameter should be the maximum principal strain. This would be in agreement with observations of damage development.

It is also well known that Miner's postulate introduces an unrealistic linear relationship into the damage summation scheme. Damage has been shown to accumulate in a non-linear fashion [37] for the 1045 used in this study. Tests on smooth uniaxial specimens tested in strain control under service loading spectrums [57] indicate that the influence of small cycles is not adequately predicted with the current life estimation scheme (Fig. 4). This may be a result of the interaction of the damage established at different loading levels. For instance, do small amplitude cycles promote the development of damage introduced by large amplitude events? Further investigation of these factors is required for improved life predictions.

6.1 Thin-Wall Tube Tests

Constant amplitude, completely reversed, strain control tests have been performed on thin-wall tube specimens for a variety of multiaxial loading conditions. The development of fatigue damage has been observed and five multiaxial life prediction models implemented using smooth uniaxial fatigue constants. These results are summarized below for the normalized 1045 steel investigated.

Damage development in a uniform multiaxial strain field follows the classic stages of shear initiation, stage I and stage II growth. The proportion of life spent in each of these stages depends on the applied loading conditions.

In high amplitude tests, stage I crack development occupies most of the life of the thin-wall tube. Multiaxial damage initiates very early in life, and most of the life is spent in development of damage sites on

the order of the grain size. Rapid linking to failure occurs in a small number of cycles. Fracture mechanics concepts are not applicable to the latter stages of this growth process.

In long life, low amplitude tests, initiation occurs on planes that experience the maximum range of shear strain. The extent of stage I crack development is dependent on strain state and strain amplitude. Stage I growth is more extensive and occupies a larger percentage of life with increasing strain ratio, λ. For the fatigue lives tested, the extent of stage I growth decreases with decreasing amplitude resulting in a larger percentage of life spent in stage II growth. The transition from stage I to stage II cracking is responsible for the two phase damage curves reported previously [13,37]. Failure occurs by stage II growth. Fracture mechanics concepts are applicable to the later stages of this growth process. Only at "fatigue limit" stress levels for torsion does stage II crack growth occur.

The most appropriate fatigue damage model is dependent on the test conditions. At short lives or large strain ratios, λ, shear strain based parameters relate best to the physical damage. At long lives and smaller strain ratios, most of the life is stage II growth; consequently, the maximum principal strain parameter best relates to the physical damage.

6.2 Notched Shaft Tests

Constant amplitude, completely reversed fatigue tests have been performed on a notched shaft specimen to study the influence of a notch during multiaxial fatigue. Comparison of the damage development and life predictions with the thin-wall tube can be summarized as follows.

The notch geometry has a significant influence on the development of damage in the shaft. Crack initiation and early growth occur in the notch plane rather than on planes of maximum shear strain. Both the stress gradients in the notch and the surface finish of the shaft influence this behavior.

The number of cracks that initiate is dependent on load amplitude. A single crack initiates and grows to failure at long lives. More cracks initiate and interact as the load amplitude increases. At high amplitudes, extensive damage accumulates at the notch, and failure is constrained to the notch plane by the extensive damage and crack linking.

At long lives, stage II growth occurs on planes of maximum principal stress. For this condition, fracture mechanics concepts are applicable. At short lives, extensive damage and crack linking constrain the failure to the notch plane and fracture mechanics concepts are not applicable.

Torsional cracking occurs in longitudinal shear planes. At long lives, the shear cracks branch to stage II (mode I) growth as they extend out of the notch stress concentration. At shorter lives, shear cracks grow the entire length of the notched shaft.

Correlation of the experimental results with the five multiaxial life prediction models reflects the observed damage processes. As the load ratio (M_t/M_b) increases, the correlation between the experimental results and the predicted lives decreases. This is a reflection of the early damage development occurring in the notch plane rather than on planes of maximum shear.

Similitude between the thin-wall tube and the notched shaft does not exist for initiation and early growth (except in torsion). Similitude does exist in the failure process, with stage II growth occurring at long lives and a crack linking process occurring at short lives.

7. CONCLUSIONS

1. Damage development in thin-wall tube (smooth) specimens subjected to multiaxial fatigue follows the classical stages of initiation, stage I, and stage II growth.
2. For high amplitude LCF damage conditions in unnotched specimens almost the entire life is stage I growth. Shear based life prediction parameters are most appropriate for this life regime.
3. For low amplitude HCF damage conditions in unnotched specimens growth perpendicular to the maximum principal stress/strain predominates the damage process for the life regime tested. Maximum principal strain amplitude should best correlate these data.
4. The cyclic life when the transition from LCF to HCF behavior occurs varies with strain state.
5. For a constant effective strain amplitude, the extent of stage I crack development is a function of strain state.
6. Similitude does not exist in the initiation and early growth processes between the smooth specimen and the notched component. Crack initiation and early growth in the notched shaft occur in the circumferential direction in the shaft rather than on stage I planes for bending and mixed loading. Surface finish and longitudinal stress-strain gradients influence this behavior. Macroscopic growth depends on the extent of damage established in the nucleation process.

7. At low amplitudes, growth to failure in notched specimens proceeds on stage II planes, perpendicular to the maximum principal stress (mode I in fracture mechanics terminology). This is similar to the thin-wall tube growth process at long lives.
8. At high amplitudes, growth to failure is constrained to the notch and occurs by a crack linking process. This is similar to the short life growth processes in the thin-wall tube. The stress gradient along the length of the shaft is important in constraining the damage process to the notch region.
9. Surface finish has a larger effect than expected and significantly influences the initiation and early growth.
10. During torsional loading magnesium sulphide inclusions, aligned in the longitudinal direction, significantly influence the initiation and growth of fatigue damage for both specimens.

Table 1 Chemical Composition and Microstructure Characterization for SAE-1045 Steel

Chemistry*

C	Mn	P	S	Si	Ni	Cr
0.44	0.77	0.024	0.053	0.210	0.050	0.06

Mo	Cu	Aℓ	V	Nb	Ti
Nil	0.03	0.043	0.002	0.002	0.002

Microstructure*

Grain size 6-7 (Per ASTM E112)
(approximately 35-40 μm)
Inclusion (Per ASTM E45)

Type	Rating
A & C Thin	2-3
B Thin	1

* Courtesy of Deere and Company

Table 2 Static Tensile Properties

BHN	= 153
E	= 205000 MPa
%RA	= 51
σ_y	= 380 MPa (lower)
σ_{uts}	= 621 MPa
σ_f	= 985 MPa
ε_f	= 0.71
n	= .23
K	= 1185 MPa

Table 3 Smooth Specimen Uniaxial Fatigue Constants

Test Series	σ_f' (MPa)	b	ε_f'	c	E(MPa)
2.5 mm ϕ Longitudinal	953.0	-0.106	0.213	-0.470	205000
2.5 mm ϕ Tangential	809.2	-0.100	0.173	-0.468	205000
5.0 mm ϕ Ford	1049.0	-0.105	0.229	-0.454	202000
6.0 mm ϕ Deere	948.2	-0.092	0.239	-0.435	202375

Table 4 Thin-Wall Tube Test Results*

ID	λ	$\frac{\Delta\varepsilon}{2}$	$\frac{\Delta\sigma}{2}$(MPa)	$\frac{\Delta\gamma}{2}$	$\frac{\Delta\tau}{2}$ (MPa)	N_f
4527	0.0	10000	450.0	0	0.0	1137
4553	0.0	10000	450.0	0	0.0	1107
4545	0.0	4300	352.0	0	0.0	7839
4511	0.0	2200	273.0	0	0.0	142541
4552	0.0	2200	273.0	0	0.0	78271
4529	0.0	2200	273.0	0	0.0	94525

ID	λ	$\frac{\Delta\varepsilon}{2}$	$\frac{\Delta\sigma}{2}$(MPa)	$\frac{\Delta\gamma}{2}$	$\frac{\Delta\tau}{2}$ (MPa)	N_f
4524	0.5	9600	427.0	4800	79.0	1258
4523	0.5	4130	338.0	2060	55.0	11777
4516	0.5	2100	266.0	1060	52.0	115462
4528	0.5	2100	266.0	1060	52.0	80000
4519	0.5	1440	224.0	720	43.0	611780

ID	λ	$\frac{\Delta\varepsilon}{2}$	$\frac{\Delta\sigma}{2}$(MPa)	$\frac{\Delta\gamma}{2}$	$\frac{\Delta\tau}{2}$(MPa)	N_f
4525	1.0	8660	381.0	8660	131.0	1616
4533	1.0	8660	381.0	8660	131.0	1229
4515	1.0	3720	305.0	3720	107.0	11611
4520	1.0	3720	305.0	3720	107.0	10377
4514	1.0	1900	238.0	1900	88.0	123544
4550	1.0	1900	238.0	1900	88.0	90000
4517	1.0	1300	212.0	1300	80.0	595613
4554	1.0	1300	212.0	1300	80.0	393633

Table 4 (Cont'd)

ID	λ	$\frac{\Delta\varepsilon}{2}$	$\frac{\Delta\sigma}{2}$(MPa)	$\frac{\Delta\gamma}{2}$	$\frac{\Delta\tau}{2}$(MPa)	N_f
4526	2.0	6550	288.0	13100	195.0	1758
4501	2.0	2600	234.0	5200	153.0	20031
4503	2.0	2600	234.0	5200	153.0	16887
4522	2.0	1440	179.0	2880	126.0	98778
4548	2.0	1440	179.0	2880	126.0	87500
4521	2.0	980	147.0	1960	111.0	545840

ID	λ	$\frac{\Delta\varepsilon}{2}$	$\frac{\Delta\sigma}{2}$(MPa)	$\frac{\Delta\gamma}{2}$	$\frac{\Delta\tau}{2}$(MPa)	N_f
4549	INF	0	0.0	17300	251.0	890
4537	INF	0	0.0	17300	251.0	889
4506	INF	0	0.0	7200	197.0	8710
4512	INF	0	0.0	3809	168.0	102083
4551	INF	0	0.0	3809	168.0	57369
4531	INF	0	0.0	3809	168.0	93052
4518	INF	0	0.0	2600	147.0	1010210
4587**	INF	0	0.0	2250		3200000

* Strain values reported as microstrain.

**Torsional test with initial overload.

Table 5 Notched Shaft Test Results

Load Condition	Test* Lab	Symbol	Bending Moment(Nm)	Torsion Moment(Nm)	Life (Cycles) Initiation	Failure	Estimated
BR3	JD	B	2800	0	2571	8262	
BR3	AOS	B	2600	0	7930	13060	3918
BR3	IL	B	2600	0	3000	13761	
BR3	AOS	B	2586	0	14000	17450	5235
BR3	JD	B	2600	0	8111	18310	5676
BR2	RN	B	1730	0	30000	83600	
BR2	JD	B	1875	0	41361	106717	
BR2	BC	B	1875	0	55000	117678	43540
BR2	IL	B	1730	0	60000	184343	
BR2	AOS	B	1730	0	130000	228290	84467
BR2	AOS	B	1708	0	163770	249890	92459
BR2	IL	B	1730	0	49200	132292	
BR1	AOS	B	1475	0	230000	403770	201800
BR1	JD	B	1475	0	463976	709000	354500
BR1	AOS	B	1460	0	430000	764000	382000
BR1	IL	B	1400	0	4493950	**	
TR3	JD	T	0	3000	4057	9528	
TR3	IL	T	0	3000	14720	14720	6329
TR3	BC	T	80	2534	33328	33328	14331
TR2	BC	T	0	2400	65000	101050	46483
TR2	IL	T	0	2400	75700	164070	
TR1	RN	T	0	2000	750000	1293400	505107
TR1	IL	T	0	2000	1584000	2238000	874000
TR1	GKN	T	0	2000	700000	2000000	
TR	JD	T	0	1500	1514960	**	
TR	JD	T	0	1700	2324070	**	2324070

Table 5 (Cont'd)

Condition	Test* Lab	Symbol	Bending Moment(Nm)	Torsion Moment(Nm)	Life (Cycles) Initiation	Failure	Estimated
XR3	IL	X	1850	2550	5113	5113	2045
XRNS3	IL	X	1355	2550	5500	11626	
XR2	RN	X	1220	1700	60800	124500	
XR2	JD	X	1220	1710	107460	158094	71142
XR2	IL	X	1220	1710	72000	163655	
XR1	RN	X	990	1390	350000	586960	
XR1	IL	X	990	1390	933000	1193970	716382
XRNS1	IL	Q	725	1390	2000000	**	
YR3	IL	Y	2325	1350	2810	11376	
YR3	IL	Y	2325	1350	3000	12089	
YR3	IL	Y	1720	1350	17065	51775	
YR3	IL	Y	1720	1350	21450	65799	
YR2	IL	Y	1550	1090	80000	159907	68760
YR2	IL	Y	1550	1090	97500	220460	
YRNS2	IL	R	1150	1090	2293930	**	
YRNS2	IL	R	1150	1090	2380730	**	
YR1	IL	Y	1250	880	600000	722480	325116
YR1	RN	Y	1250	880	325000	747000	
YRNS1	IL	R	920	880	3472900	**	

Table 5 (Cont'd)

Condition	Test* Lab	Symbol	Bending Moment(Nm)	Torsion Moment(Nm)	Life (Cycles) Initiation	Failure	Estimated
ZR3	JD	Z	1250	2700	6402	10418	4479
ZR3	IL	Z	1150	2700	3000	12701	
ZR3	IL	Z	851	2700	9000	17730	7092
ZR3	IL	Z	851	2700	10000	24538	
ZR2	IL	Z	780	2180	70000	142708	
ZR2	IL	Z	780	2180	70681	169509	
ZR2	IL	Z	570	2180	76100	177754	
ZR2	IL	Z	570	2180	99560	186715	80287
ZR	JD	Z	845	1800	259857	396798	200000
ZRNS1	IL	S	460	1760	3026740	**	
ZRNS1	IL	S	460	1760	2350000	**	

* IL - University of Illinois
JD - Deere and Company
RN - Rexnord Corporation
AOS - A. O. Smith Corporation
BC - Battel Columbus
GKN - Guest, Keen, and Nettelfolds

** Did not fail.

Table 6 Notched Shaft Finite Element Strain Analysis (Node 801)*

Test Condition	M_b(Nm)	M_t(Nm)	ε_{11}	ε_{22}	ε_{33}	γ_{12}	γ_{13}	γ_{23}
BENDING								
Elastic	1400	--	-219	- 611	1675	0	0	571
Elastic/Plastic	1475	--	-239	- 644	1765	0	0	602
	1730	--	-366	-1218	2504	0	0	912
	2000	--	-438	-1588	3074	0	0	1126
	2200	--	-524	-1903	3570	0	0	1306
	2300	--	-579	-2115	3868	0	0	1402
	2400	--	-640	-2362	4227	0	0	1533
	2600	--	-758	-2802	4876	0	0	1748
TORSION								
Elastic	--	2000	0	0	0	-359	-2770	0
Elastic/Plastic	--	2000	0	0	0	-359	-2770	0
	--	2400	0	0	0	-739	-4821	0
	--	2600	0	0	0	-757	-5118	0
	--	2800	0	0	0	-813	-5625	0
	--	3000	0	0	0	-892	-6284	0
XR COMBINED								
Elastic	990	1390	-153	- 433	1182	-249	-1925	400
Elastic/Plastic	990	1390	-153	- 433	1182	-249	-1925	400
	1220	1710	-279	- 908	1831	-420	-3020	651
	1850	2550	-859	-2589	4421	-995	-7442	1553

Table 6 (Cont'd)

	M_b(Nm)	M_t(Nm)	ε_{11}	ε_{22}	ε_{33}	γ_{12}	γ_{13}	γ_{23}
YR COMBINED								
Elastic	1250	880	-194	- 546	1494	-158	-1219	508
Elastic/Plastic	1250	880	-194	- 546	1494	-158	-1219	508
	1550	1090	-264	- 792	1952	-205	-1591	683
	12325	1350	-679	-2333	4231	-366	-2950	1513
ZR COMBINED								
Elastic	625	1760	- 96	- 274	745	-316	-2437	251
Elastic/Plastic	625	1760	- 96	- 274	745	-316	-2437	251
	770	2180	-132	- 416	993	-437	-3293	342
	1150	2700	-418	-1221	2225	-922	-6580	817
XRNS COMBINED								
Elastic	725	1390	-112	- 317	865	-249	-1925	292
Elastic/Plastic	725	1390	-112	- 317	865	-249	-1925	292
	895	1720	-149	- 443	1114	-320	-2489	380
	1155	2550	-464	-1410	2607	-832	-6147	941
YRNS COMBINED								
Elastic	916	880	-142	- 400	1094	-158	-1219	371
Elastic/Plastic	916	880	-142	- 400	1094	-158	-1219	371
	1135	1090	-180	- 510	1368	-192	-1522	462
	1700	1350	-393	-1338	2618	-318	-2460	941
ZRNS COMBINED								
Elastic	460	1760	- 7	- 201	545	-316	-2437	183
Elastic/Plastic	460	1760	- 7	- 201	545	-316	-2437	183
	568	2180	- 10	- 302	727	-434	-3270	247
	840	2700	-157	-489	1129	-582	-4399	389

* Strain values reported as microstrain.

Table 7 Crack Sizes and Life at the Transition from Stage I Crack Development

$\bar{\varepsilon}$	λ	ID	a_s (μm)	N_s	N_f
0.22	0.0	4511	40	38000	142541
0.22	0.0	4529	25	30000	94525
0.22	0.5	4516	44	20000	115462
0.22	0.5	4528	70	40000	80000
0.22	1.0	4514	84	60000	123544
0.22	1.0	4550	40	30000	90000
0.15	0.5	4519	25	<100000	611780
0.15	1.0	4517	32	200000	595613
	1.0	4554	30	5000	393633
0.43	0.0	4545	40	7000	7839
0.43	0.5	4523	64	11000	11777
0.43	1.0	4515	64	11000	11611
1.0	0.0	4527	64	1100	1137
1.0	0.0	4553	64	1100	1107
1.0	0.5	4524	50	1200	1258
1.0	1.0	4533	40	1200	1229
1.0	1.0	4525	50	1600	1616
1.0	2.0	4526	32	1700	1758

Table 8 Unnotched Shaft Finite Element Strain Analysis (Node 801)*

Test Condition	M_b(Nm)	M_t(Nm)	ε_{11}	ε_{22}	ε_{33}	γ_{12}	γ_{13}	γ_{23}
BENDING								
Elastic	1950	----	- 600	- 850	2090	0	0	-460
Elastic/Plastic	1950	----	- 600	- 850	2090	0	0	-460
	2200	----	- 680	-1060	2510	0	0	-500
	2600	----	-1025	-1725	4075	0	0	-730
TORSION								
Elastic/Plastic	----	2550	0	0	0	-140	-3750	0
	----	3000	0	0	0	-280	-5300	0
COMBINED								
Elastic/Plastic	1330	1800	- 470	- 690	1500	- 50	-2400	330
	1600	2176	- 750	-1150	2320	-145	-3700	480
	2000	2720	-1600	-2125	4630	-390	-7710	990

* Strain values reported as microstrain

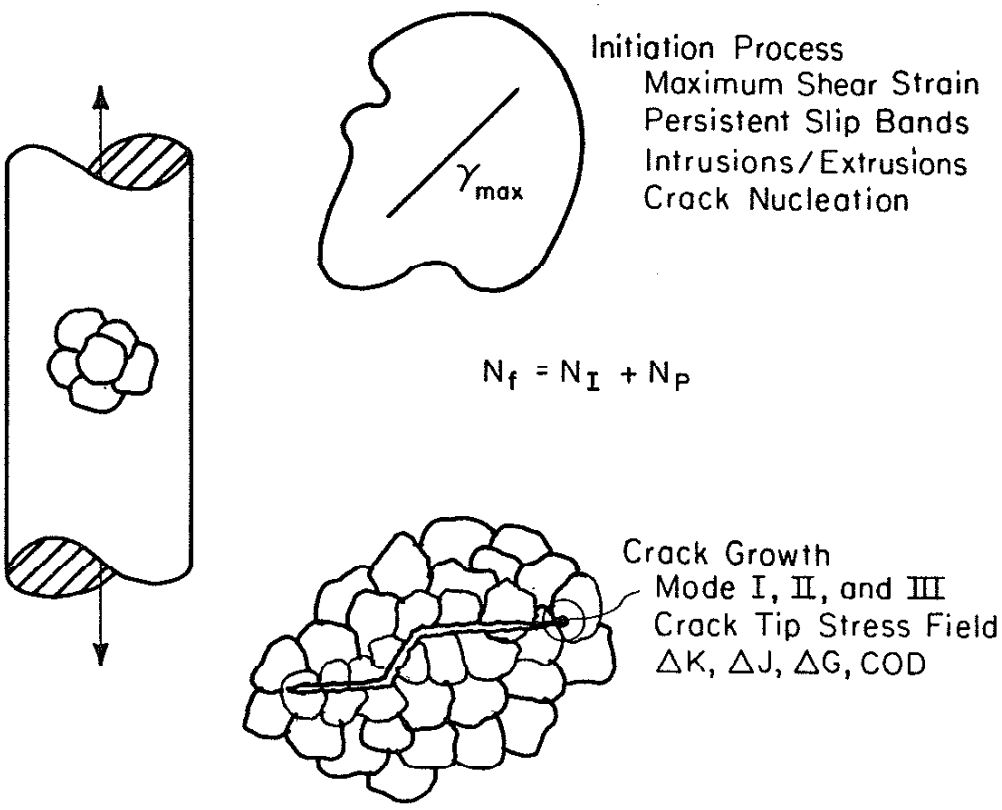

Figure 1 Stages of Crack Development, Initiation, Stage I, and Stage II Growth

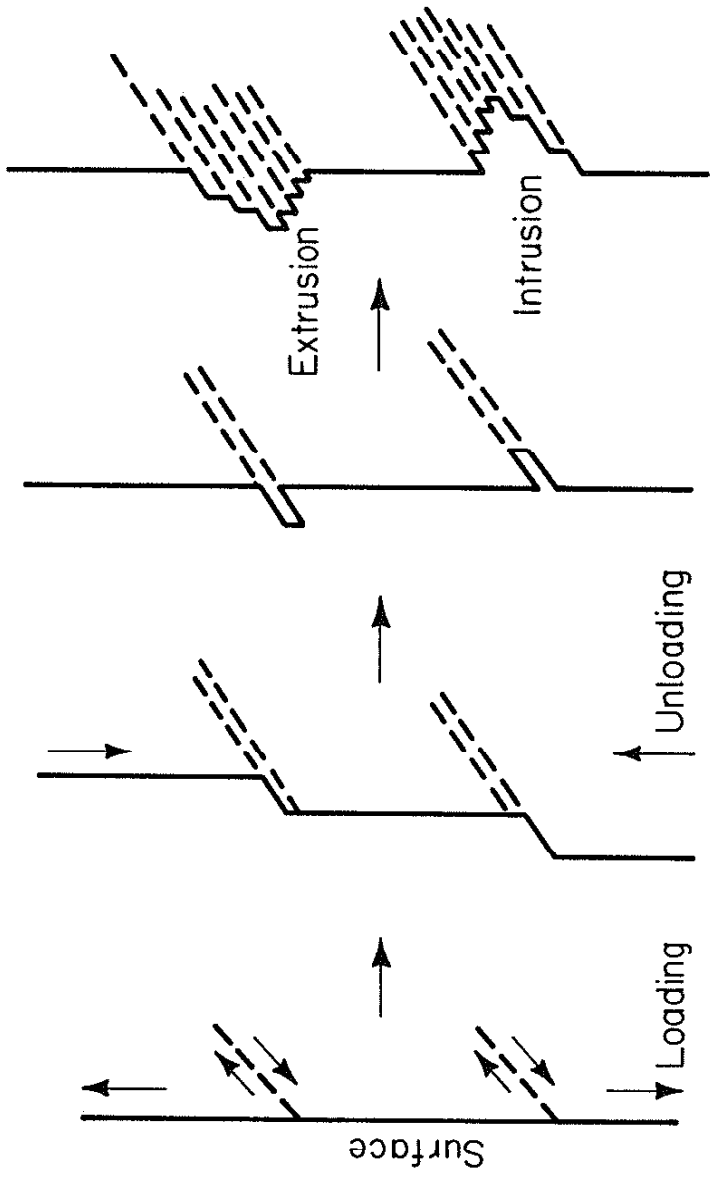

Figure 2 Crack Initiation Mechanism

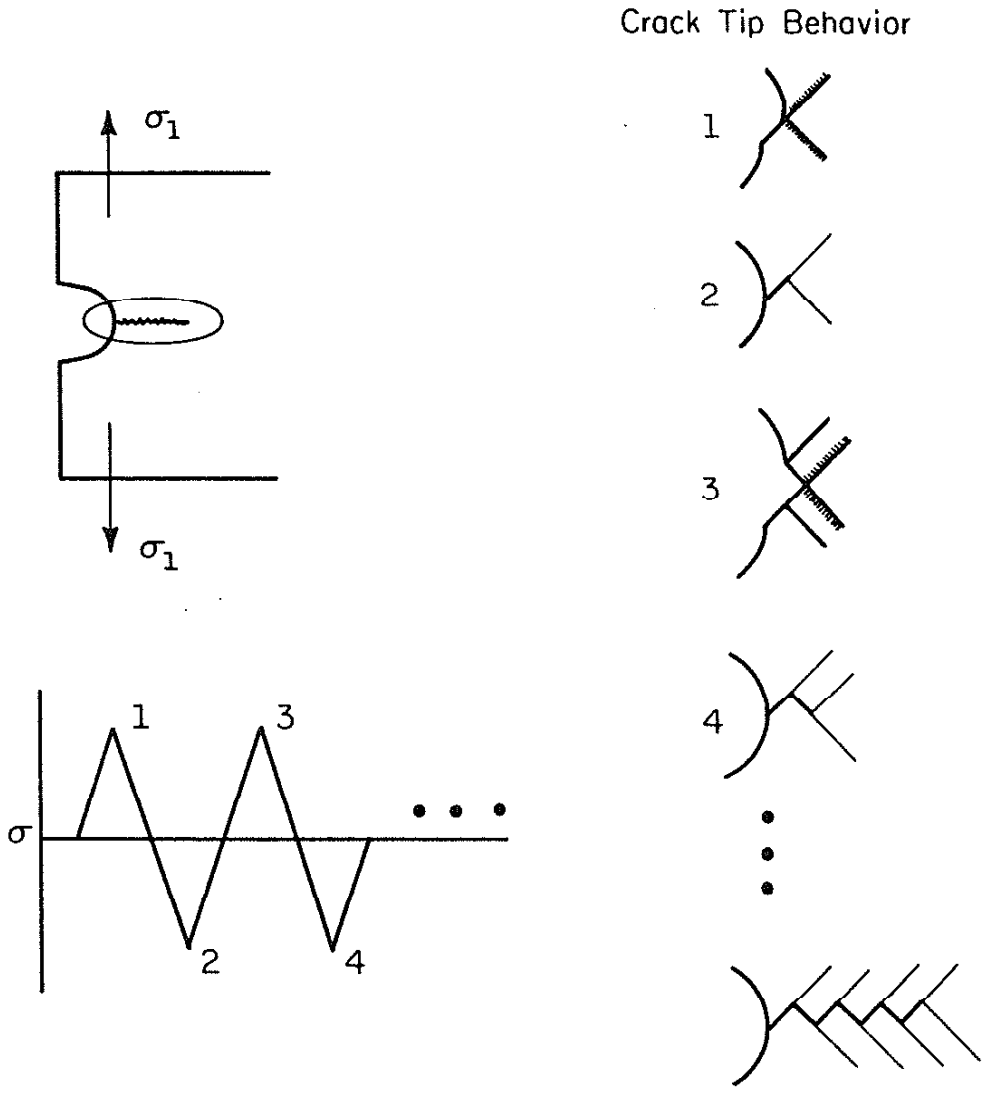

Figure 3 Coarse Slip Growth Model for Ductile Materials

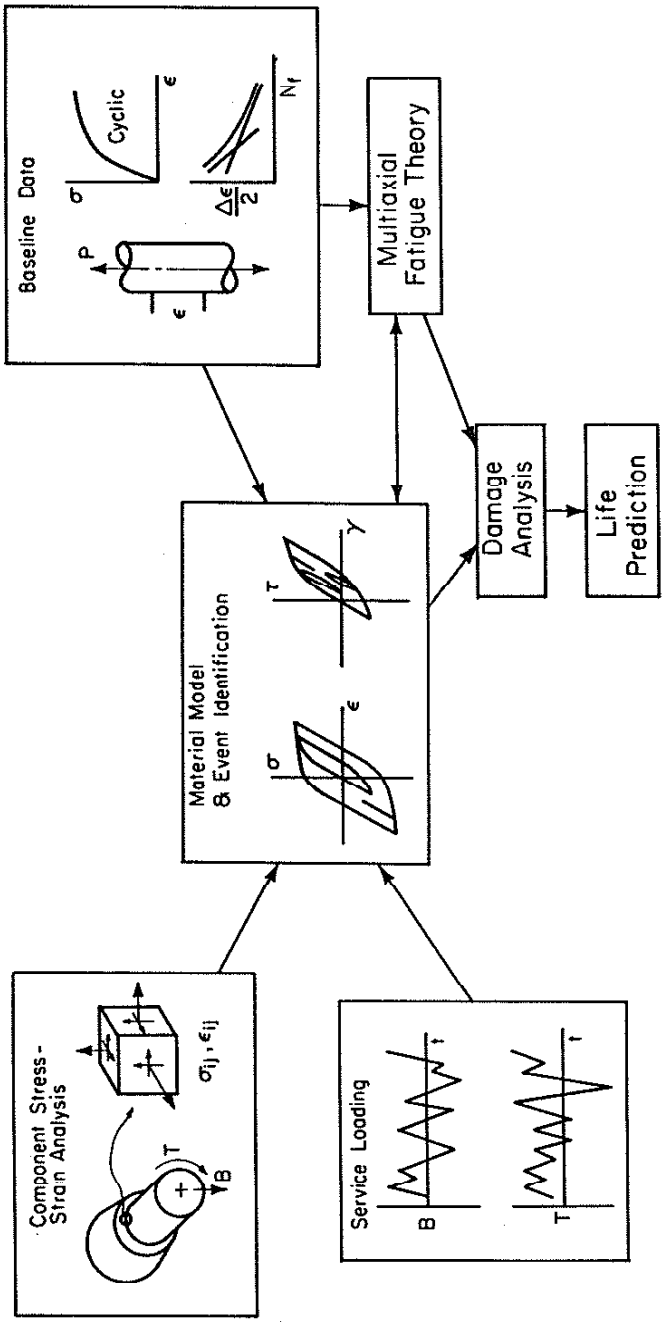

Figure 4 Schematic of Component Fatigue Analysis by the Local Stress-Strain Approach

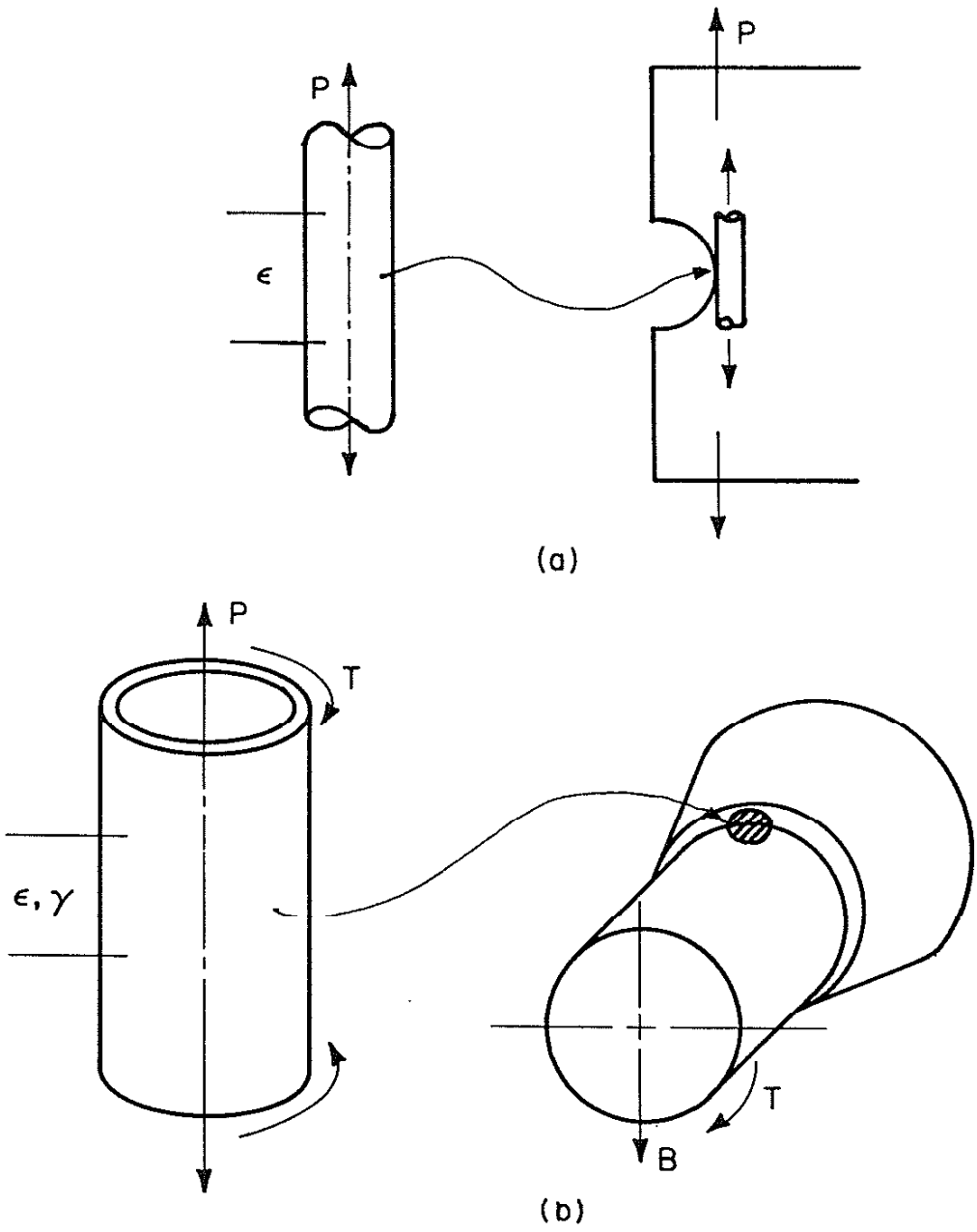

Figure 5 Similitude Assumptions for Smooth and Notched Specimens, (a) Uniaxial Loading, b) Multiaxial Loading

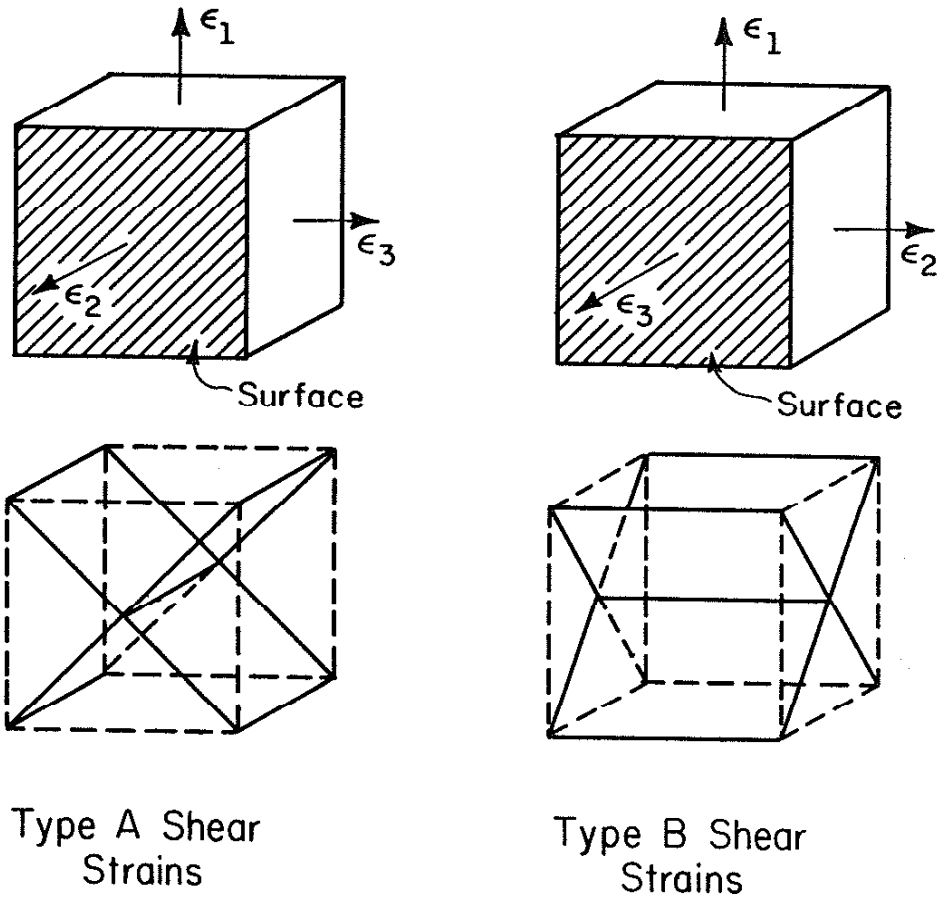

Figure 6 Type A and Type B Shear Strains

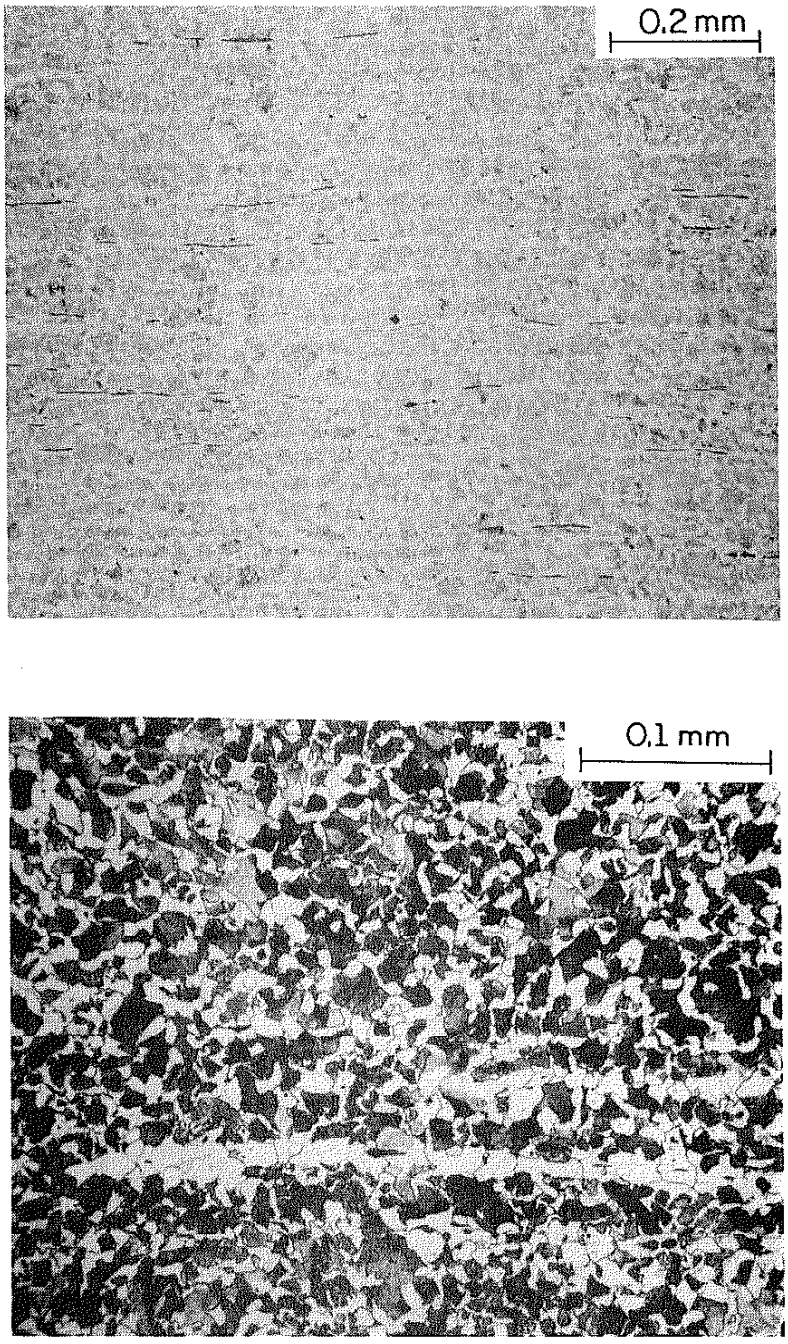

Figure 7 Etched Microstructure of SAE 1045 Steel

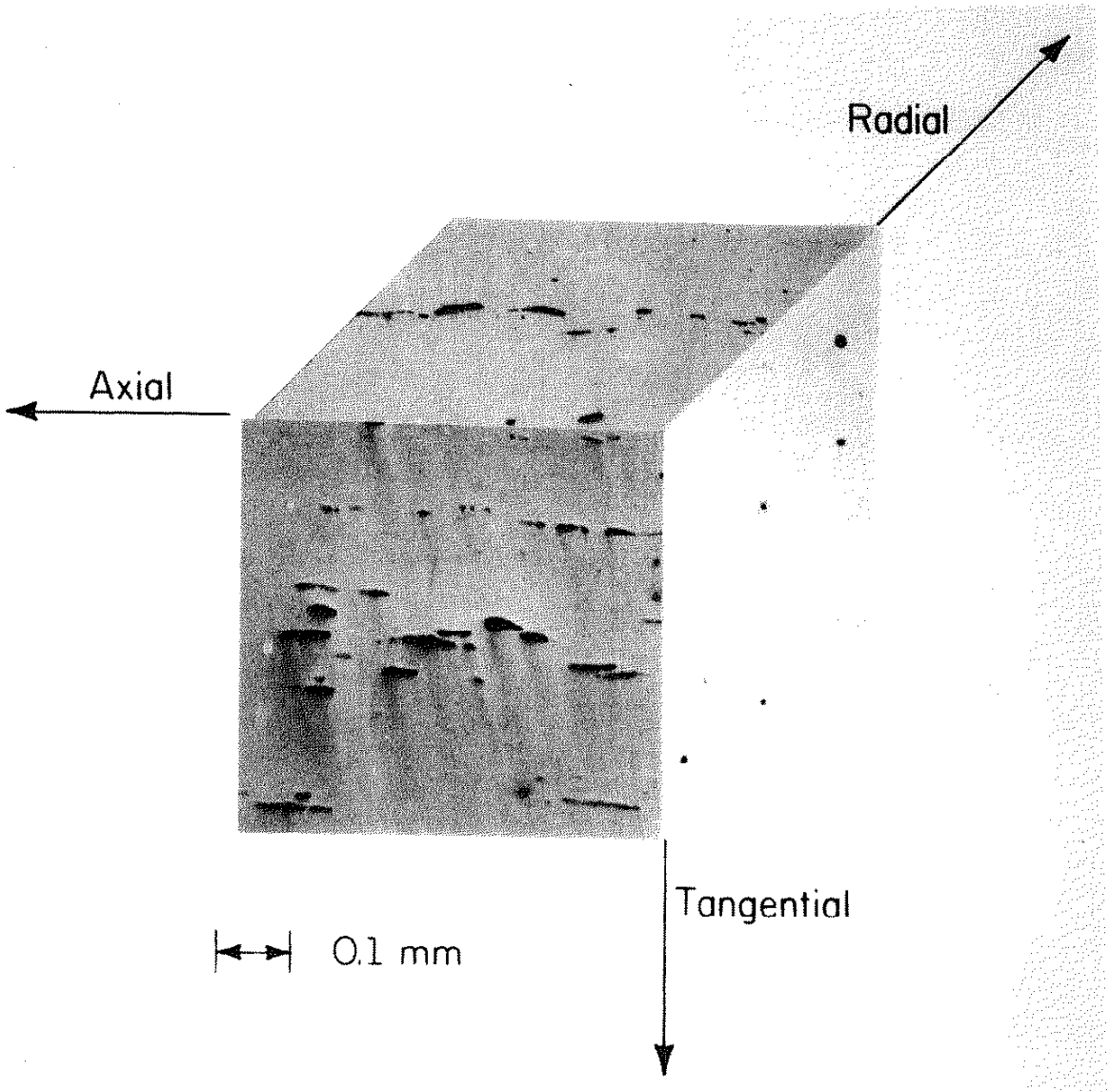

Figure 8 Unetched Microstructure Showing Magnesium Sulfide Inclusions in the Longitudinal Direction

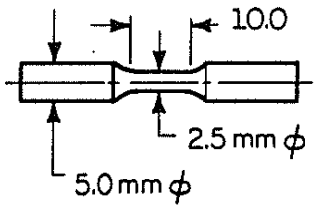

Specimen for Uniaxial Testing

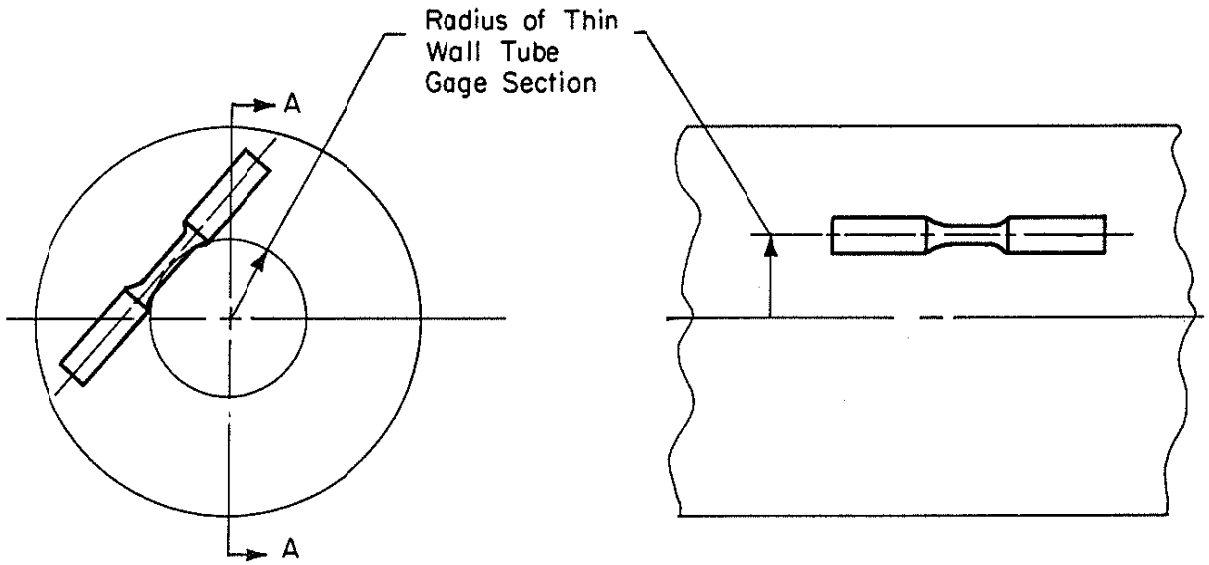

Tangential Specimen

Longitudinal Specimen

Figure 9 Position and Geometry of 2.5 mm Diameter Specimens Taken from Bar Stock

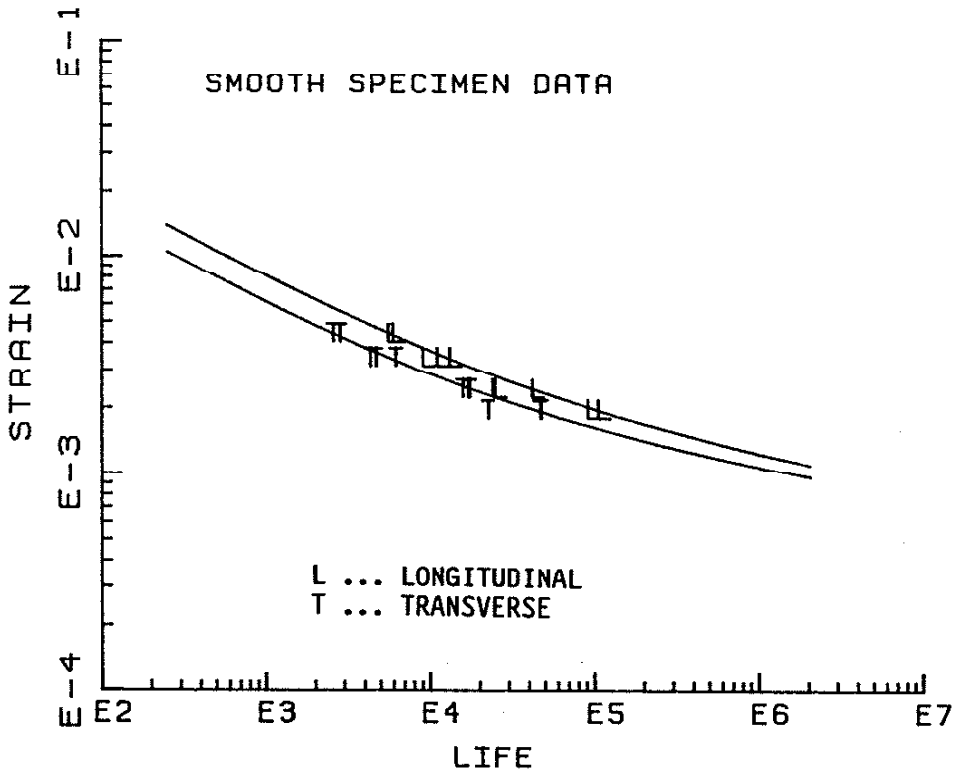

Figure 10 Baseline Fatigue Test Results from 2.5 mm Diameter Specimens

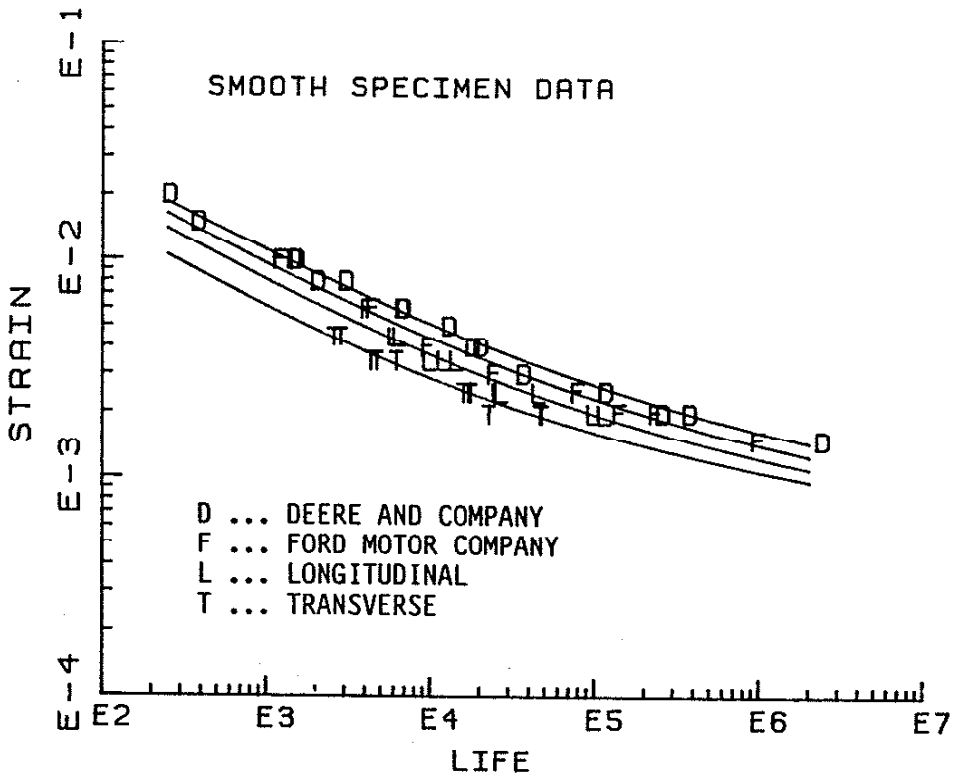

Figure 11 Baseline Data for Four Sets of Uniaxial Data Generated in the SAE Program

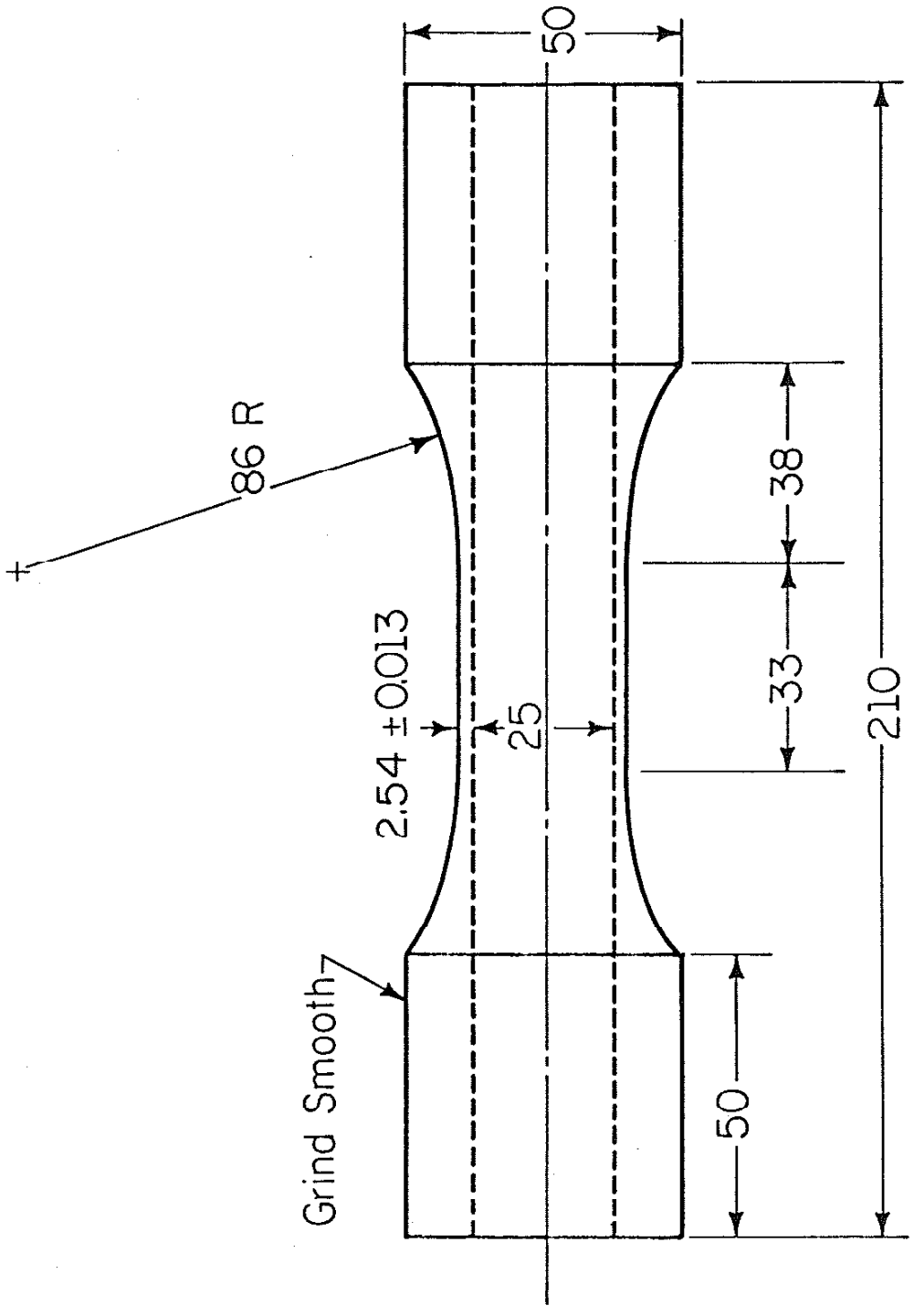

Figure 12 Thin-Wall Tube Test Specimen

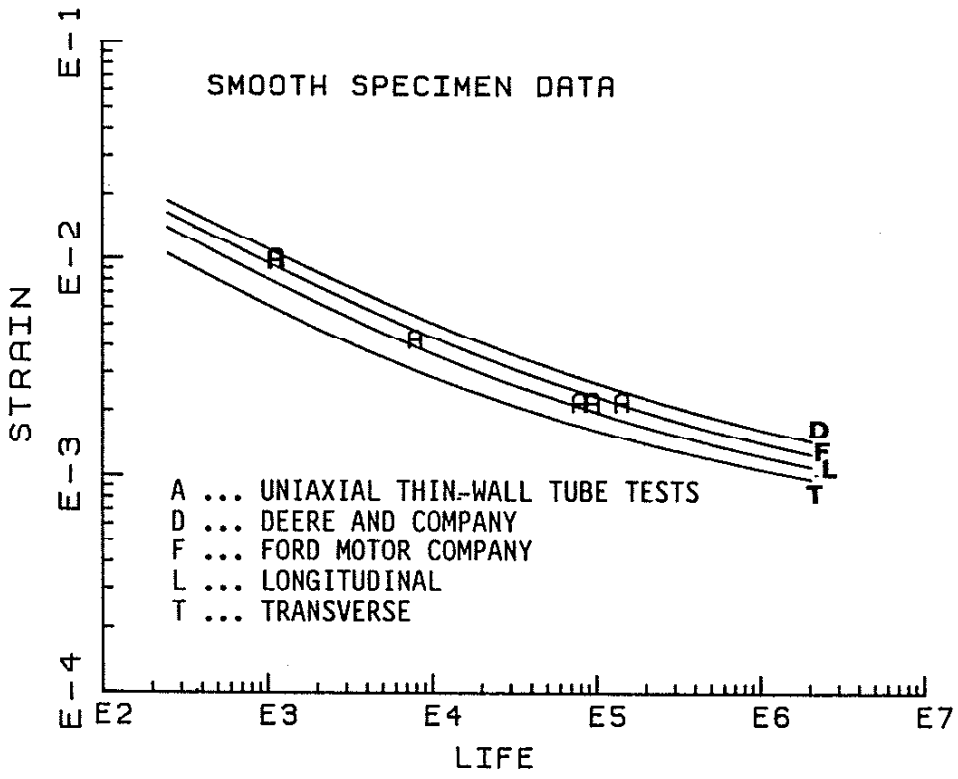

Figure 13 Comparison of Axially Loaded Thin-Wall Tube Tests with Smooth Specimen Uniaxial Data

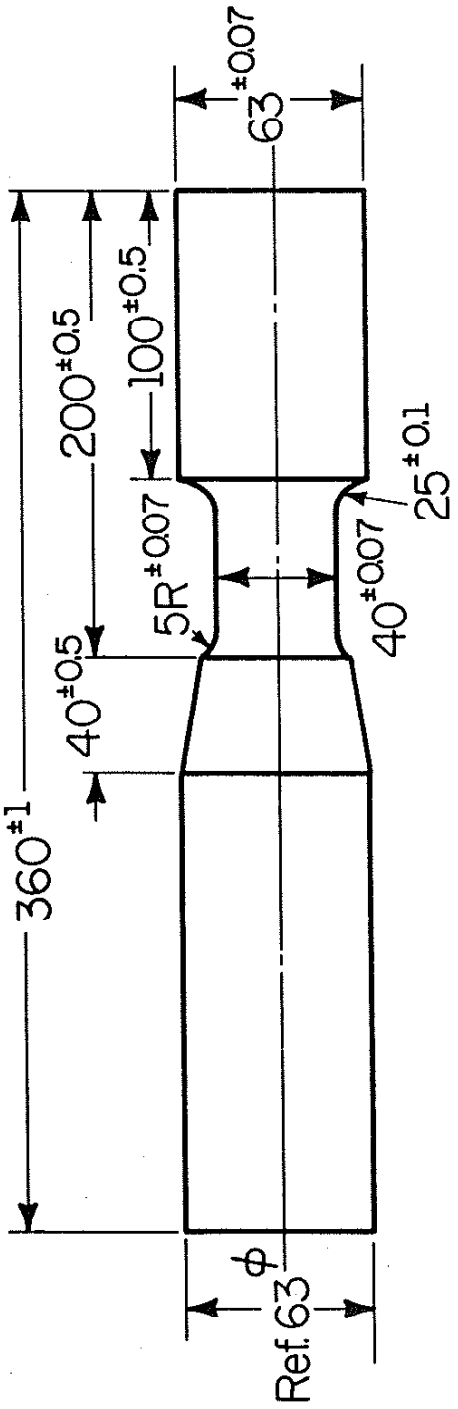

Figure 14 Notched Shaft Test Specimen

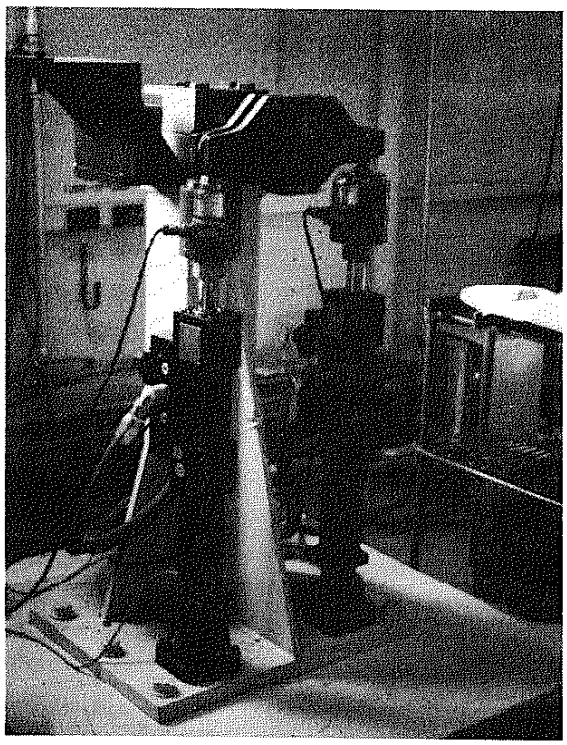

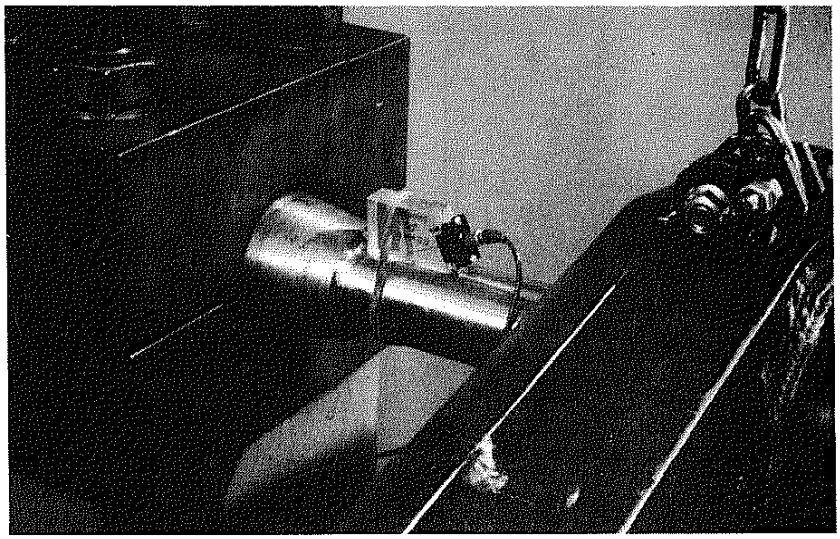

Figure 15 Test Frame for Notched Shaft Program

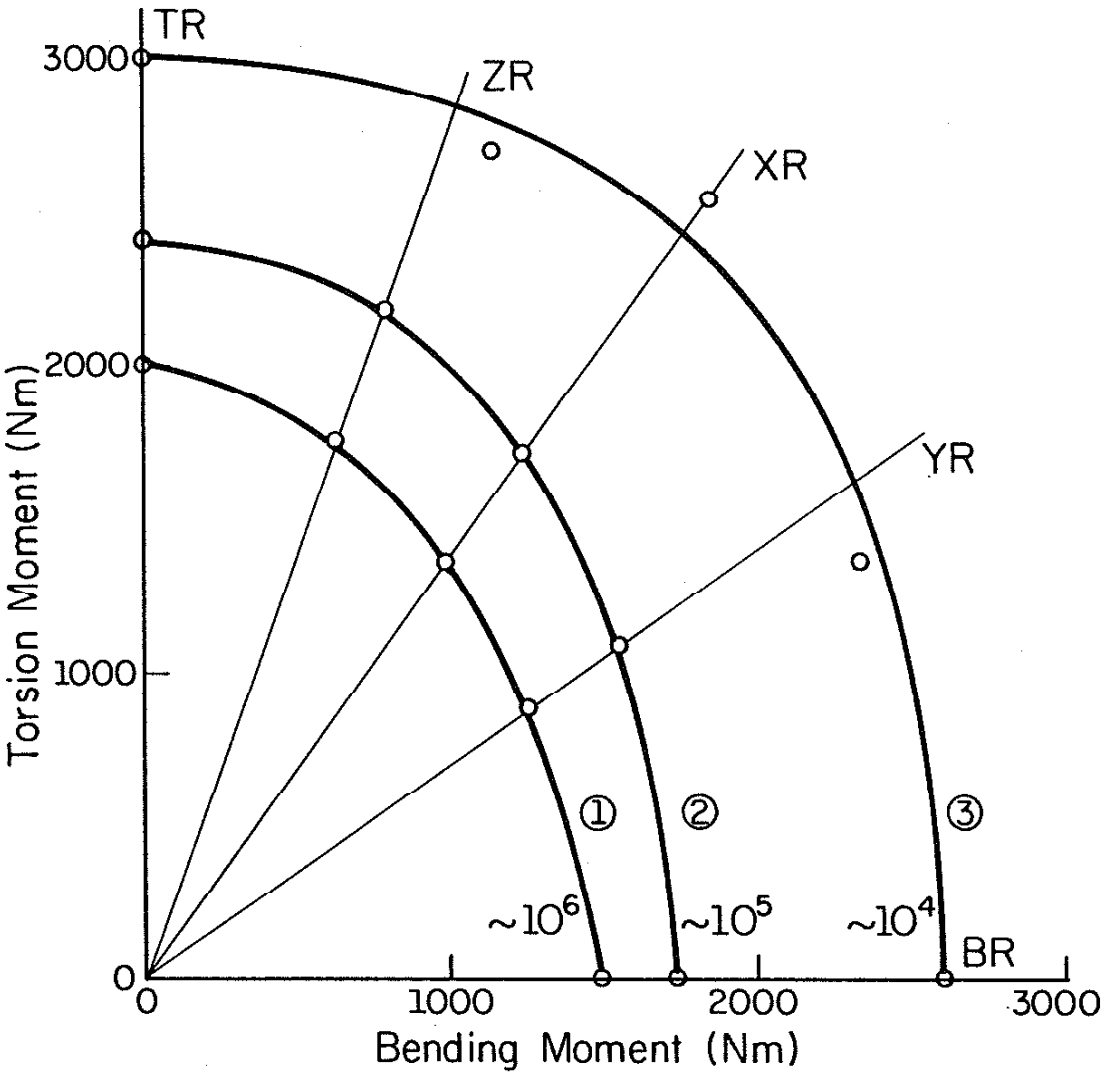

Figure 16 Test Matrix for Notched Shaft Experimental Program

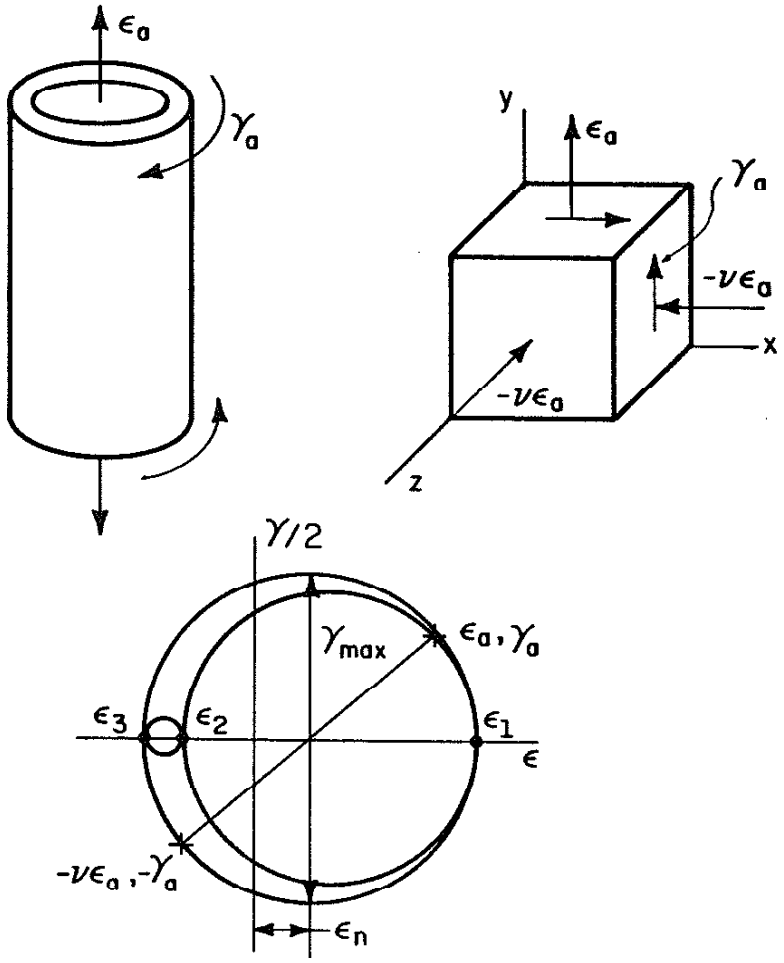

Figure 17 Strain Analysis for Thin-Wall Tube

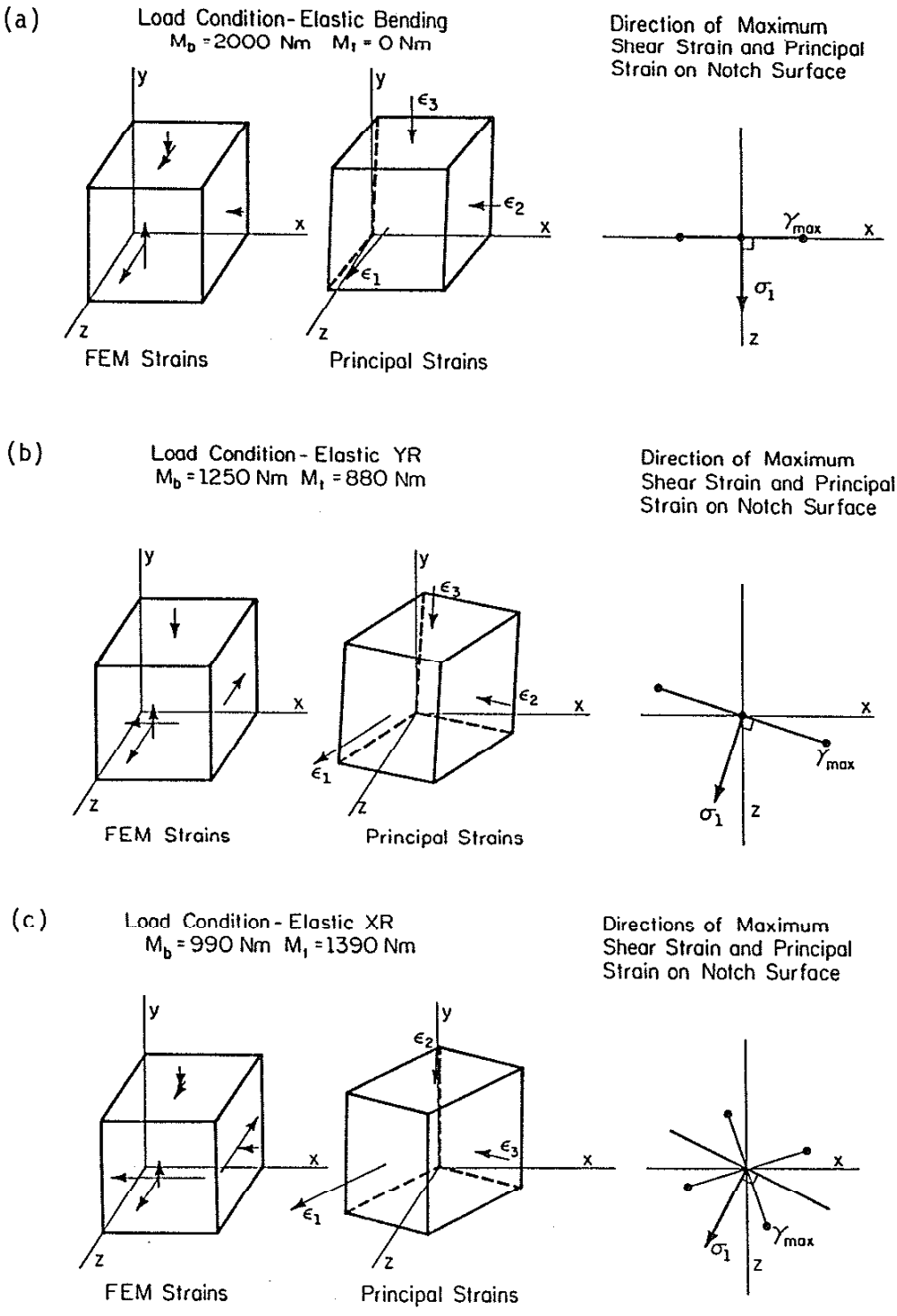

Figure 18 Strain State and Principal Directions for Notched Shaft (a) Bending, (b) YR, (c) XR, (d) ZR, (e) Torsion

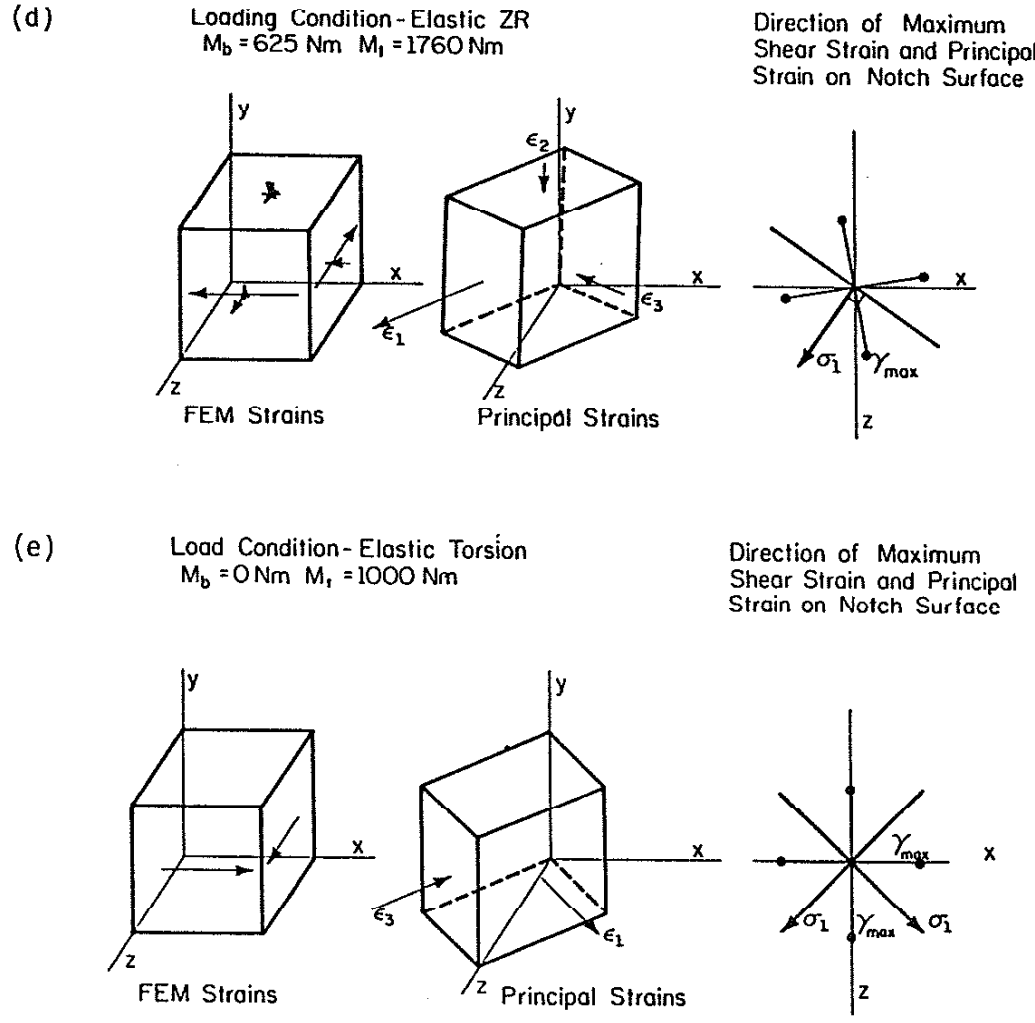

Figure 18 Strain State and Principal Directions for Notched Shaft (a) Bending, (b) YR, (c) XR, (d) ZR, (e) Torsion

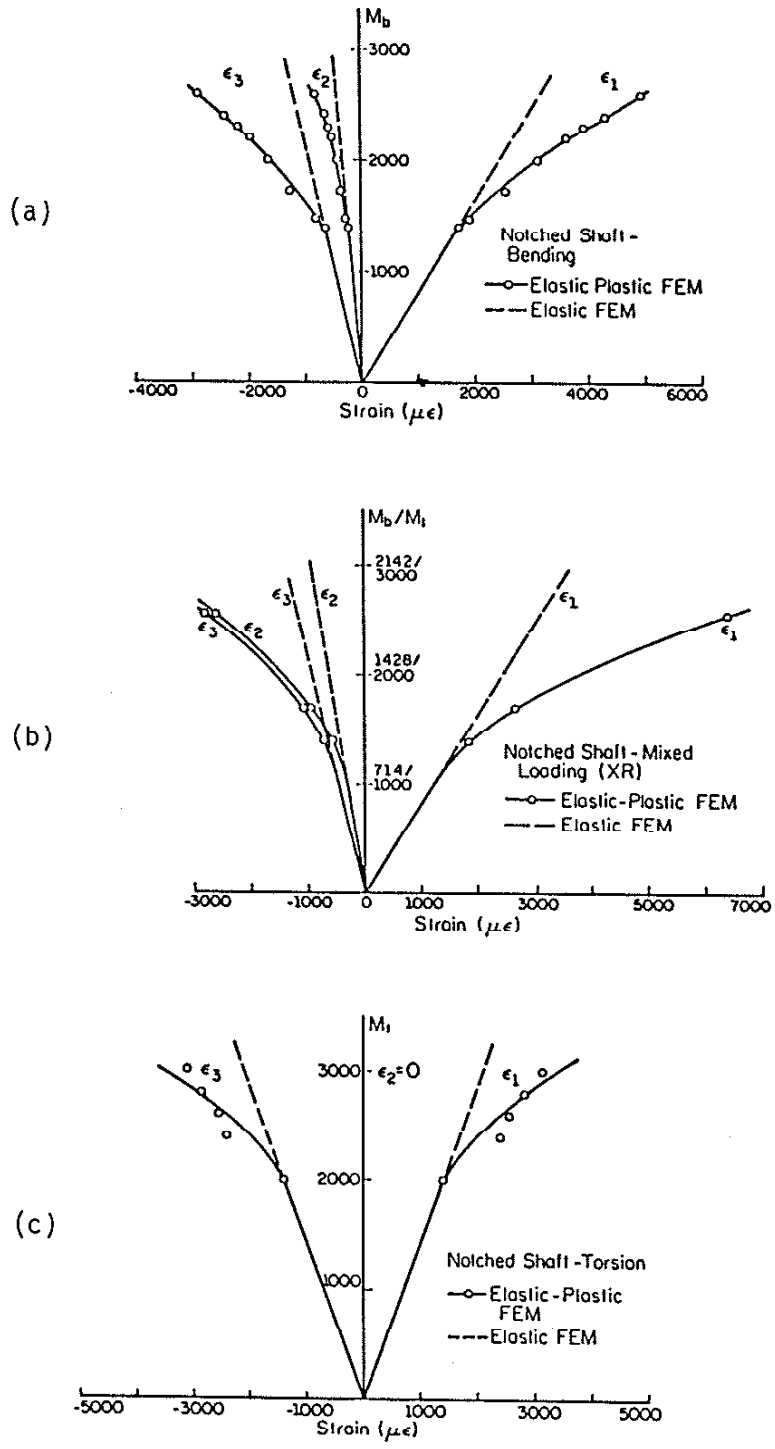

Figure 19 Elastic-Plastic Principal Strains versus Applied Moments for the Notched Shaft
(a) Bending, (b) XR, (c) Torsion

(a)

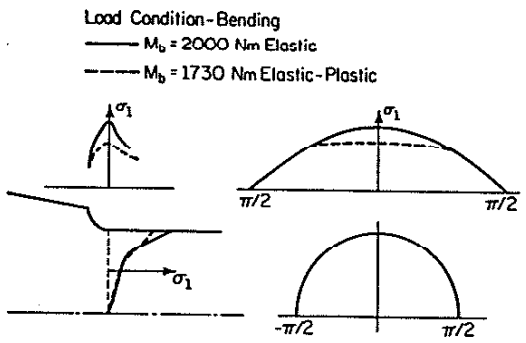

(b)

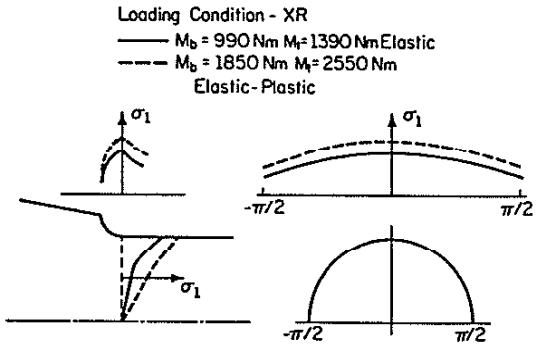

(c)

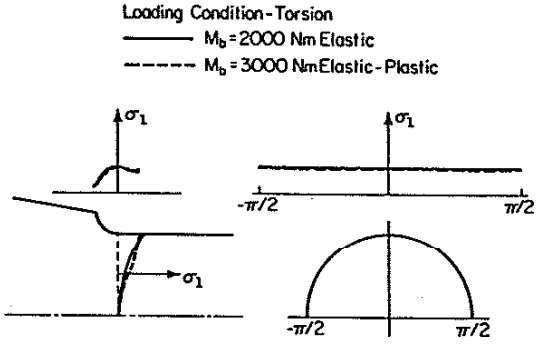

Figure 20 Principal Stress Gradients in the Notched Shaft (a) Bending, (b) XR, (c) Torsion

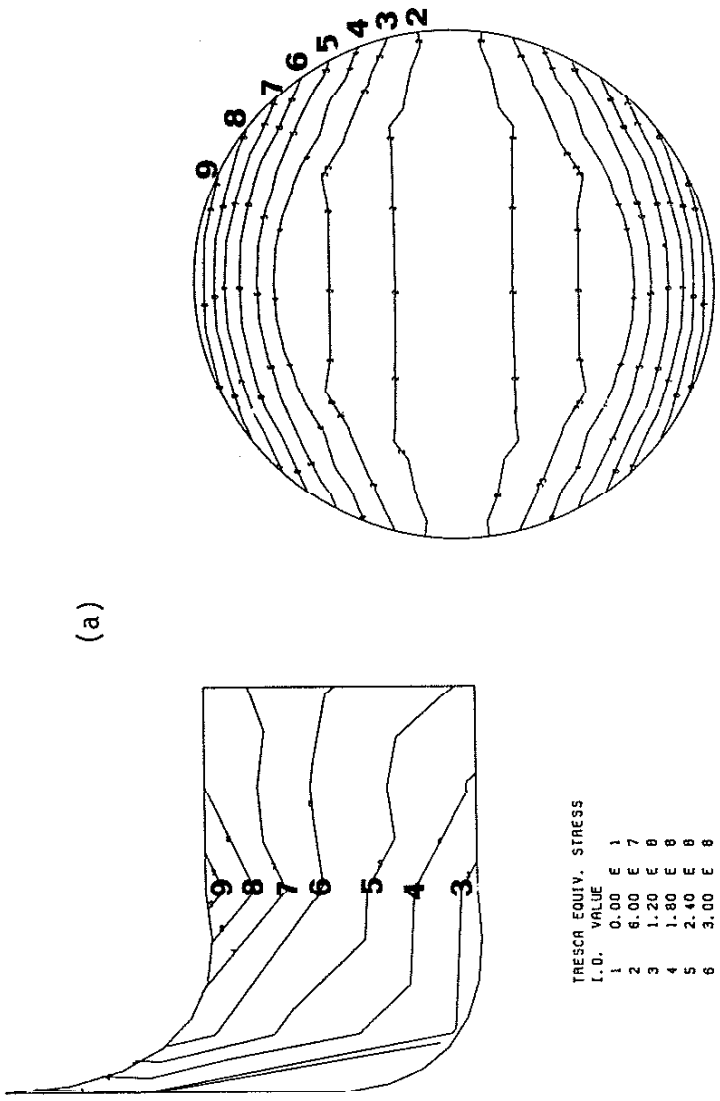

Figure 21 Contour Plot of Notch Gradients from Finite Element Analysis (a) Bending, (b) XR, (c) Torsion

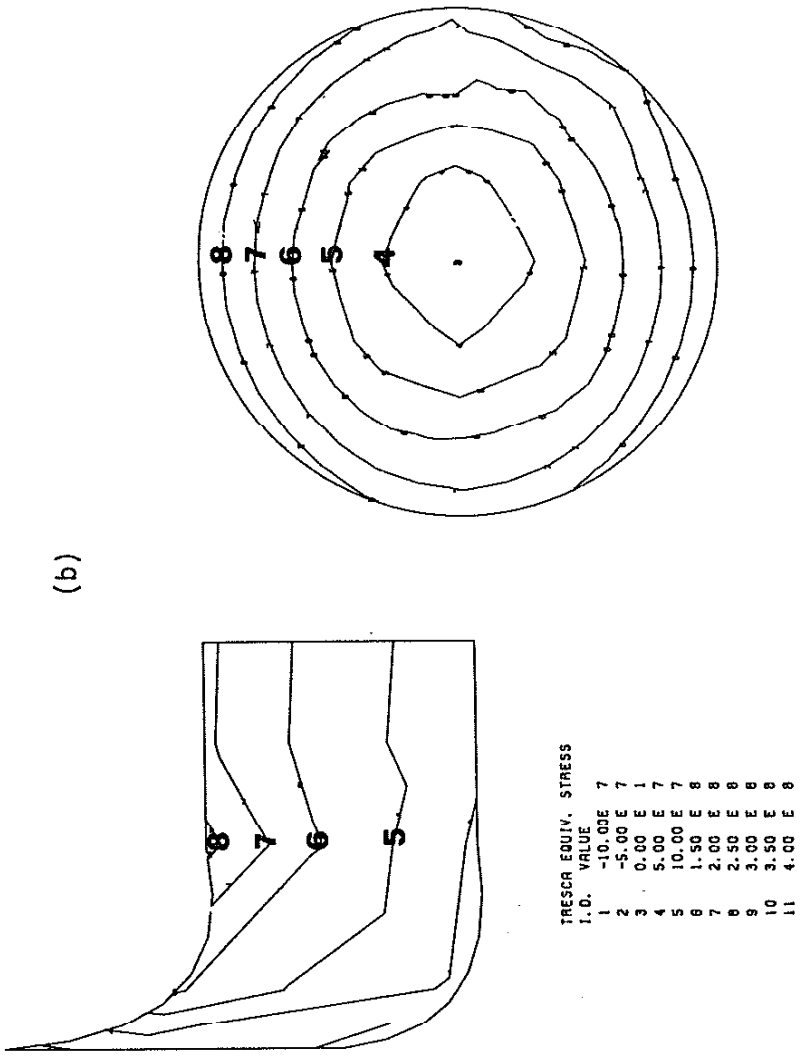

Figure 21 Contour Plot of Notch Gradients from Finite Element Analysis (a) Bending, (b) XR, (c) Torsion

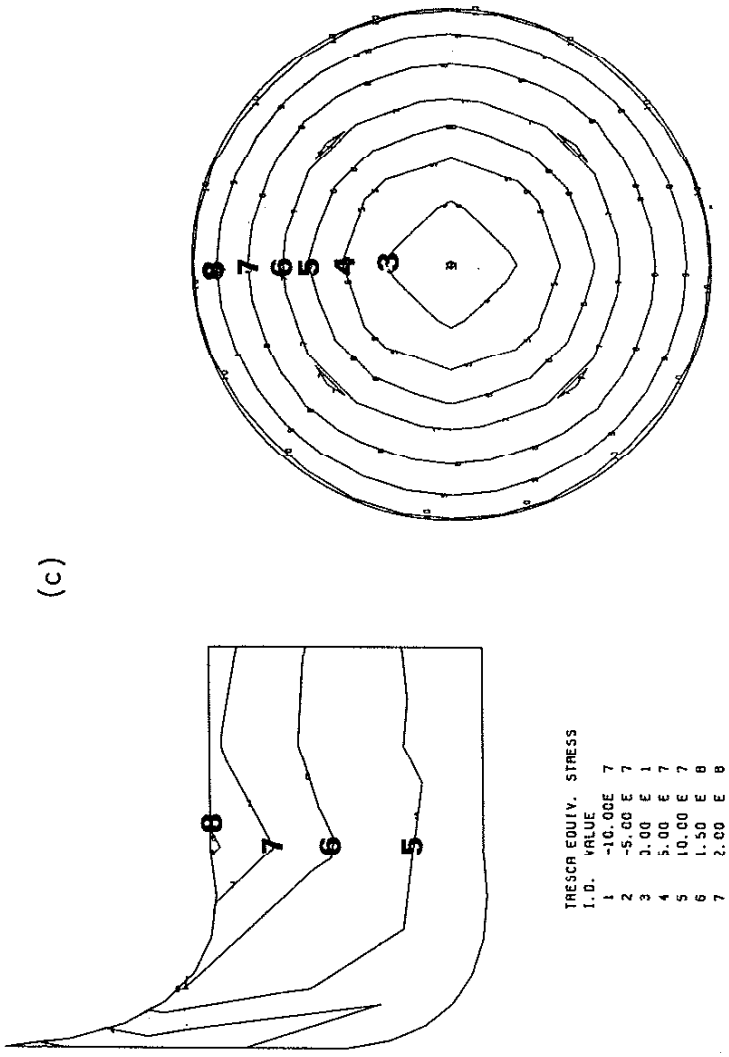

Figure 21 Contour Plot of Notch Gradients from Finite Element Analysis (a) Bending, (b) XR, (c) Torsion

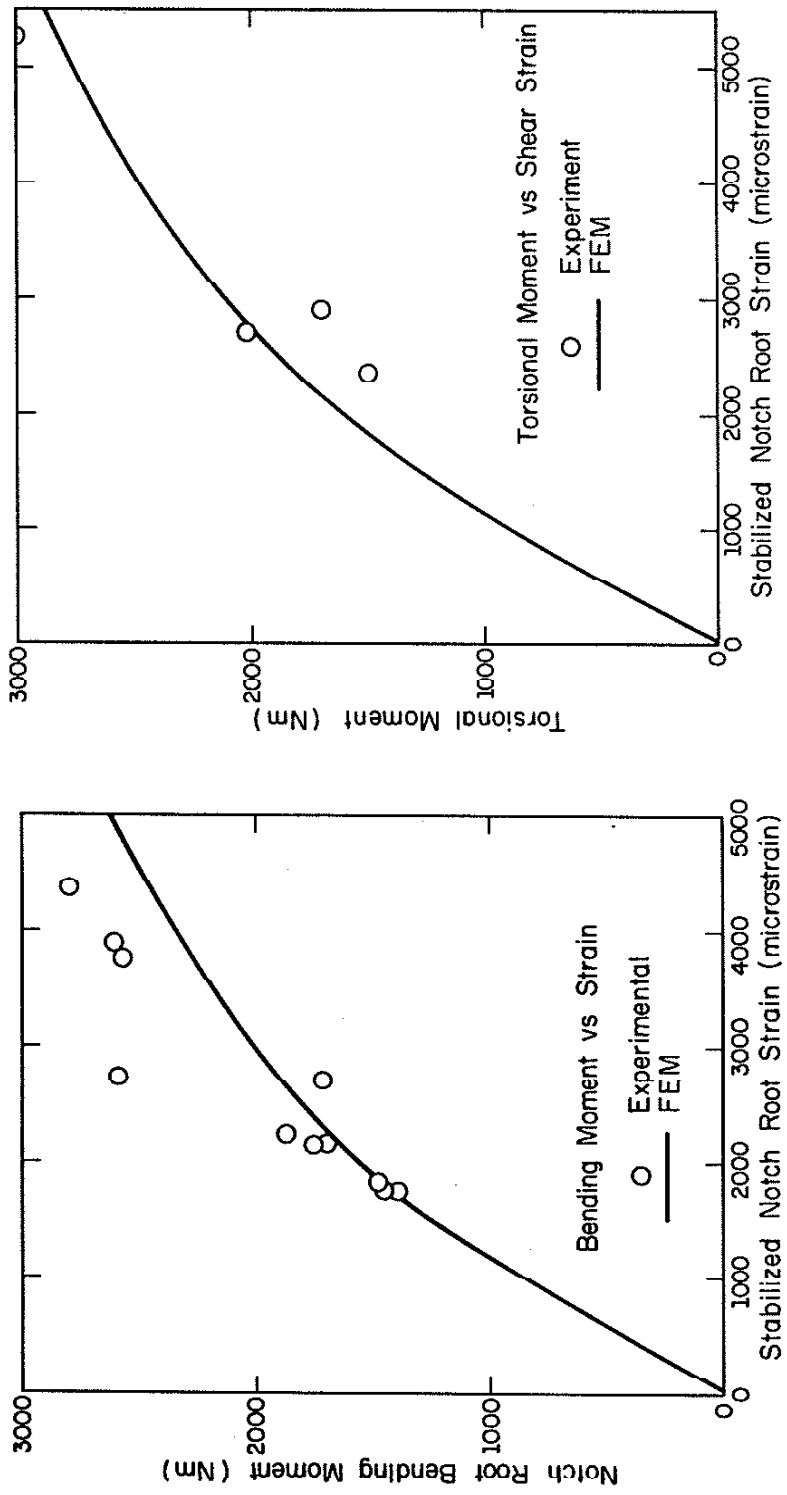

Figure 22 Comparison of Finite Element Analysis and Strain Gage Measurements (a) Results for Bending, (b) Results for Torsion

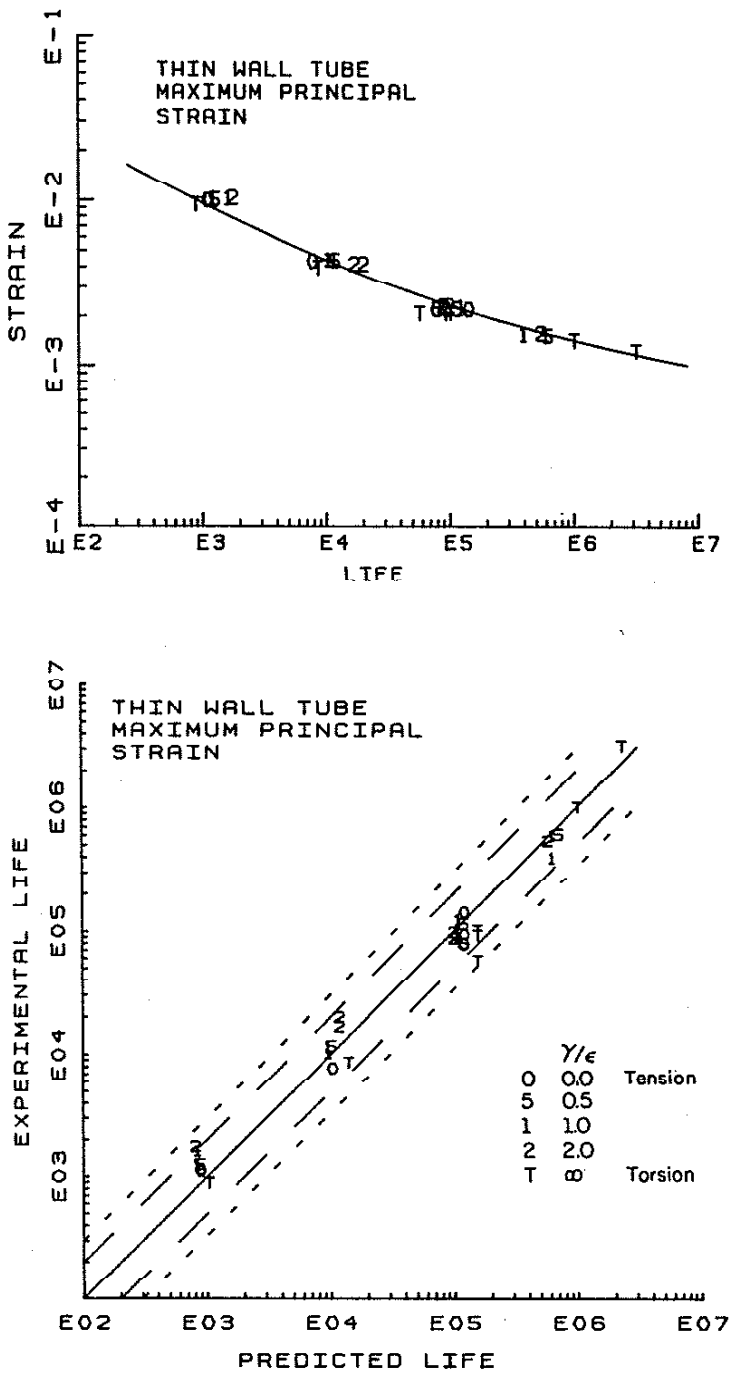

Figure 23a Thin-Wall Tube Life Predictions, Maximum Principal Strain Theory

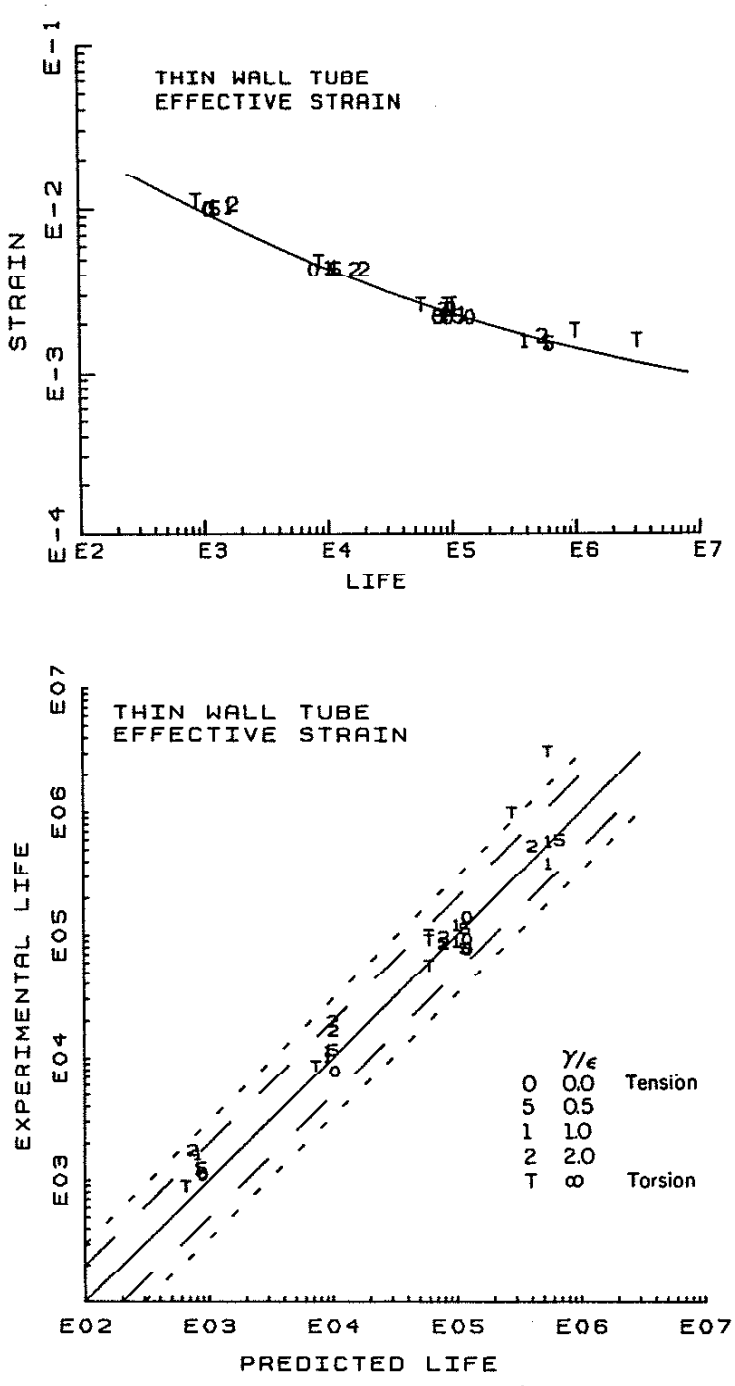

Figure 23b Thin-Wall Tube Life Predictions, Effective Strain Theory

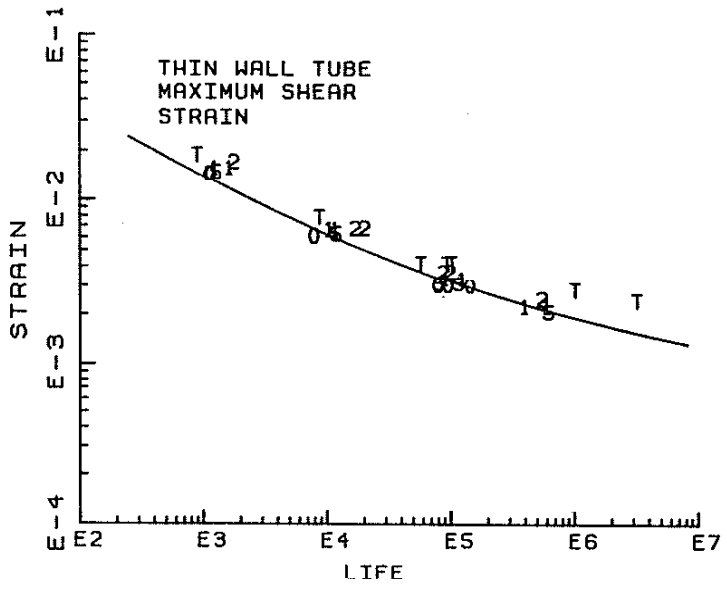

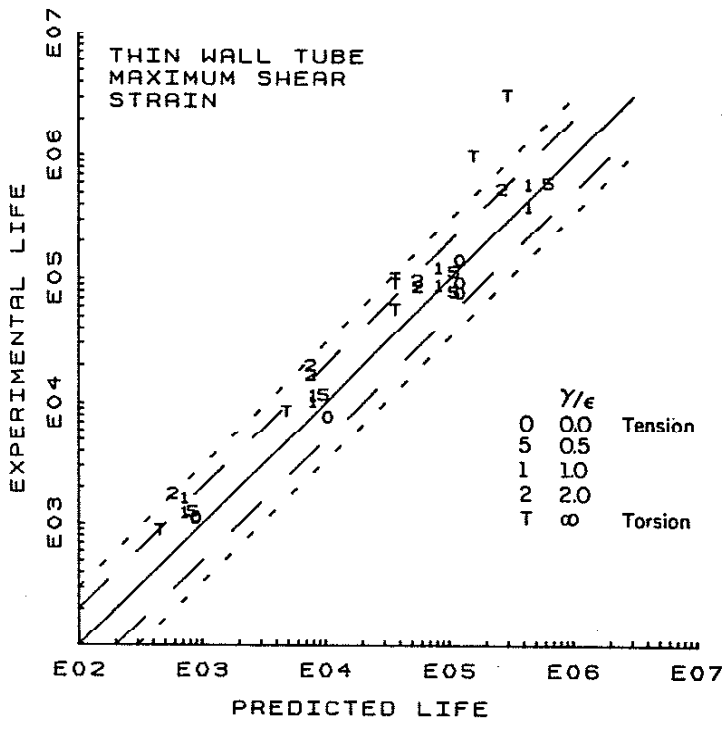

Figure 23c Thin-Wall Tube Life Predictions, Maximum Shear Strain Theory

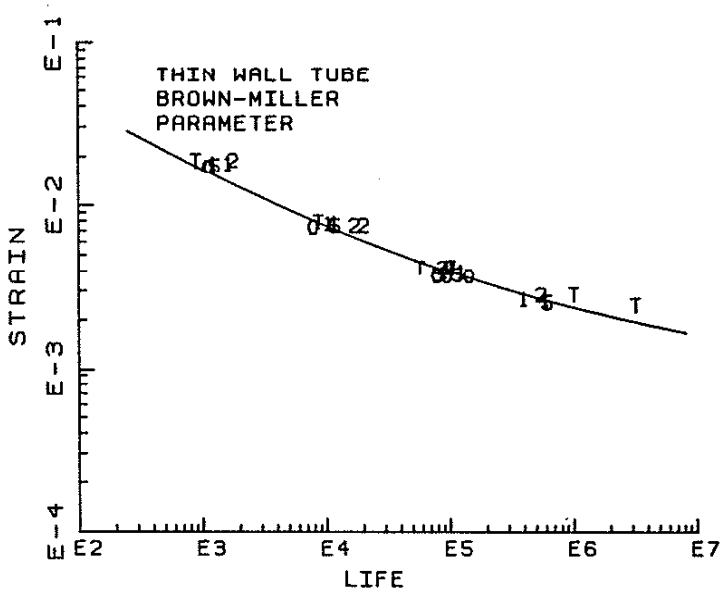

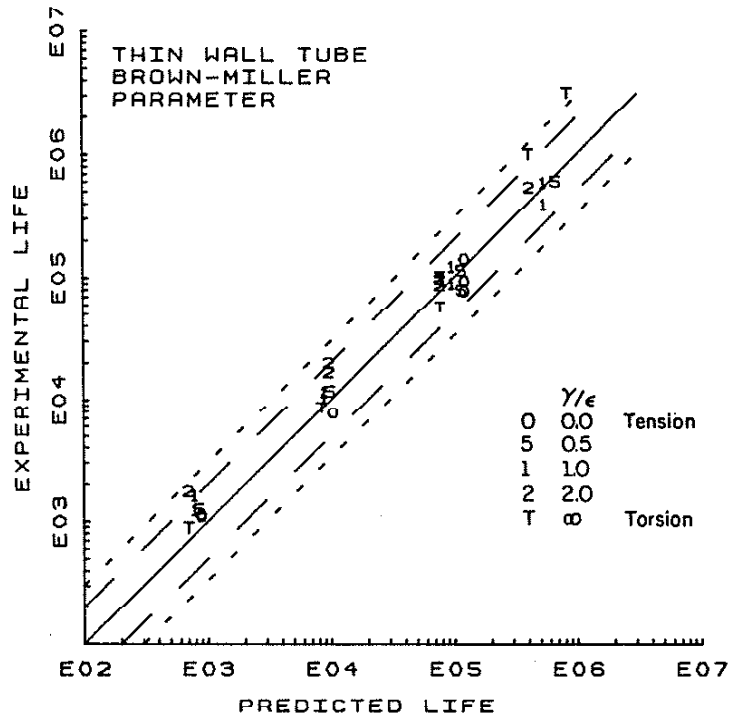

Figure 23d Thin-Wall Tube Life Predictions, Brown and Miller Theory

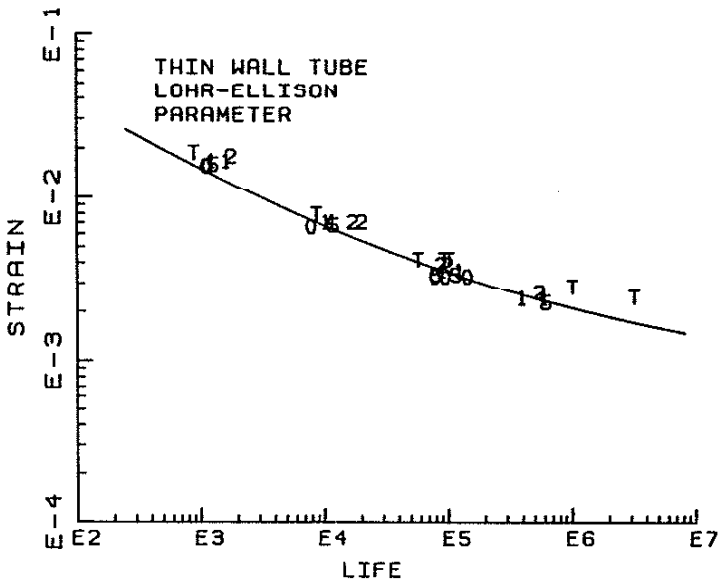

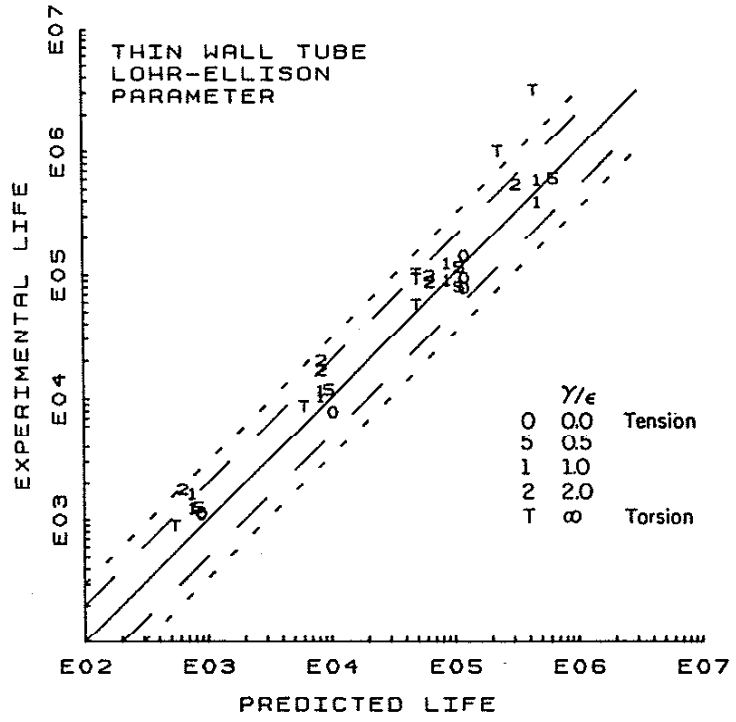

Figure 23e Thin-Wall Tube Life Predictions, Lohr and Ellison Theory

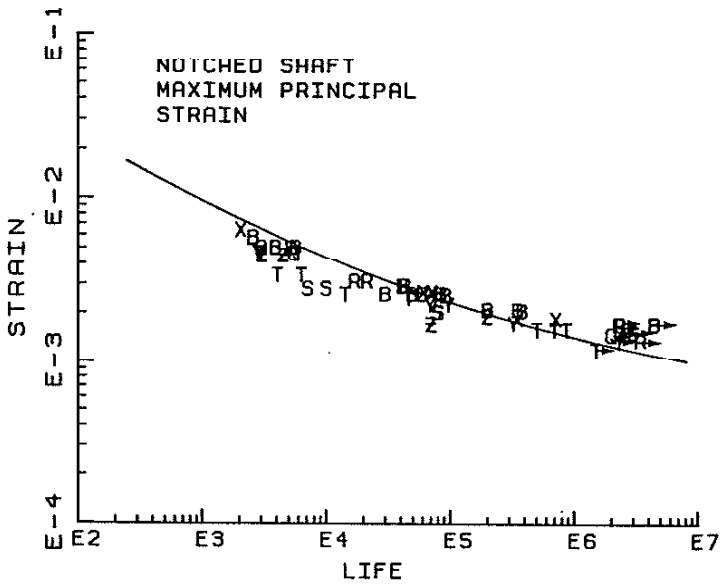

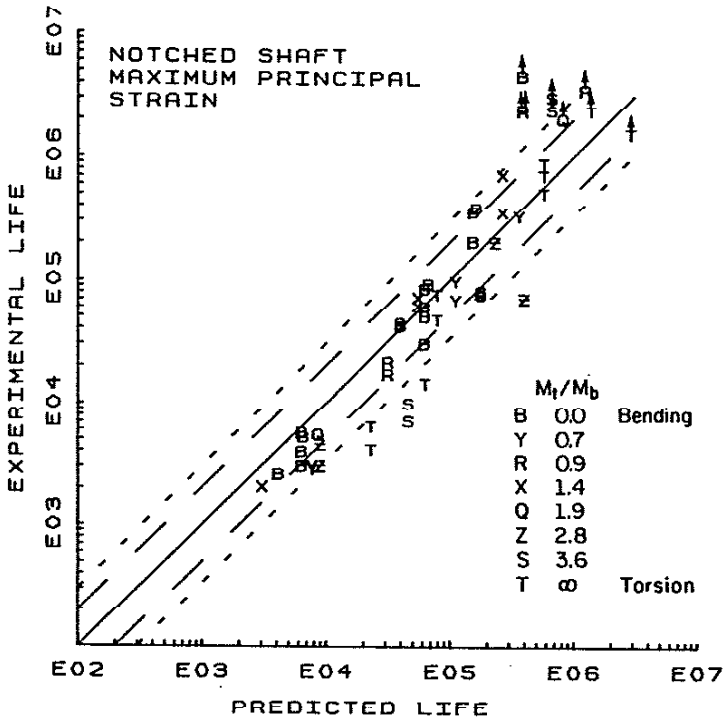

Figure 24a Notched Shaft Life Predictions. Principal Strain Theory

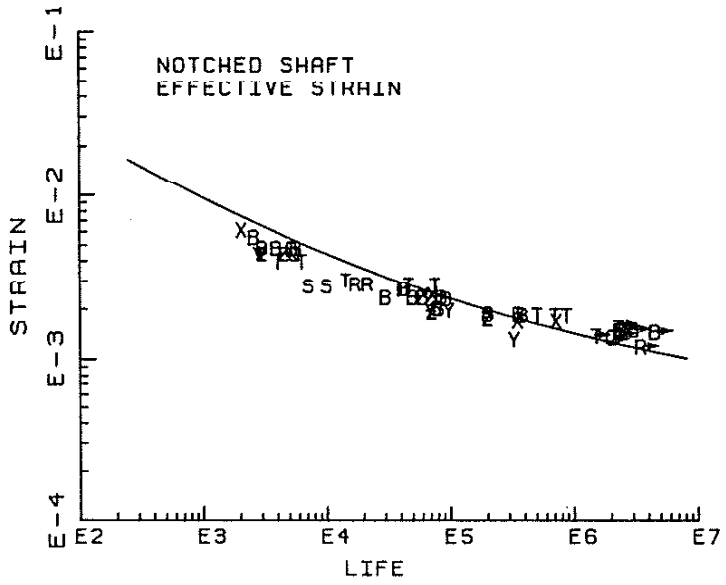

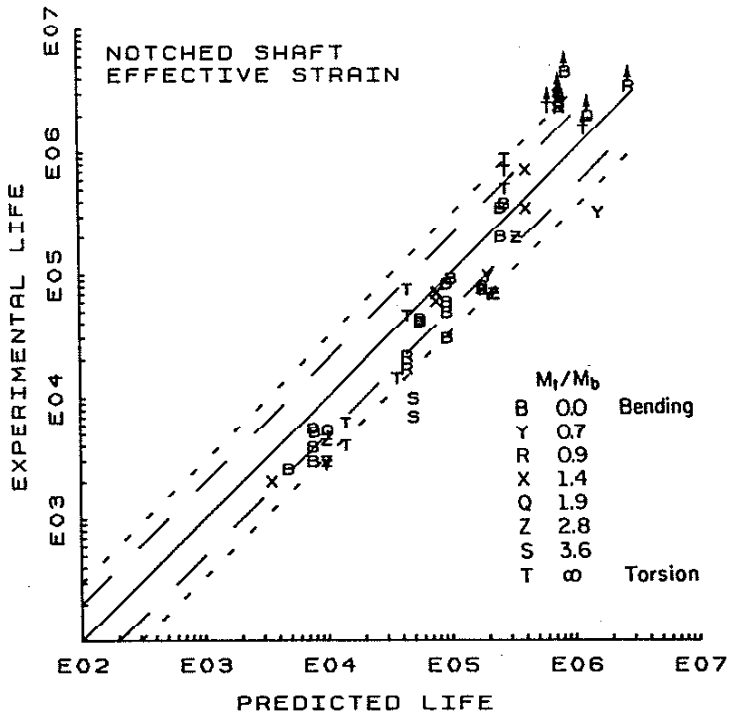

Figure 24b Notched Shaft Life Predictions, Effective Strain Theory

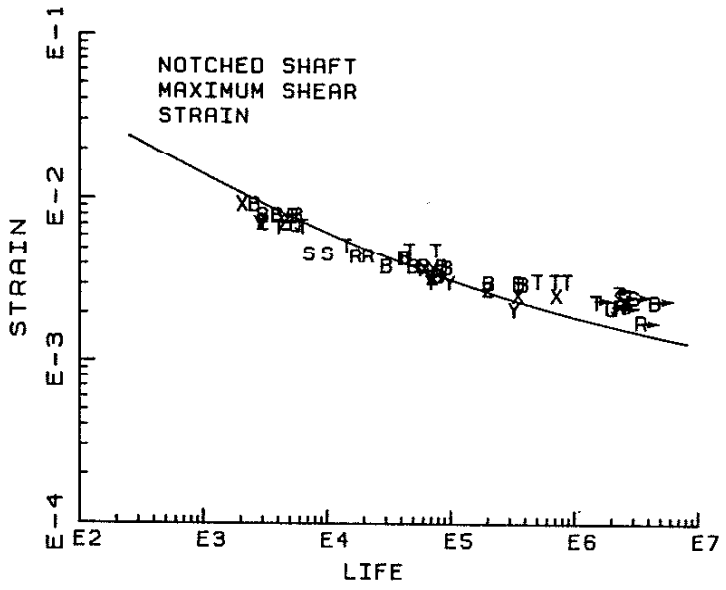

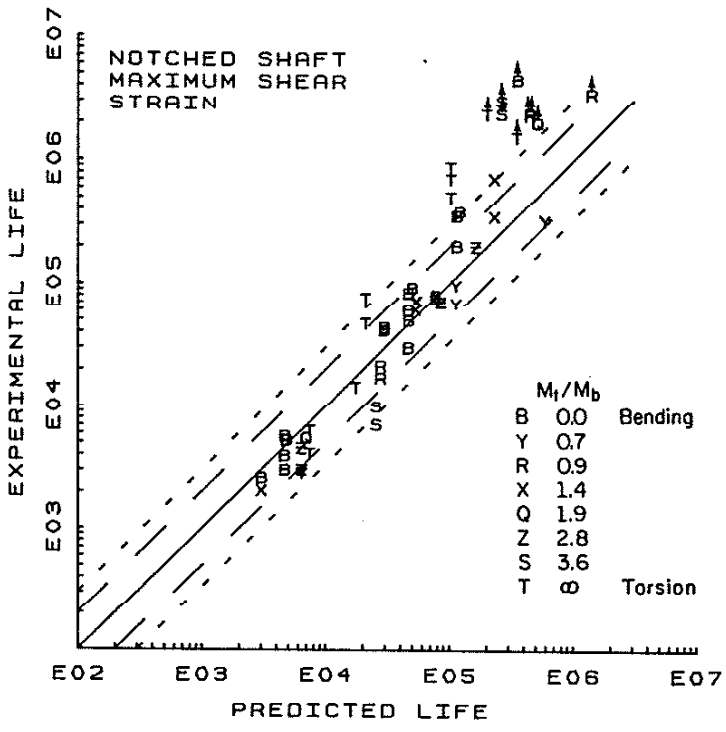

Figure 24c Notched Shaft Life Predictions, Maximum Shear Strain Theory

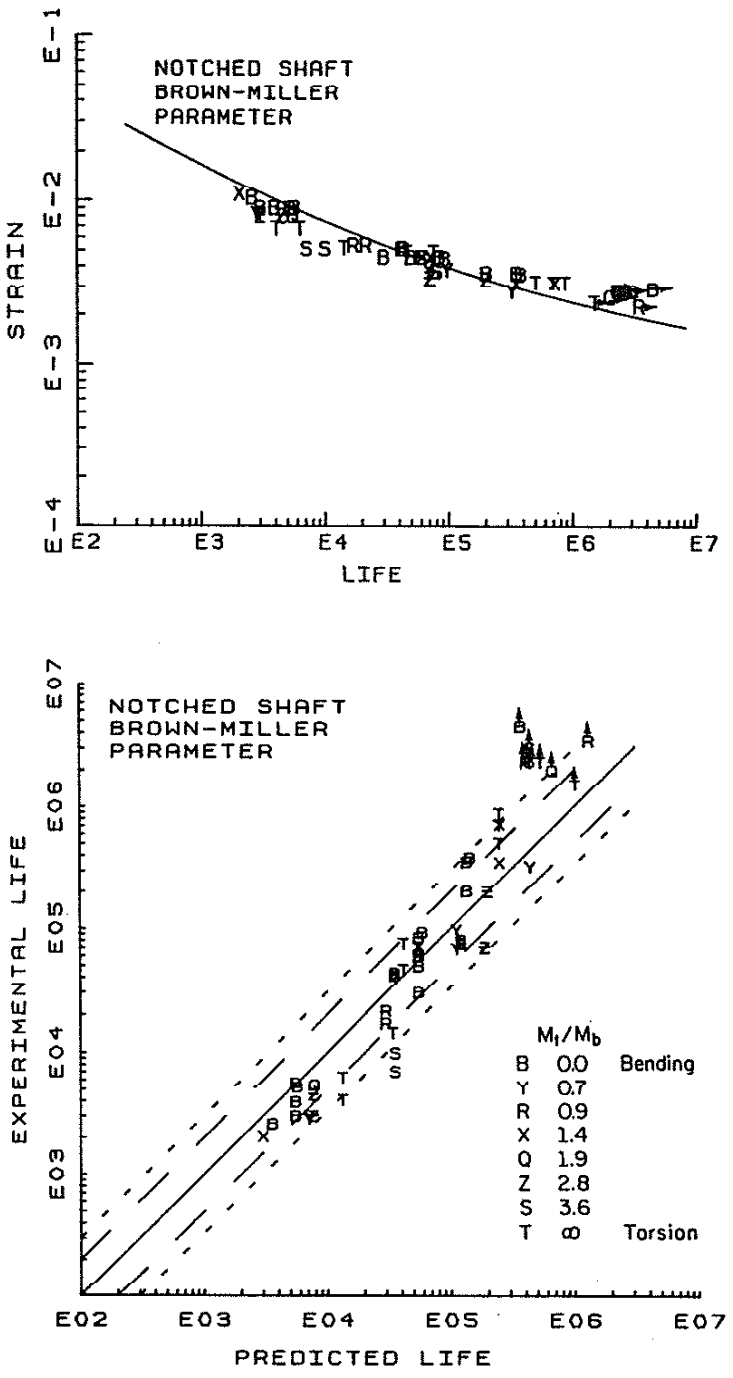

Figure 24d Notched Shaft Life Predictions, Brown and Miller Theory

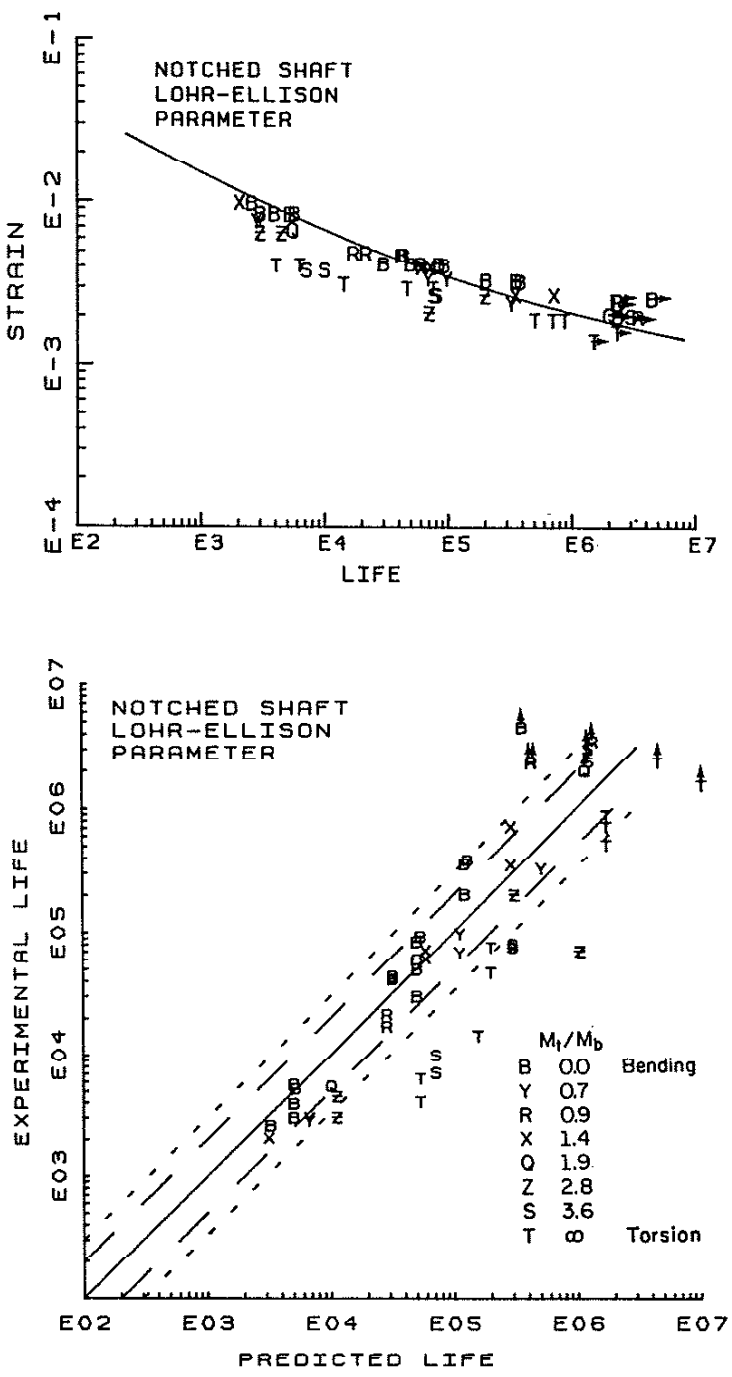

Figure 24e Notched Shaft Life Predictions, Lohr and Ellison Theory

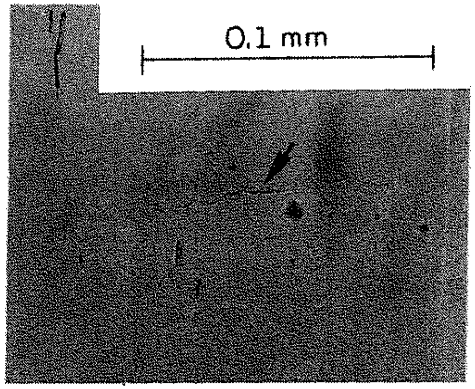

λ = 0.0 $\bar{\varepsilon}$ = 0.22%
N_f = 142541

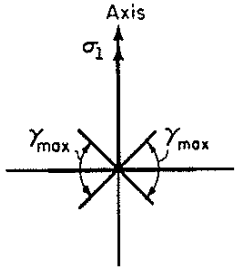

N = 80000

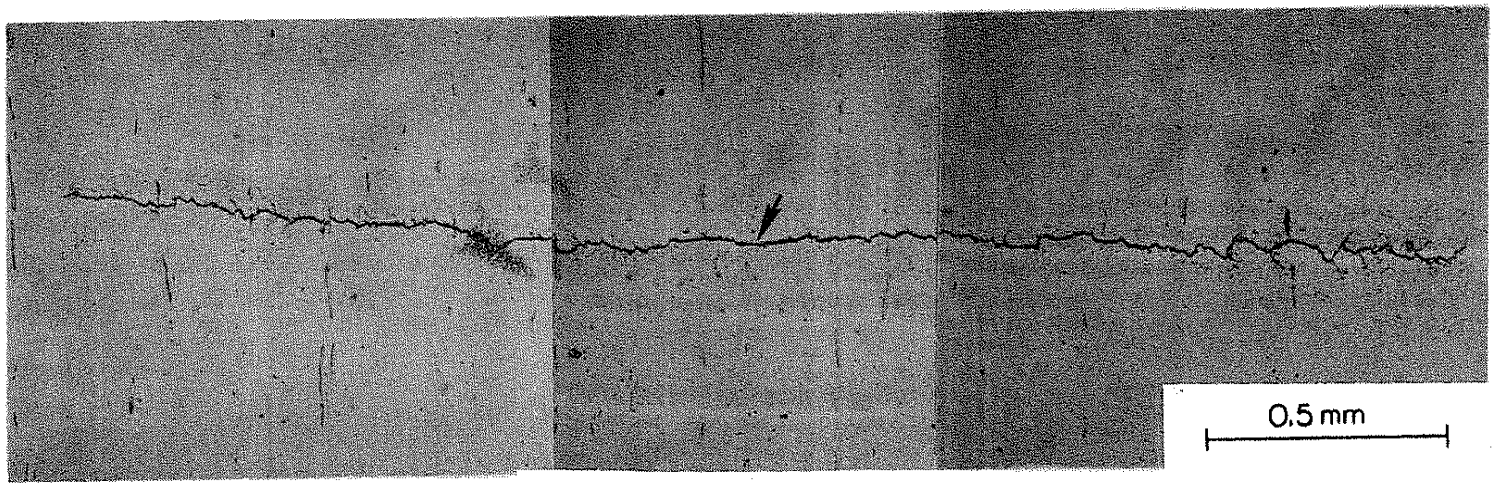

N = 140000

Figure 25 Thin-Wall Tube Crack Development for λ = 0.0, $\bar{\varepsilon}$ = 0.22%

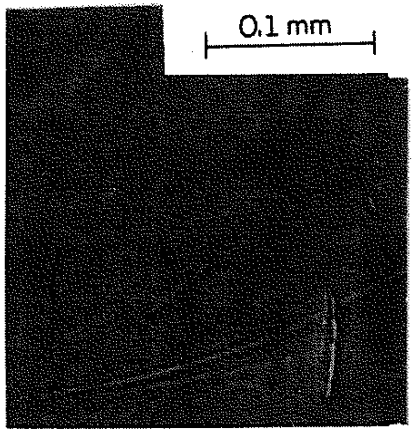

N = 20000

$\lambda = 0.5 \quad \bar{\varepsilon} = 0.22\%$
$N_f = 115462$

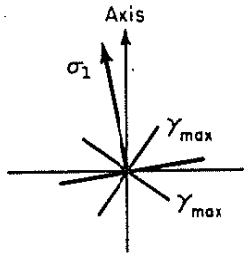

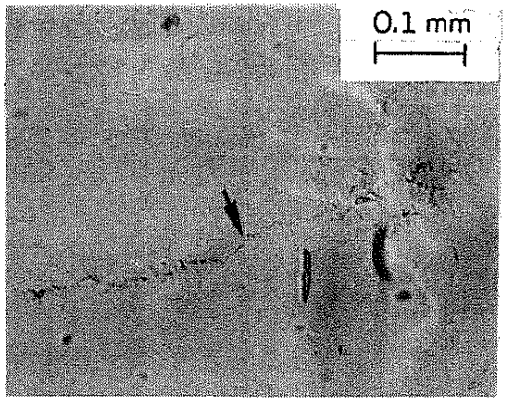

N = 80000

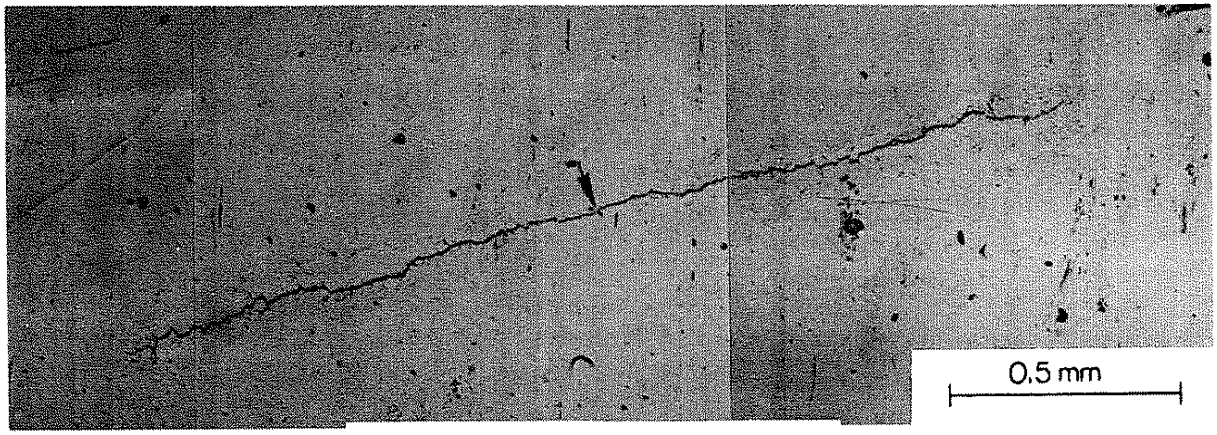

N = 110000

Figure 26 Thin-Wall Tube Crack Development for
$\lambda = 0.5$, $\bar{\varepsilon} = 0.22\%$

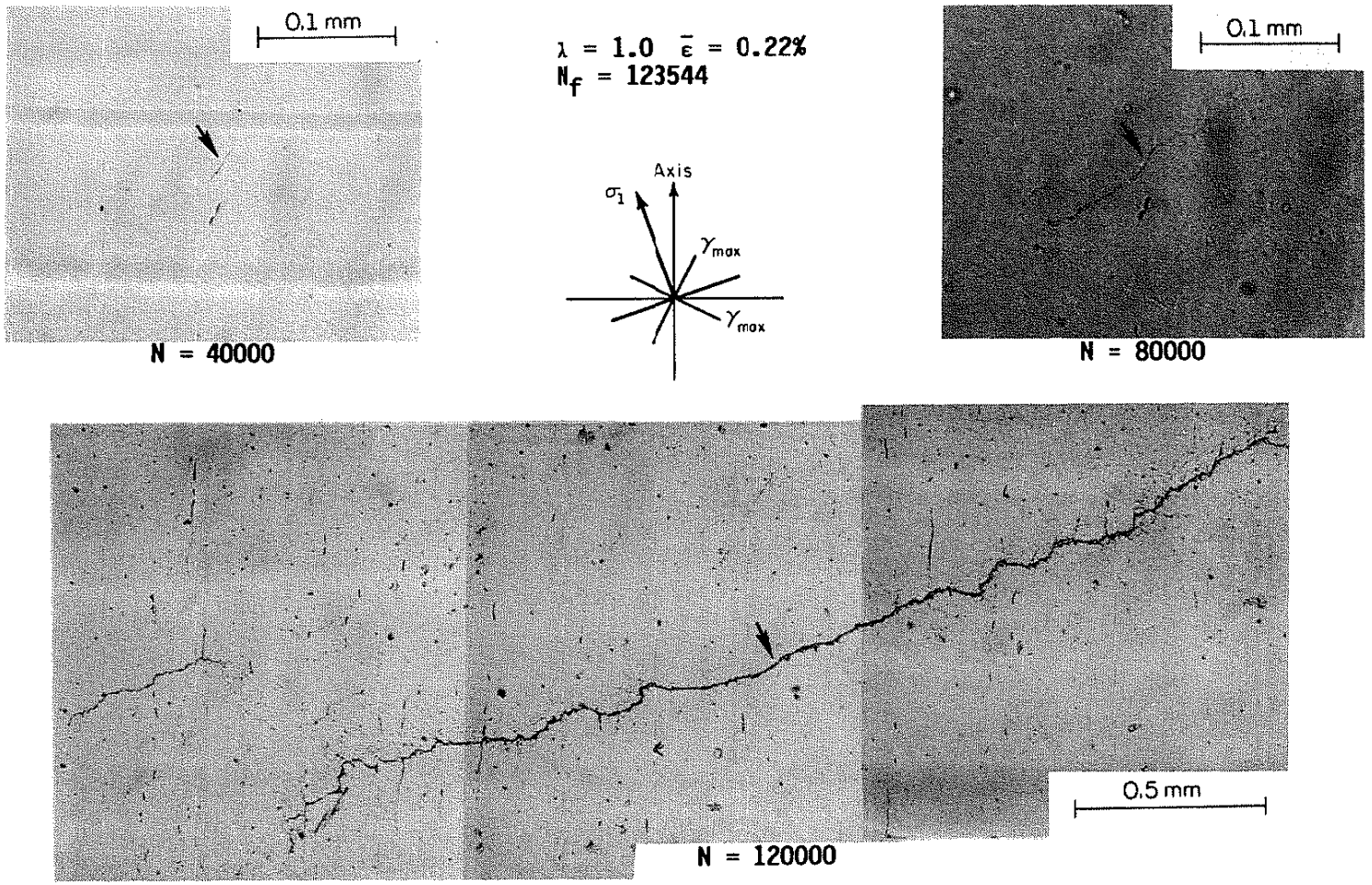

Figure 27 Thin-Wall Tube Crack Development for $\lambda = 1.0$, $\bar{\varepsilon} = 0.22\%$

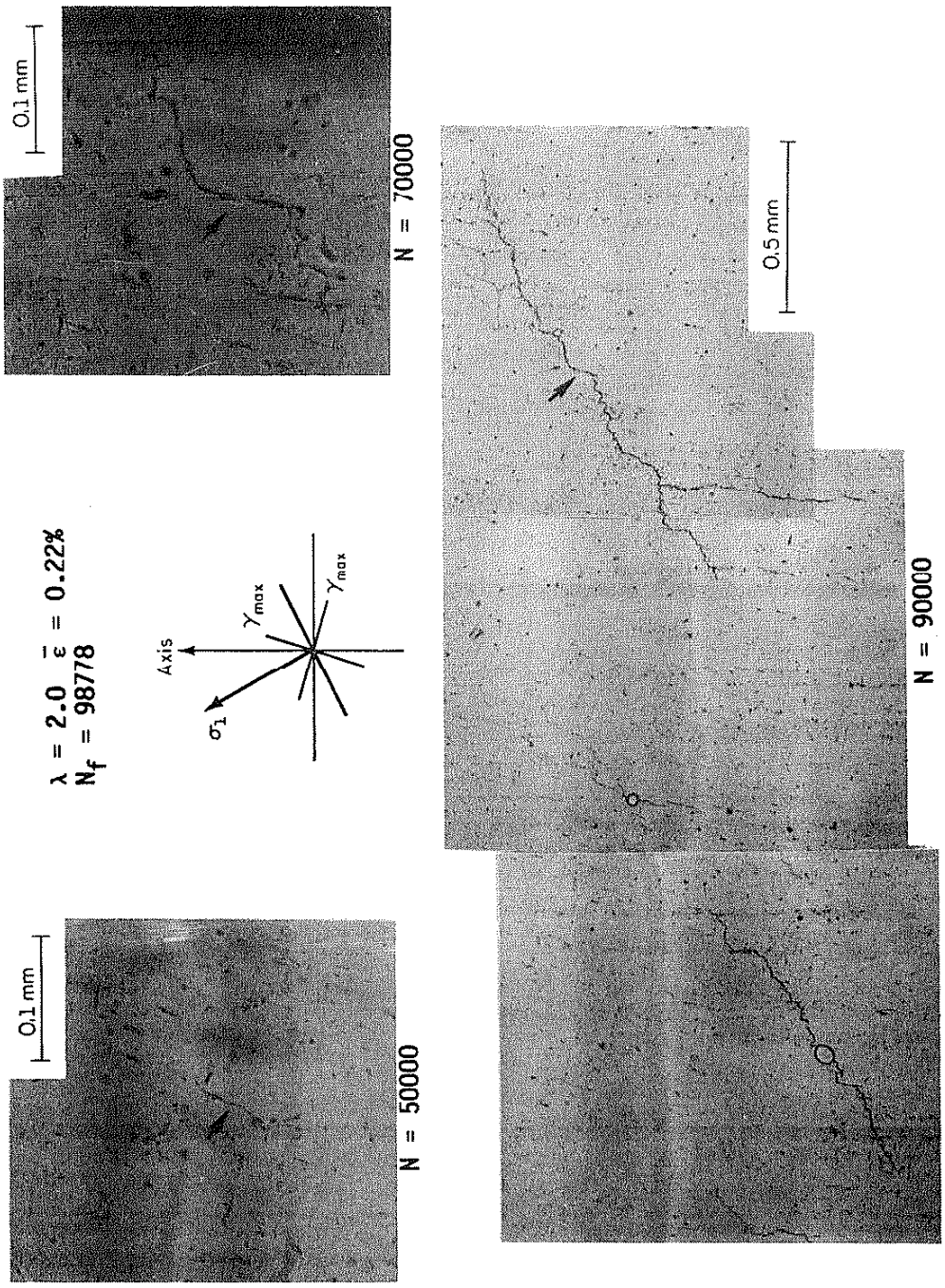

Figure 28 Thin-Wall Tube Crack Development for $\lambda = 2.0$, $\bar{\varepsilon} = 0.22\%$

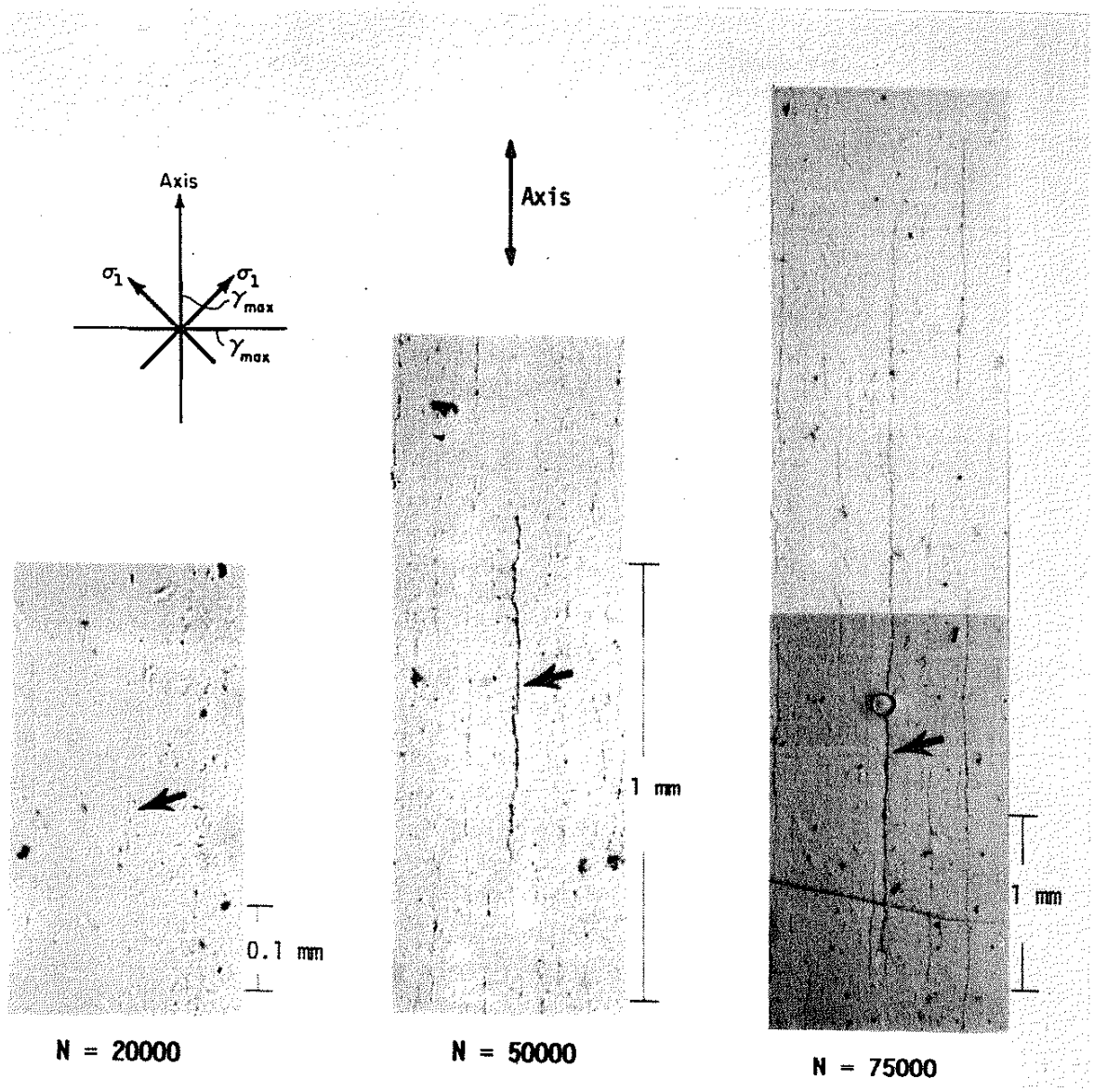

$\lambda = \infty \quad \bar{\varepsilon} = 0.22\%$
$N_f = 93052$

Figure 29 Thin-Wall Tube Crack Development for $\lambda = \infty$, $\bar{\varepsilon} = 0.22\%$

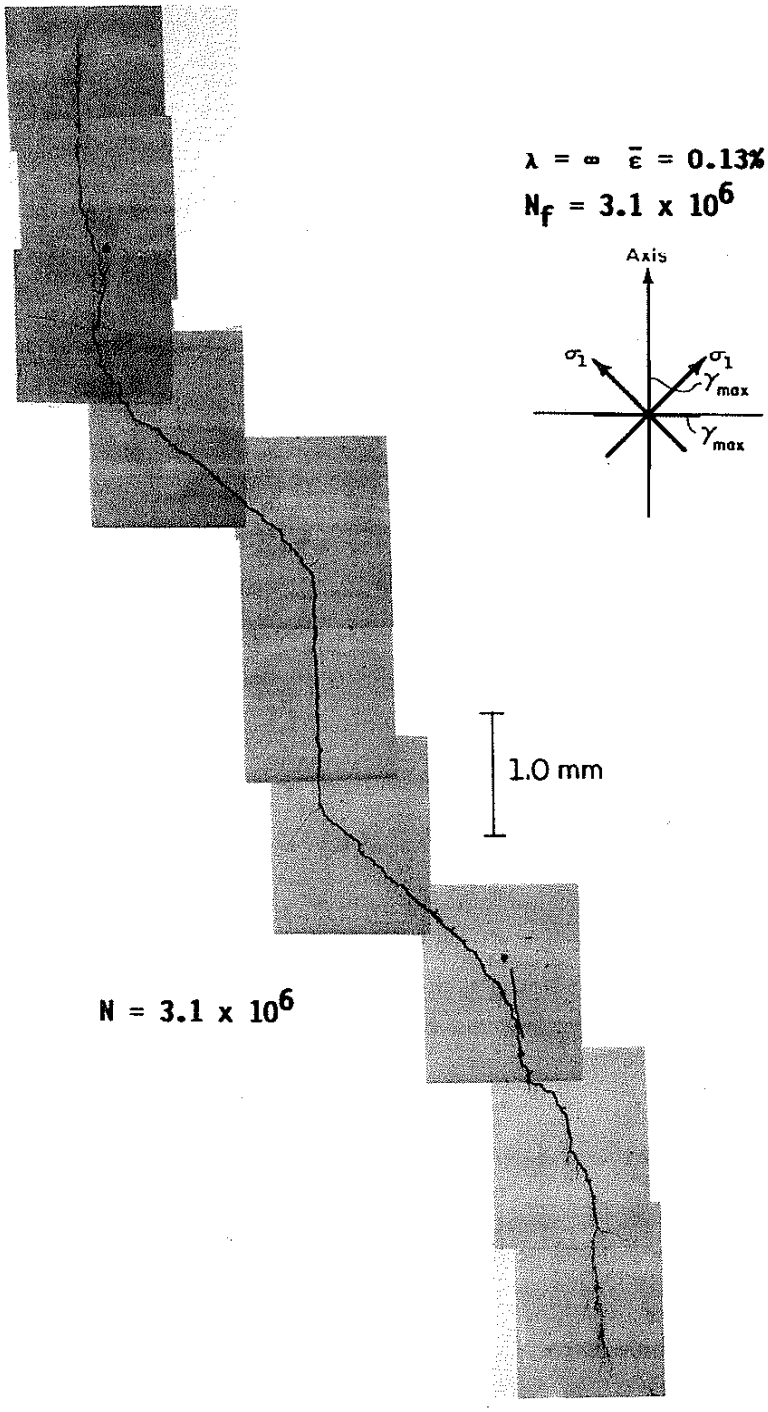

Figure 30 Thin-Wall Tube Crack Development for $\lambda = \infty$, $\bar{\varepsilon} = 0.13\%$

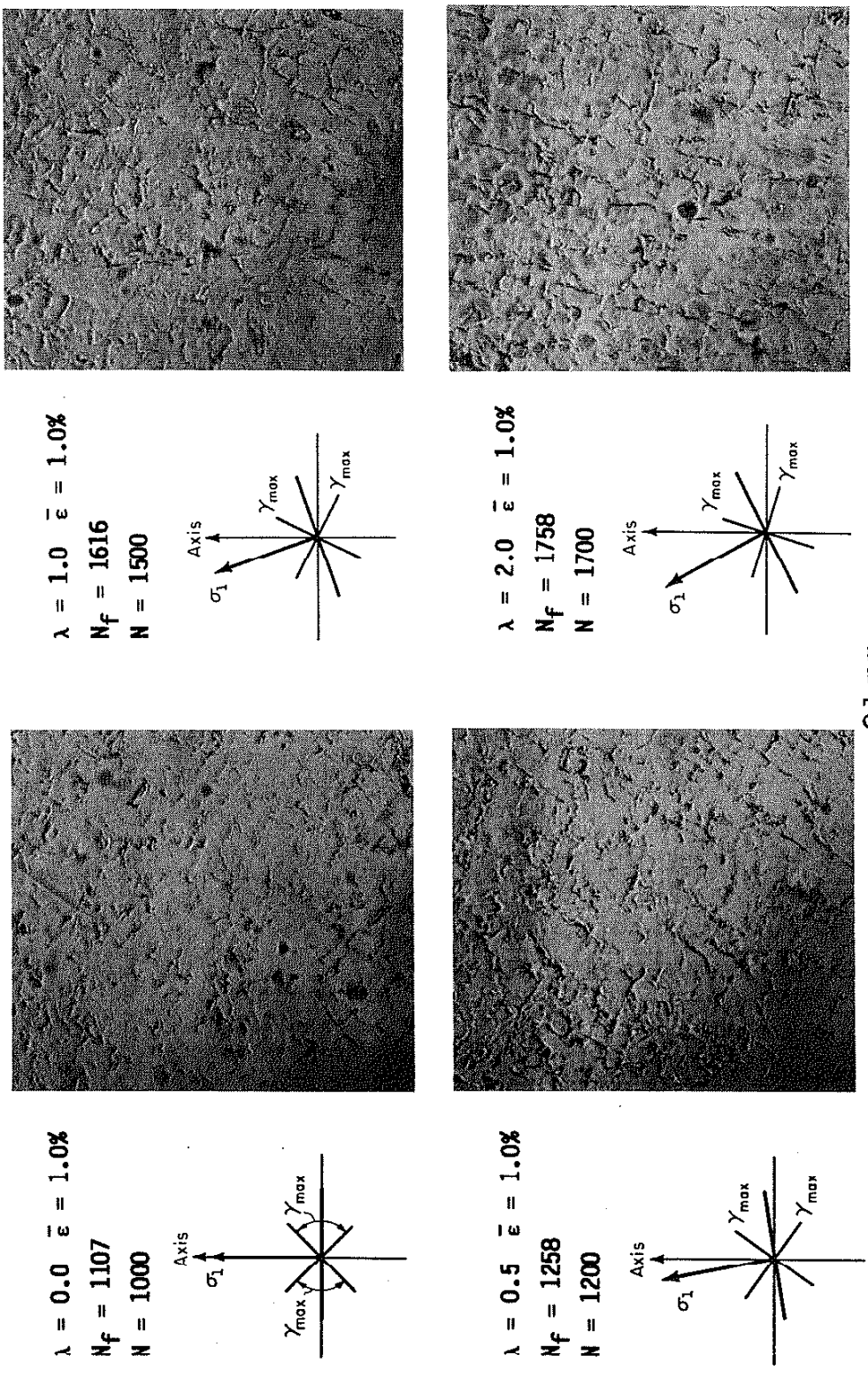

Figure 31 Thin-Wall Tube Damage Development at Short Lives, $\bar{\varepsilon}$ = 1.0% for λ = 0, λ = 0.5, λ = 1.0, λ = 2.0

$\lambda = 0.0 \quad \bar{\varepsilon} = 0.43\%$
$N_f = 7839$

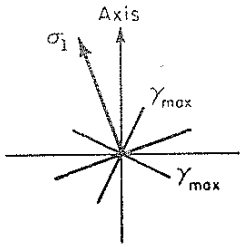

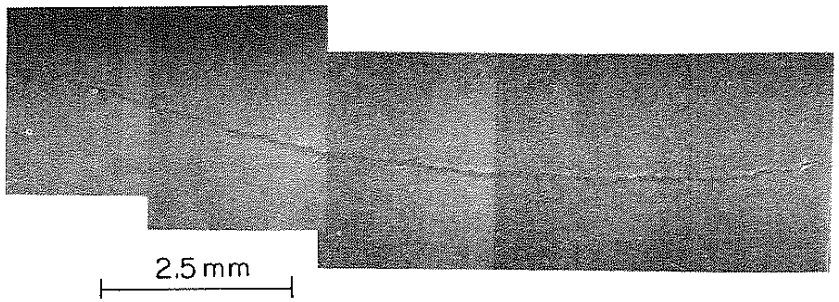

$\lambda = 1.0 \quad \bar{\varepsilon} = 0.43\%$
$N_f = 11611$

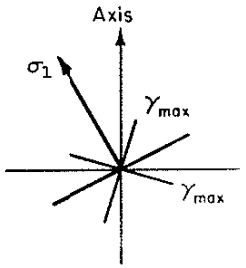

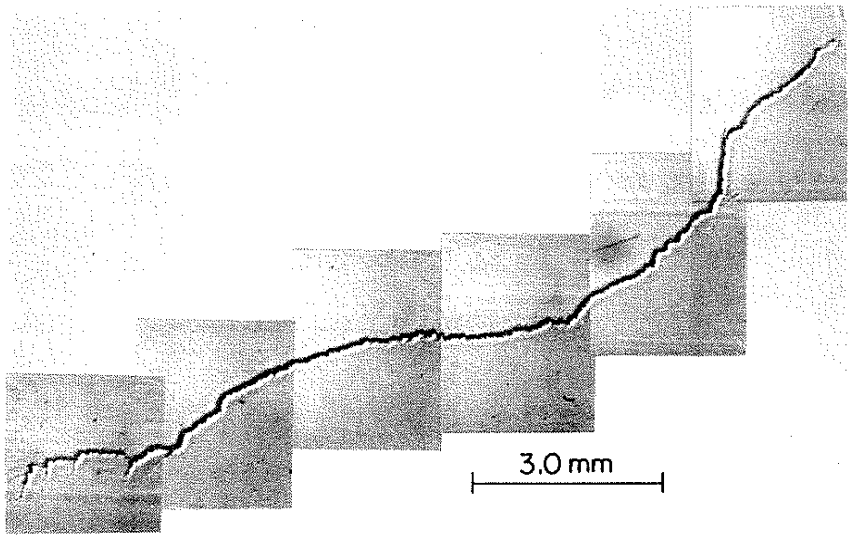

Figure 32 Thin-Wall Tube Failure Crack for Short Life Tests
$\bar{\varepsilon} = 1.0\%$ for $\lambda = 0.0$, $\lambda = 1.0$

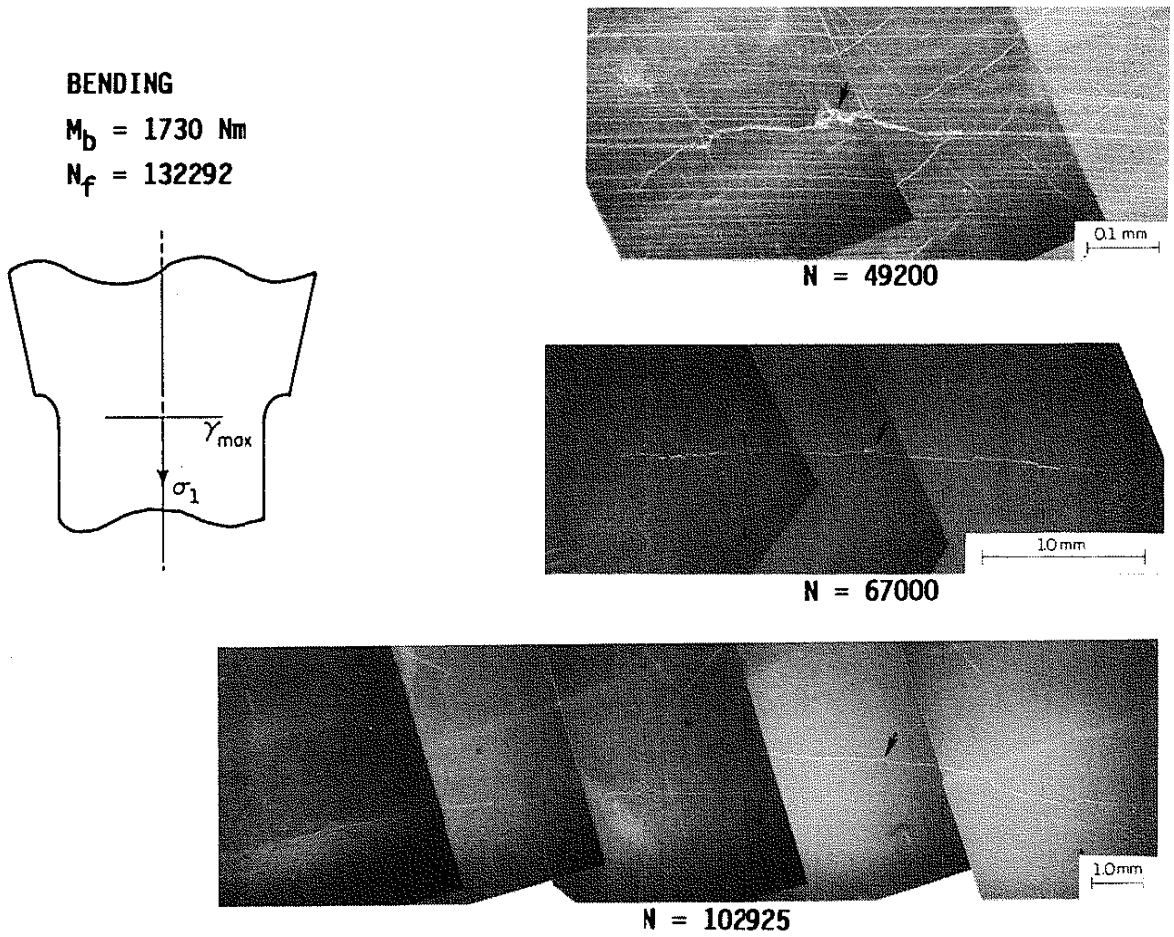

Figure 33 Crack Development for Notched Shaft in Bending

BENDING

M_b = 1475 Nm

N_f = 709000

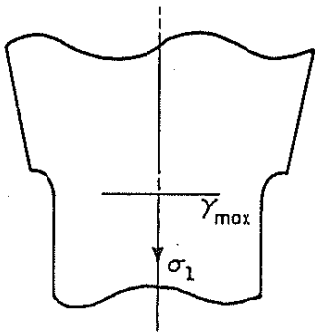

BENDING

M_b = 1875 Nm

N_f = 106717

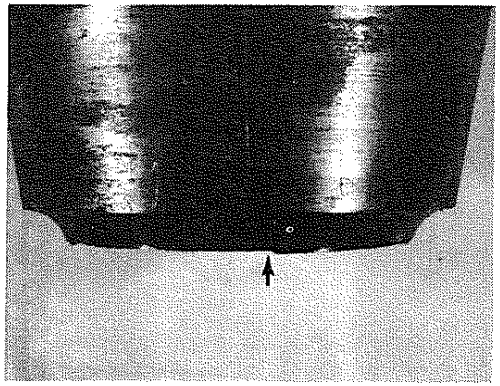

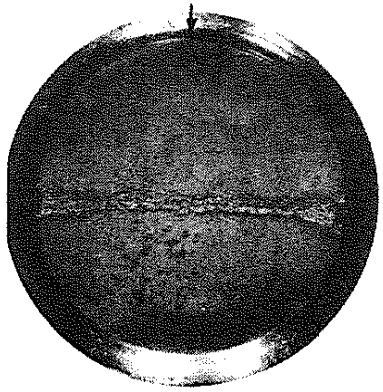

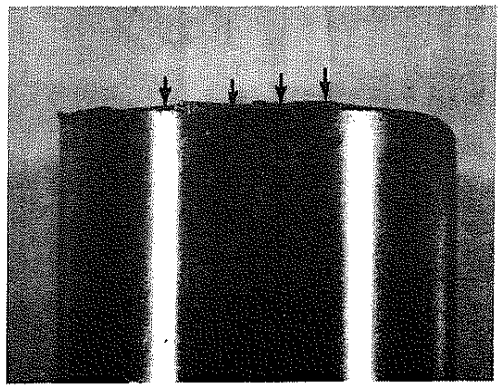

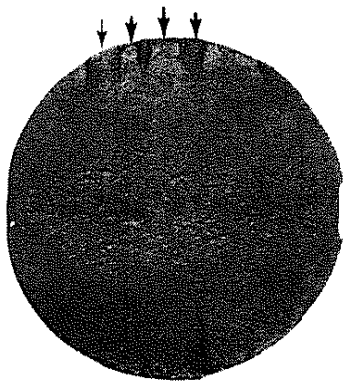

Figure 34 Fracture Surfaces of Long and Short Life Tests of the Notched Shaft in Bending

XR LOADING

M_b = 1220 Nm

M_t = 1710 Nm

N_f = 222016

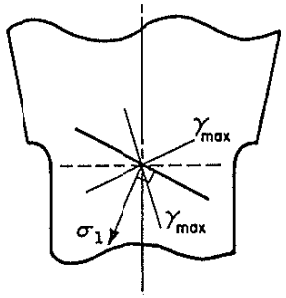

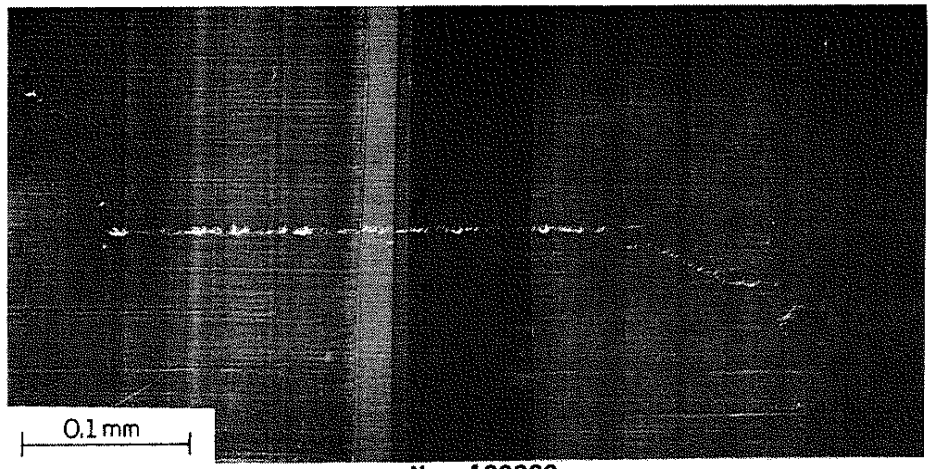

N = 100000

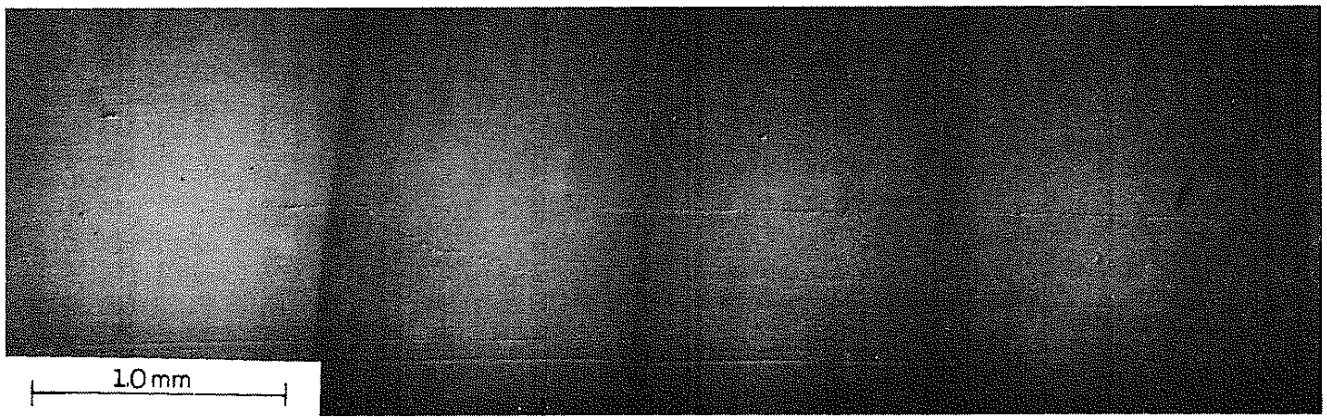

N = 130000

Figure 35 Crack Development in Notched Shaft, Combined (XR) Loading Condition

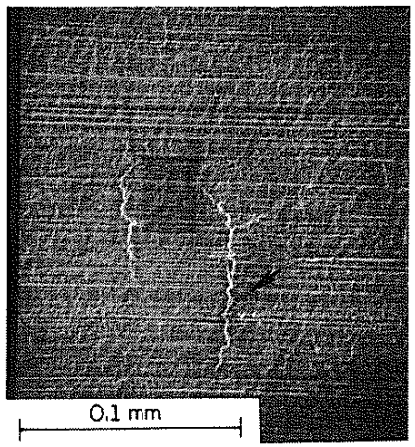

Figure 36 Crack Development from Inclusions in Notched Shaft, Combined (XR) Loading Condition

XR LOADING

M_b = 1850 Nm

M_t = 2550 Nm

N_f = 7285

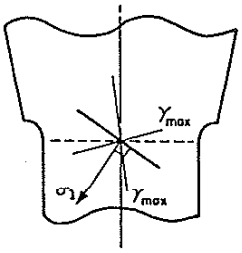

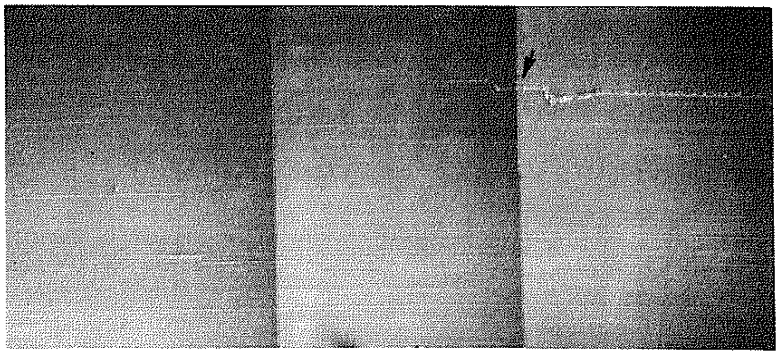

N = 4000

1.0 mm

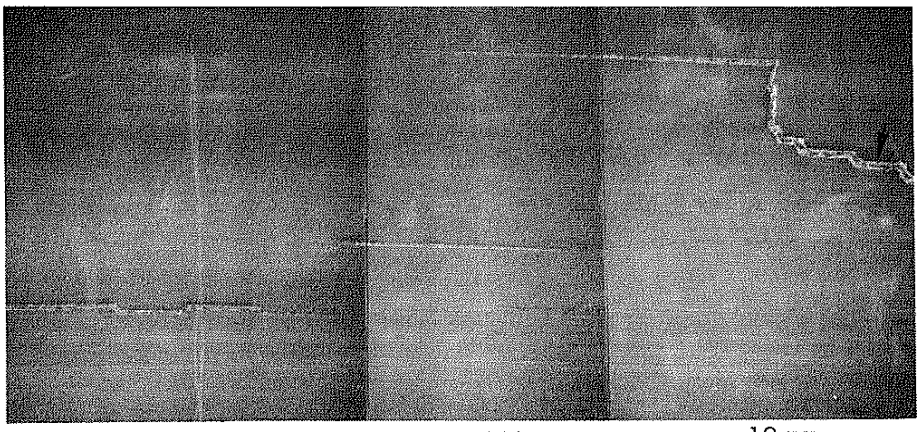

N = 5000

1.0 mm

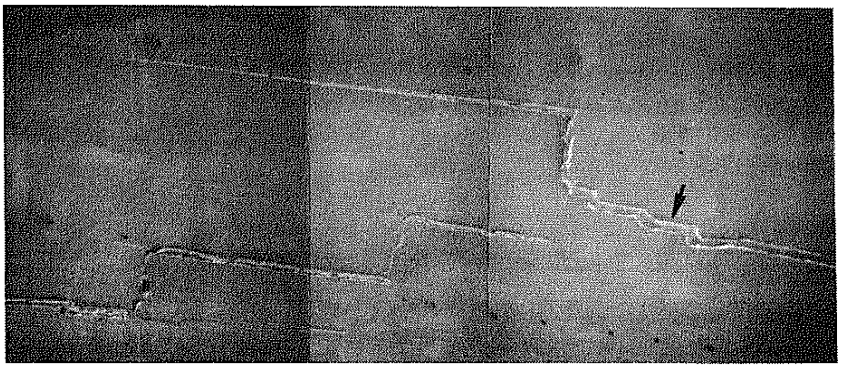

N = 6000

1.0 mm

Figure 37 Crack Development in Notched Shaft, Combined (XR) Loading Condition

XR LOADING

M_b = 1220 Nm

M_t = 1710 Nm

N_f = 222016

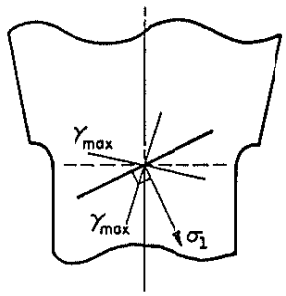

XR LOADING

M_b = 1850 Nm

M_t = 2550 Nm

N_f = 7285

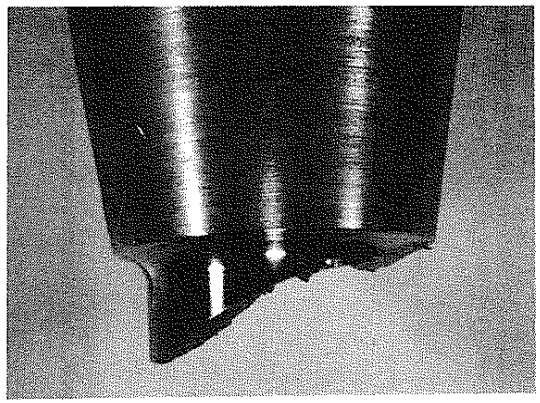

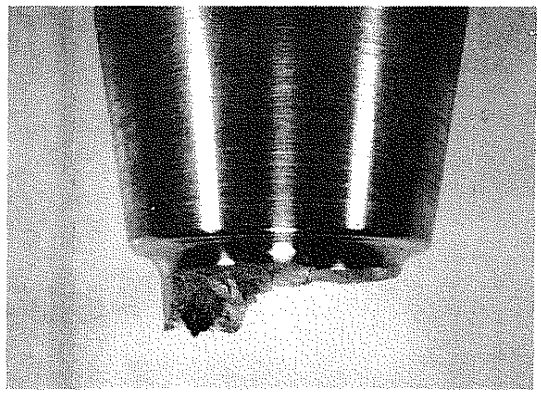

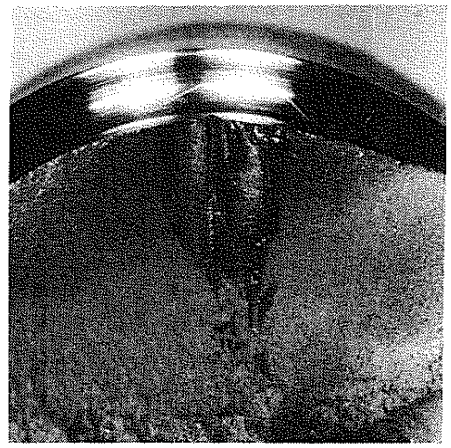

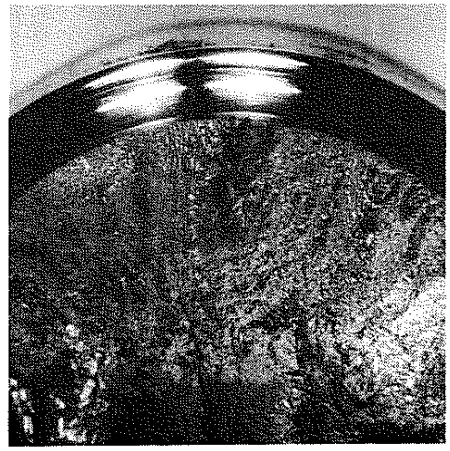

Figure 38 Macroscopic Growth Behavior for Combined (XR) Loading Conditions of the Notched Shaft

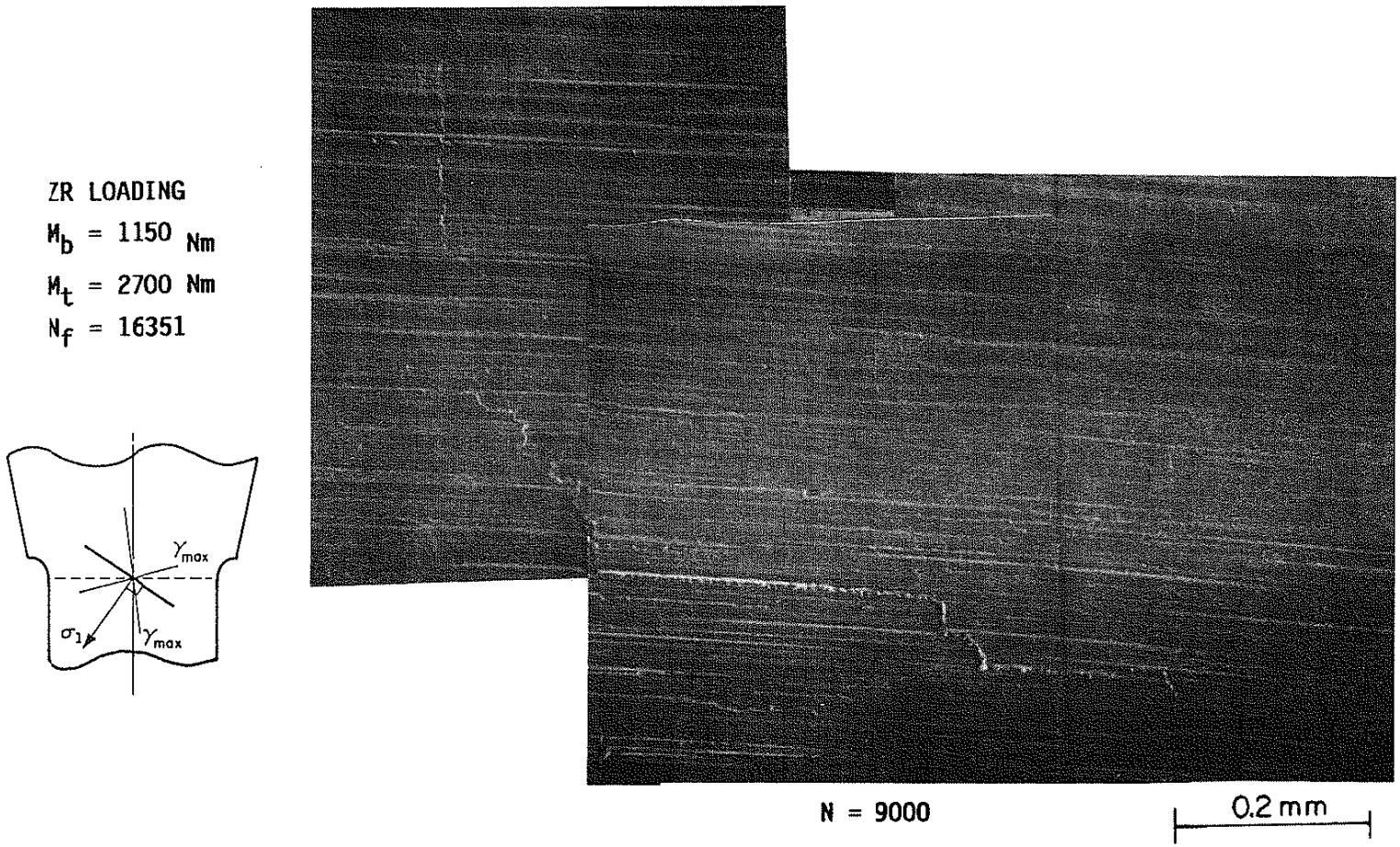

Figure 39 Crack Development in Notched Shaft, Combined (ZR) Loading Condition

ZR LOADING

M_b = 780 Nm

M_t = 2180 Nm

N_f = 171666

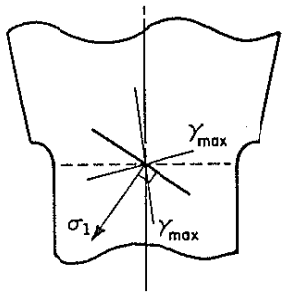

ZR LOADING

M_b = 1150 Nm

M_t = 2700 Nm

N_f = 16351

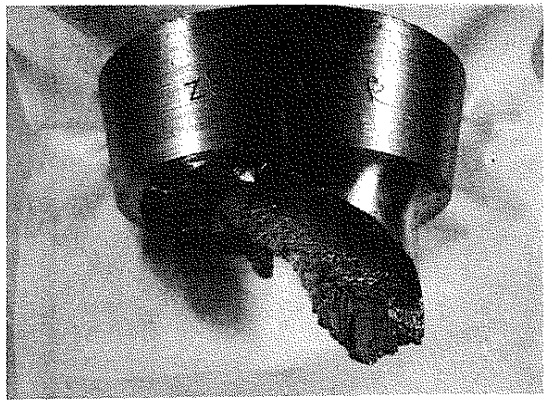

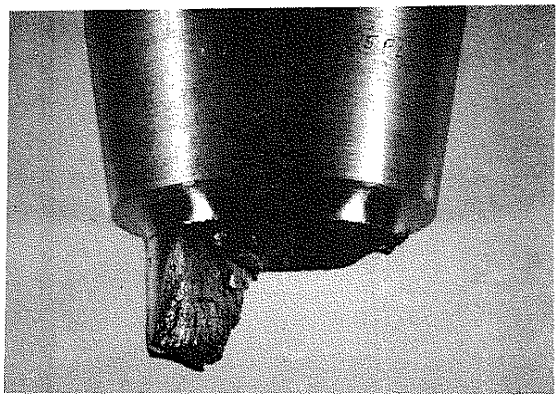

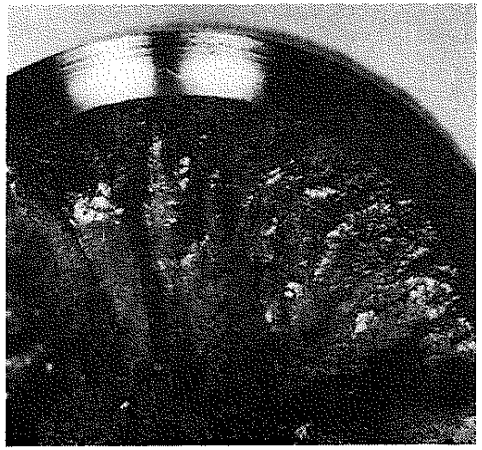

Figure 40 Macroscopic Growth Behavior for Combined (ZR) Loading Conditions of the Notched Shaft

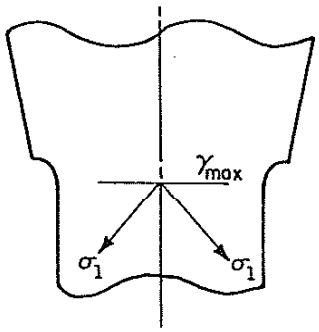

TORSION

M_t = 2000 Nm

$N_f = 2.13 \times 10^6$

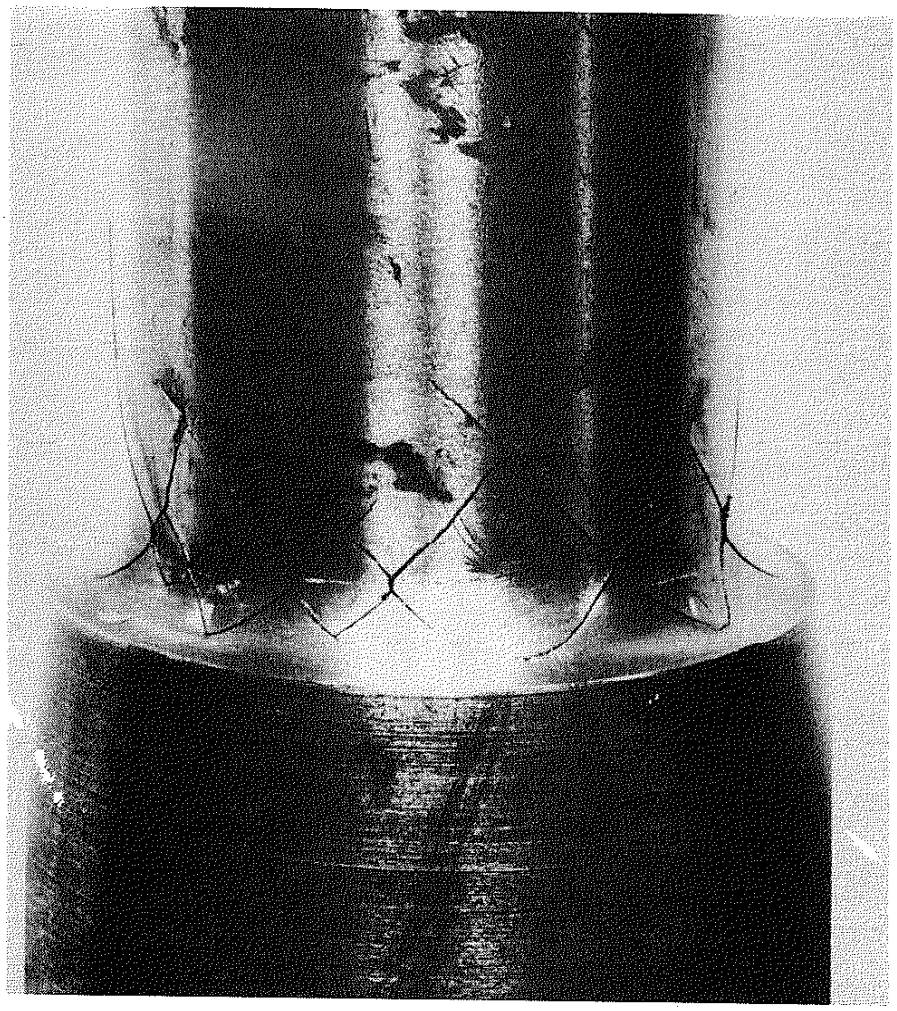

Figure 41 Torsional Cracking Behavior of the Notched Shaft at Long Lives

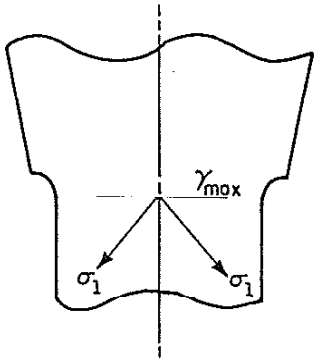

TORSION

M_t = 3000 Nm

N_f = 9528

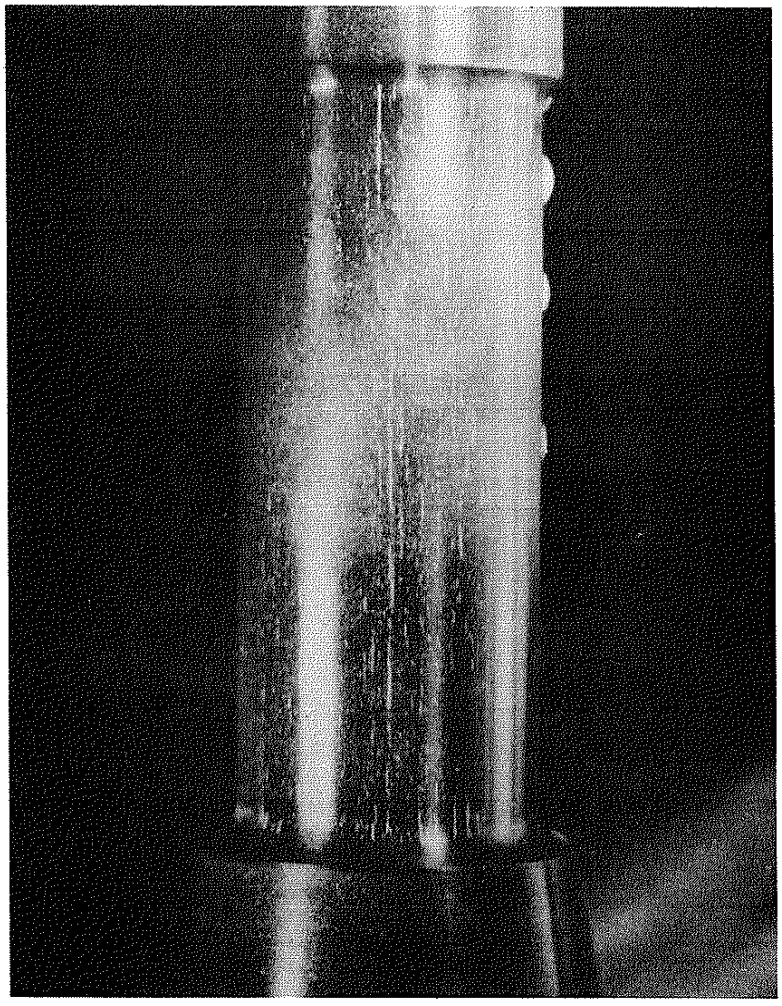

Figure 42 Torsional Cracking Behavior of the Notched Shaft at Short Lives

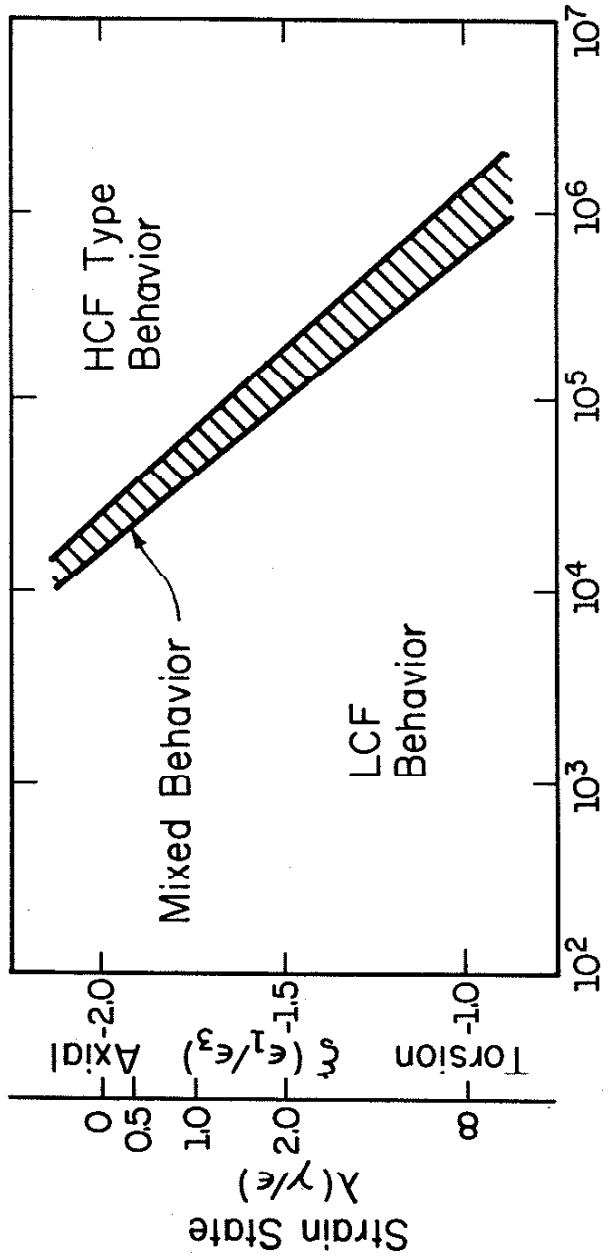

Figure 43 Schematic Representation of the Thin-Wall Tube Damage State as a Function of Strain State and Strain Amplitude

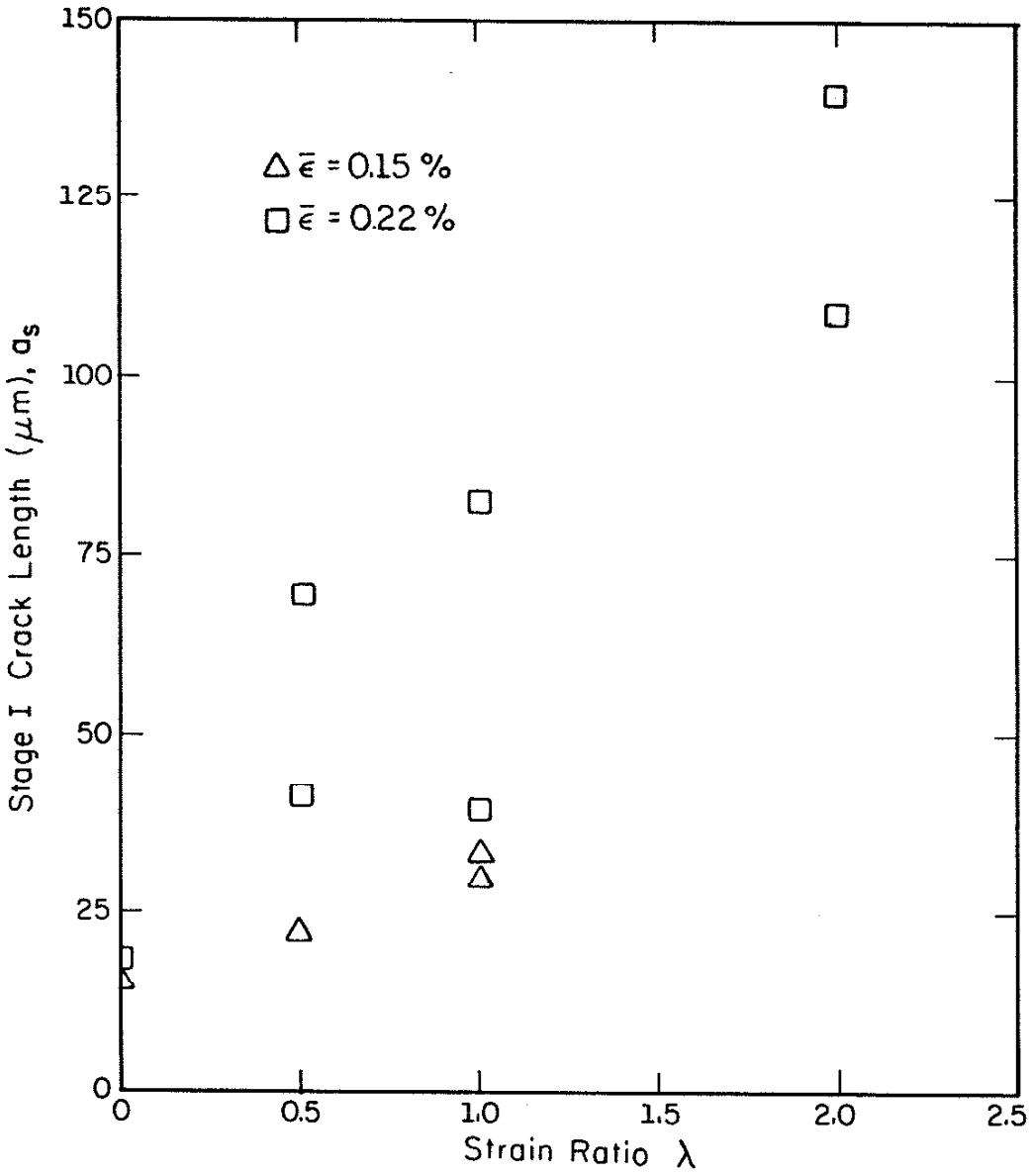

Figure 44 Crack Length Versus Strain Ratio for HCF Type Damage in the Thin-Wall Tube

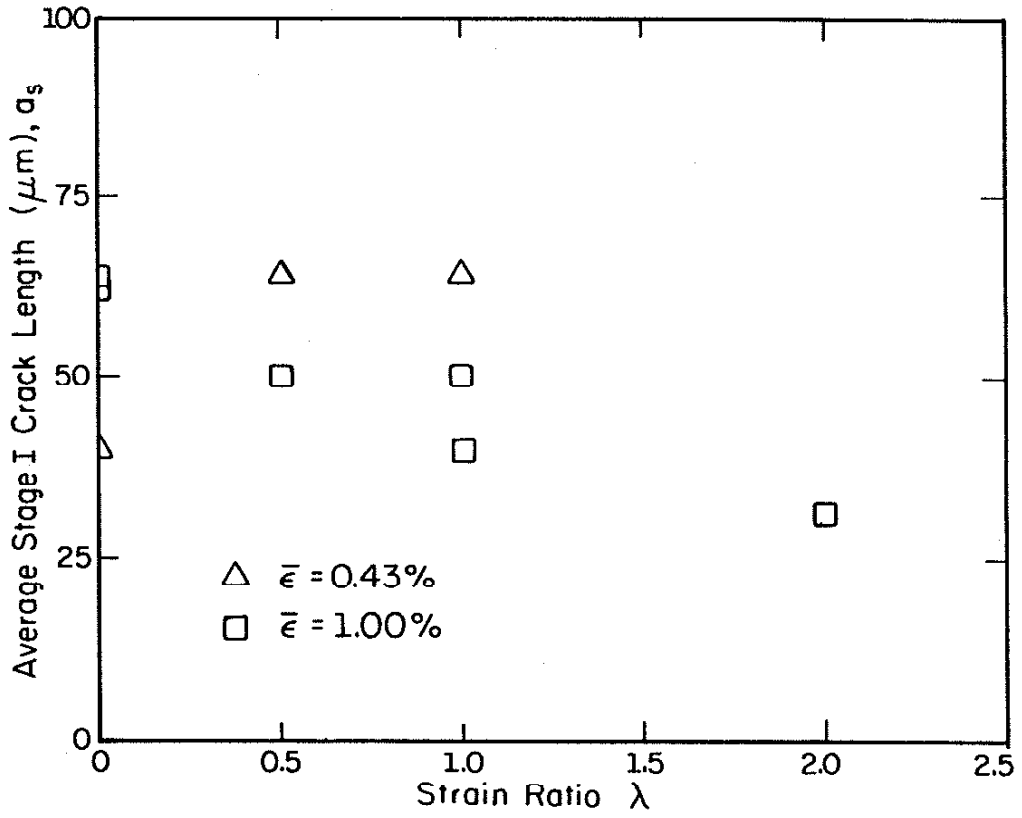

Figure 45 Crack Length Versus Strain State for LCF Type Damage in the Thin-Wall Tube

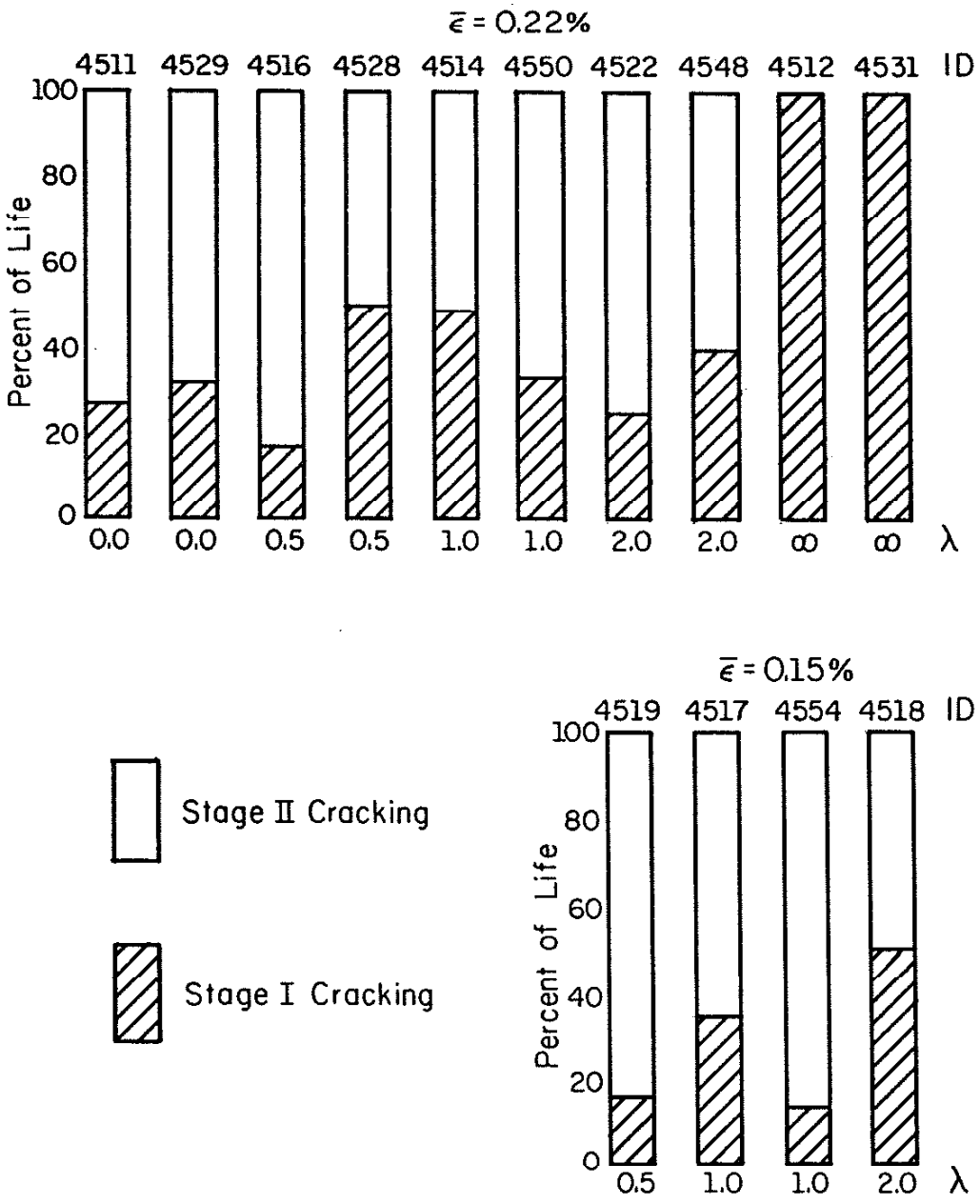

Figure 46 Percent of Life Spent in Stage I and Stage II Crack Development for HCF Type Damage

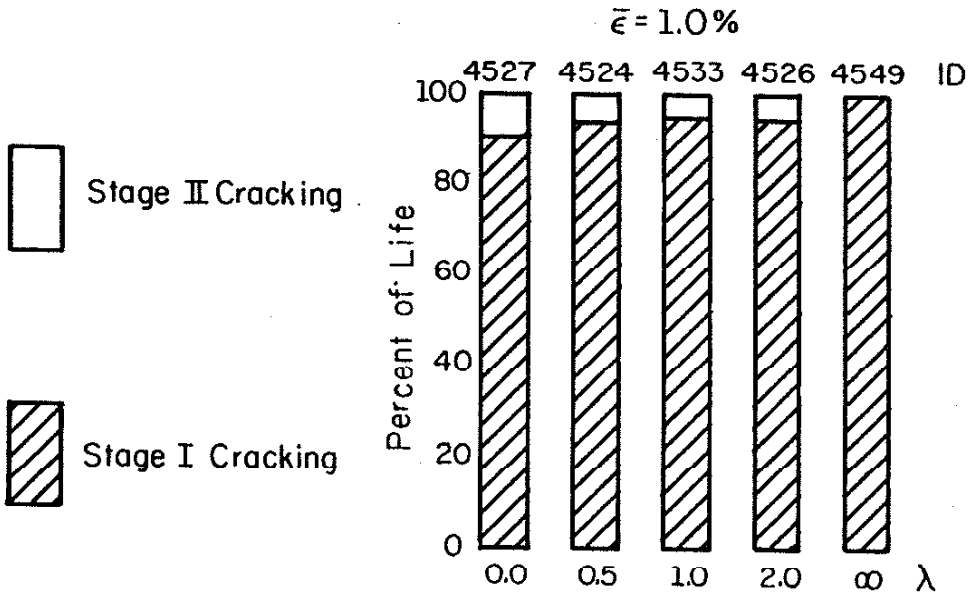

Figure 47 Percent of Life Spent in Stage I and Stage II Crack Development for LCF Type Damage

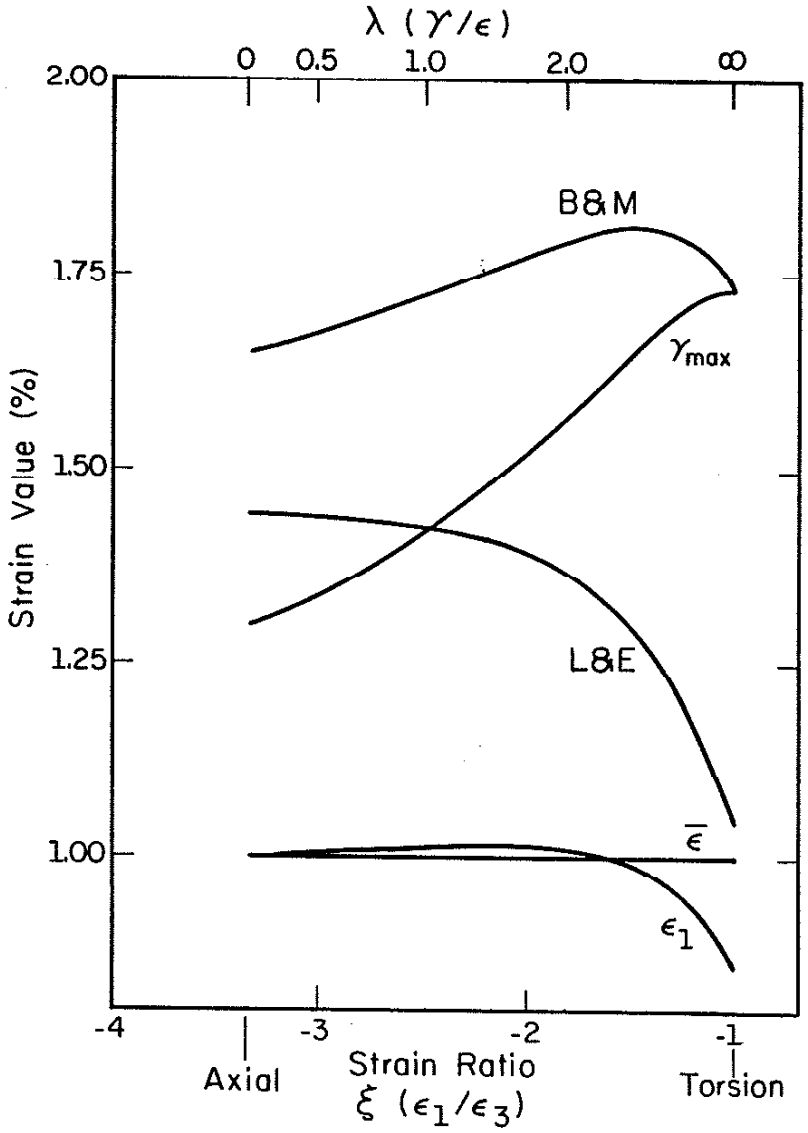

Figure 48 Change in Strain Parameters with Strain State for a Constant Effective Strain

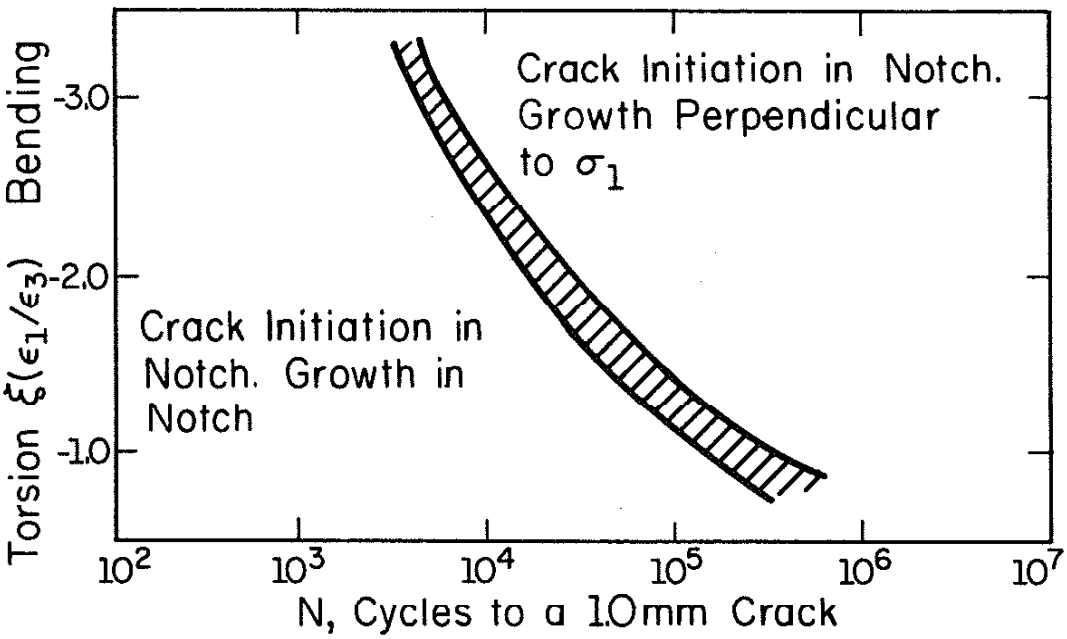

Figure 49 Schematic Representation of Damage State as a Function of the Ratio of Applied Moments and Life Regime for the Notched Shaft

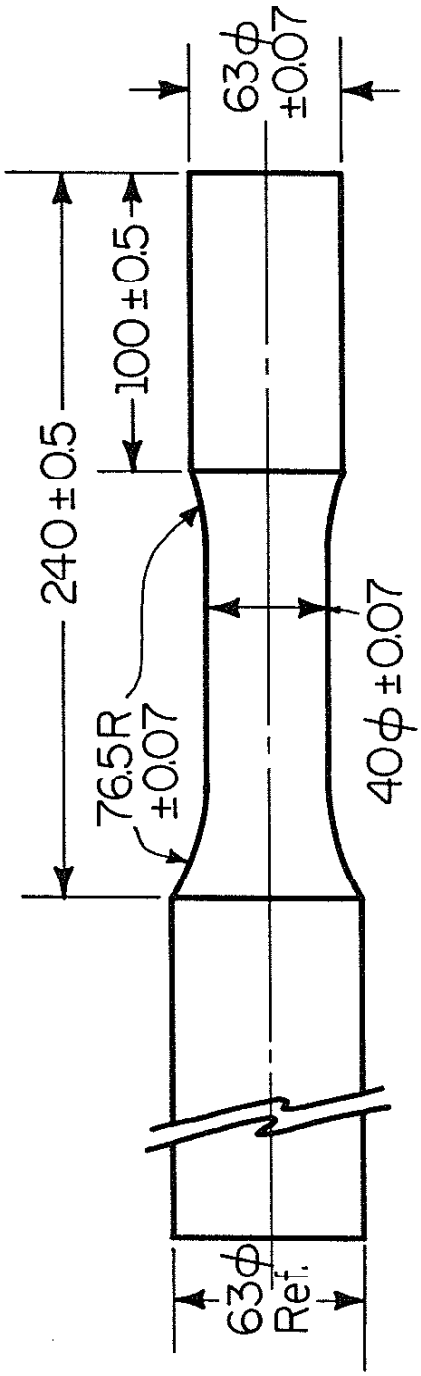

Figure 50 Unnotched Shaft Test Specimen

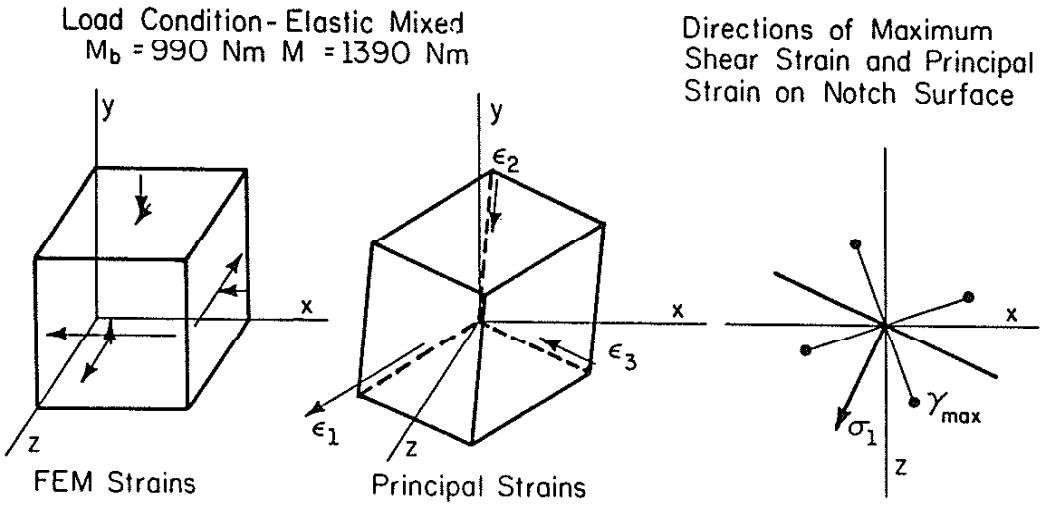

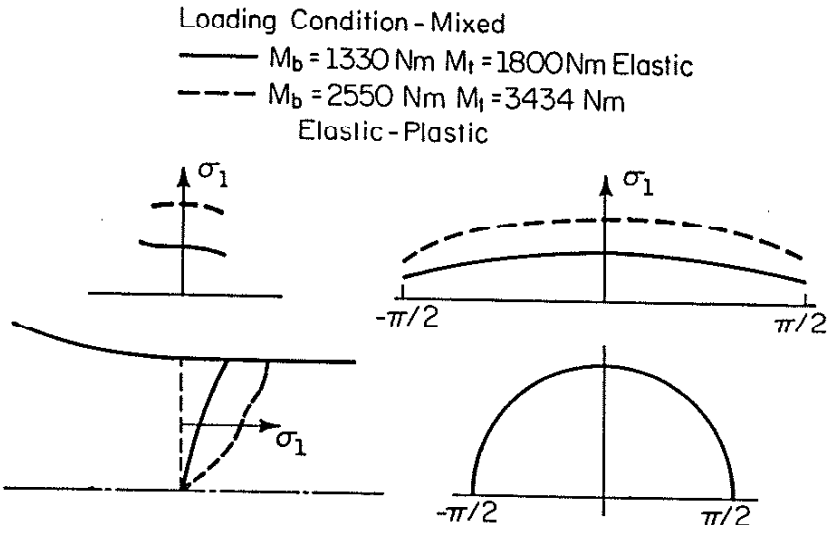

Figure 51 Stress Analysis for Combined Loading Condition of the Unnotched Shaft
(a) Strain State, (b) Stress Gradients

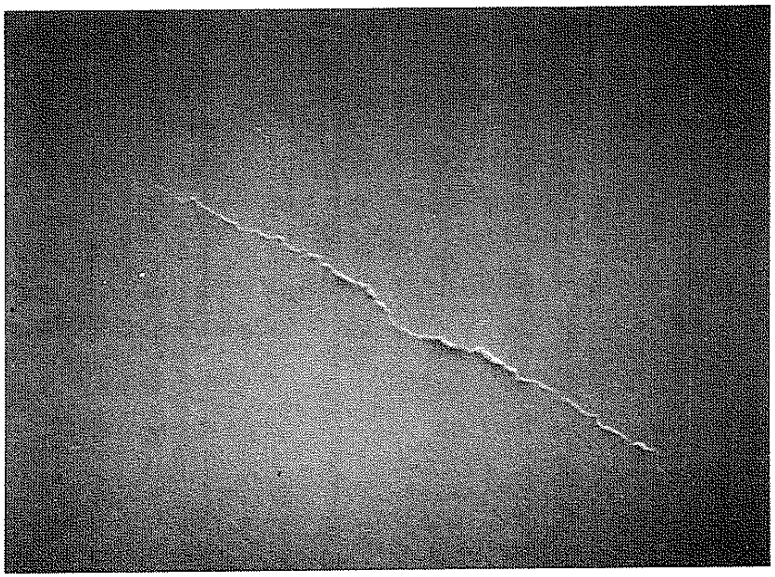

COMBINED LOADING (Polished)

UNNOTCHED SHAFT

M_b = 1330 Nm

M_t = 1800 Nm

N_f = 233150

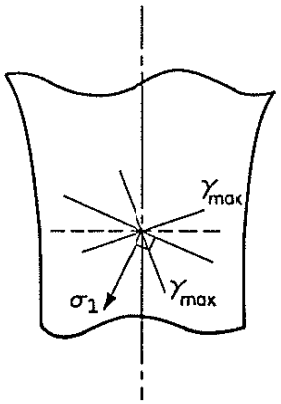

Figure 52a Crack Development During Combined Loading of the Unnotched Shaft (Polished)

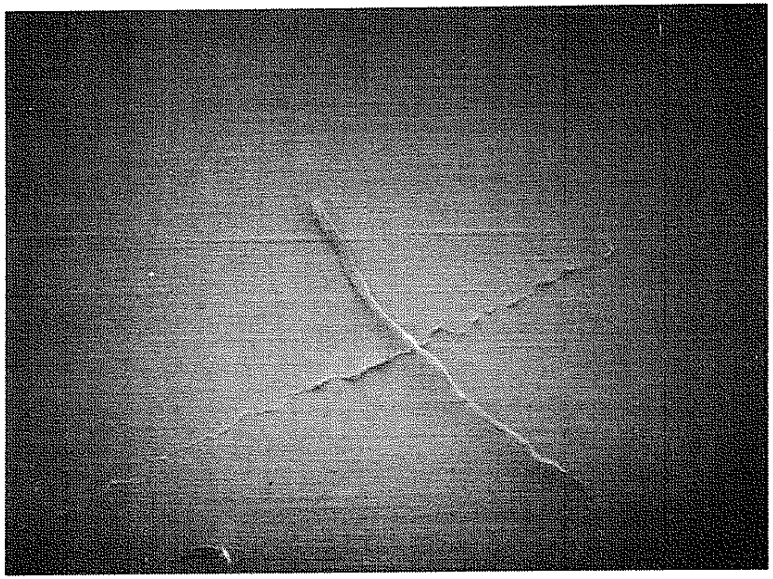

COMBINED LOADING (As Ground)

UNNOTCHED SHAFT

M_b = 1330 Nm

M_t = 1800 Nm

N_f = 211600

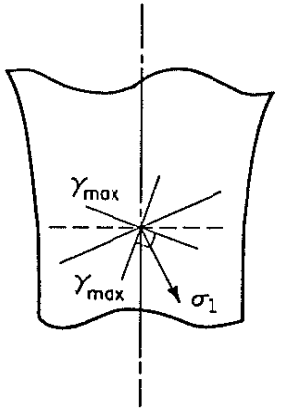

Figure 52b Crack Development During Combined Loading
of the Unnotched Shaft (as Ground)

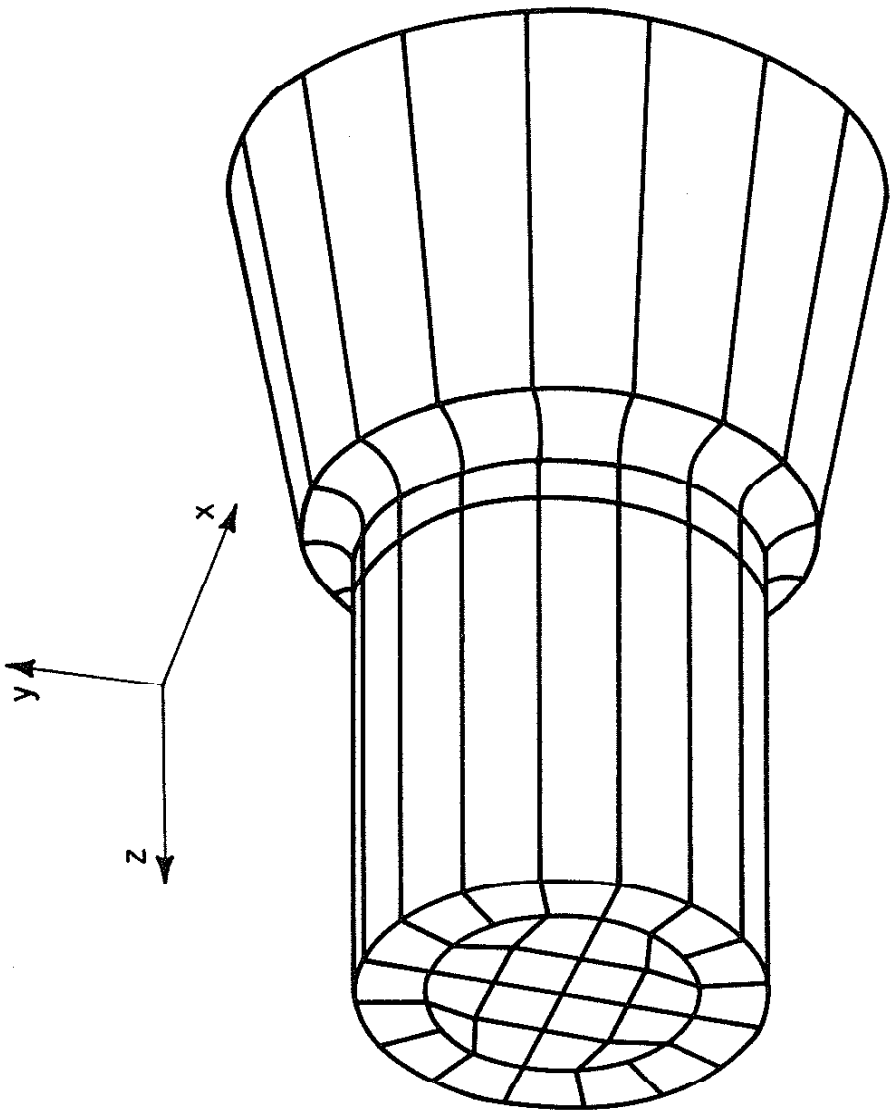

Figure A.1 Finite Element Mesh for Notched Shaft Specimen

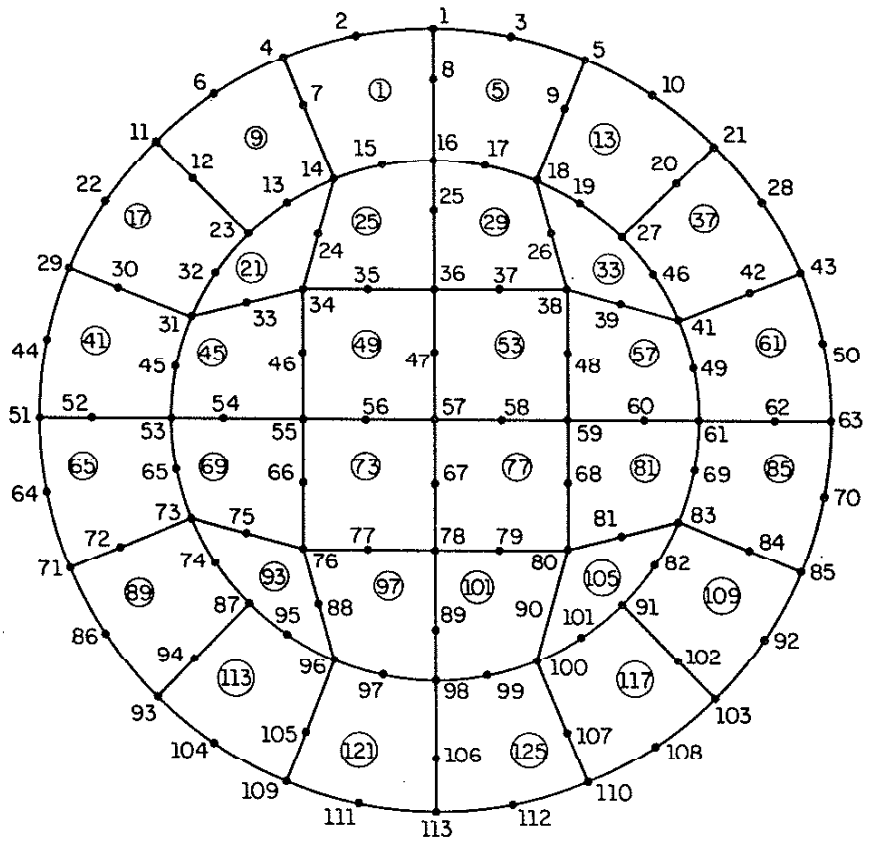

Figure A.2 Node Numbering in Cross Section of Finite Element Model

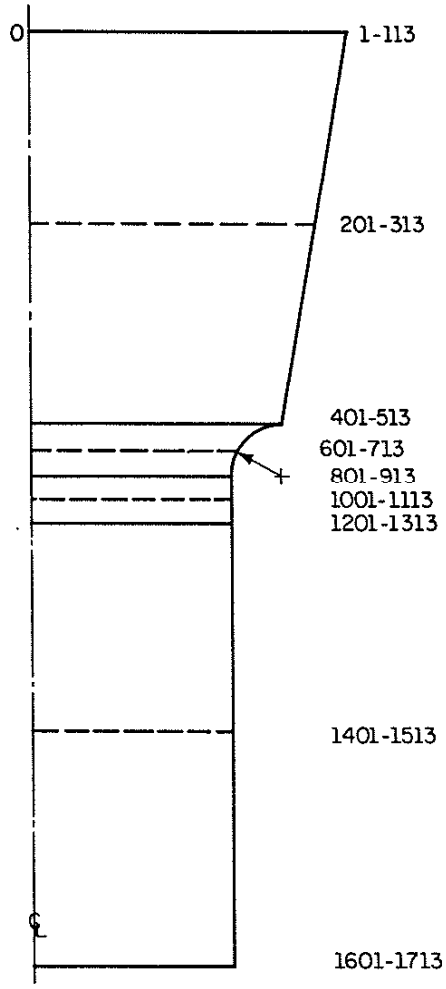

Figure A.3 Node Numbering in Layers of Notched Shaft Finite Element Model

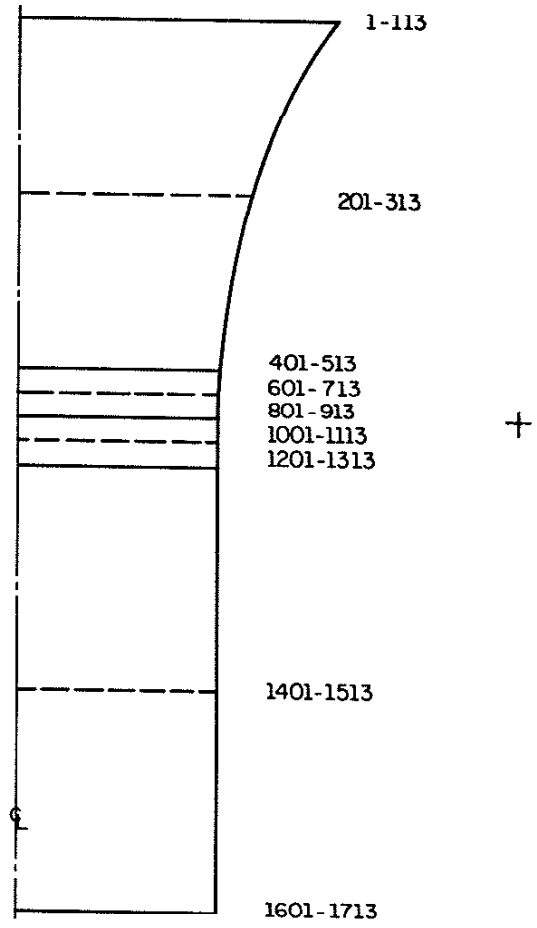

Figure A.4 Node Numbering in Layers of Unnotched Shaft Finite Element Model

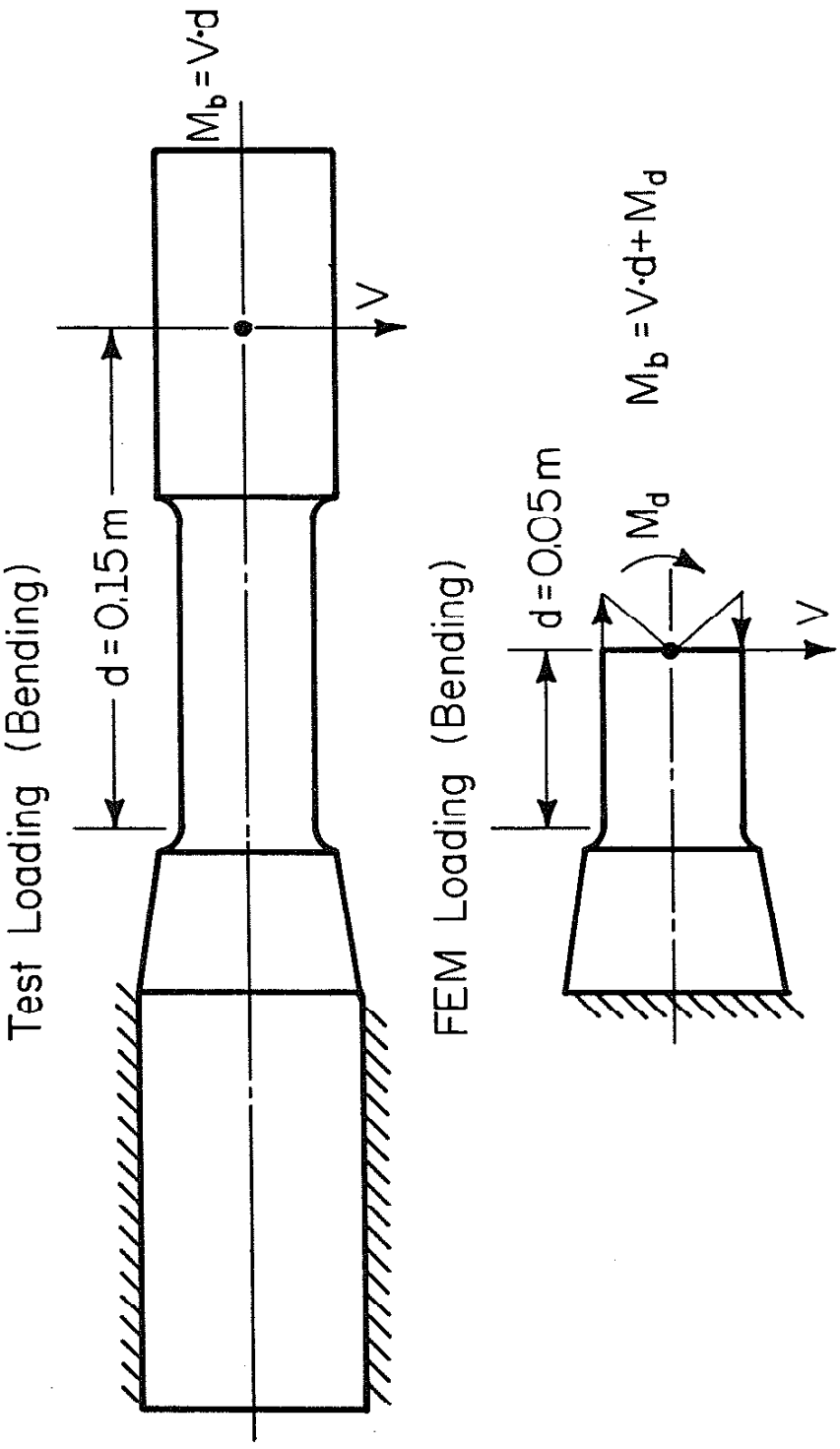

Figure A.5 Loading Conditions Applied in Finite Element Model to Achieve Correct Notch Root Bending Moments

APPENDIX A FINITE ELEMENT ANALYSIS

An elastic-plastic finite element analysis of the SAE notched shaft and the unnotched shaft has been developed using ABAQUES [48] and is given in APPENDIX B. Twenty noded, isoparameteric elements with a quadratic displacement function and a reduced integration scheme were implemented. An isotropic hardening model was employed to incorporate the strain hardening behavior of the 1045 steel. Cyclic stress-strain properties for the longitudinal smooth specimen tests were represented in a piece-wise linear manner (50 steps) for the plasticity model. A complete list of FEM results for the critical region at the point of tangency of the fillet radii and the parallel gage section are given in Table 6. The finite element mesh, node, and element definitions are presented in Figs. A.1, A.2, A.3, and A.4. Node definitions (Fig. A.2) are shown for the first layer of nodes at the big end of the specimen. Each successive layer follows the same numbering scheme with an increment of 200 (i.e. node 201, is in the same position as node 1 but in the next layer). The numbering and position of the nine layers of nodes in the model are presented in Fig. A.3 and A.4 for the notched and unnotched shafts, respectively. Nodes of particular interest at the critical tangent point of the radii and gage section are numbered 801 and 913.

The finite element model represents only the portion of the shaft required to obtain adequate solutions in the notch region, not the entire specimen. Nodes at the big end of the model were fixed in three directions to represent the clamped end of the specimen. In order to achieve the proper proportion of shear and normal stresses in the notch

root, the loading shown in Fig. A.5 was applied. A vertical force V equal to that applied in the experimental test specimen was applied by distributing this force over all end nodes. To achieve the proper bending moment in the notch root, a distributed moment (M_d) was also applied. This combination resulted in a bending moment equal to that applied in the experimental program. Torsional moments were achieved by applying point forces on the end nodes perpendicular to a radial trace.

From elastic solutions for bending and torsion the elastic stress concentration factors have been determined to be $K_{bending} = 1.61$ and $K_{torsion} = 1.39$. Petersons Handbook [50] gives values of $K_{bending} = 1.60$ and $K_{torsion} = 1.27$. Material at the specimen surface experiences a state of plane stress (i.e., no surface tractions) and accurate numerical solution should reflect this. Numerical tolerances in the FEM lead to small values of surface tractions for the analysis performed. These were always less than 5 percent of the maximum principal stress value.

APPENDIX B ABAQUES COMPUTER PROGRAM FOR SHAFT ANALYSIS

```
**************************************************************
**
**        THE FOLLOWING IS A ABAQUES JOB FILE
**        FOR PERFORMING AN ELASTIC-PLASTICE
**        FINITE ELEMENT MODEL OF THE S.A.E.
**        NOTCHED SHAFT GEOMETRY.
**
**************************************************************
**
*HEADING,CORE=80000
  ELASTIC/PLASTIC NOTCHED SHAFT MIXED LOADING  BEND=TOR
**
**************************************************************
**        NODES ARE DEFINED BY THEIR NUMBER AND THE
**        X, Y, AND Z COORDINATES.
**
**************************************************************
*NODE
  1,0.000000,0.031750,0.000000
  2,-0.006190,0.031140,0.000000
  3,0.006190,0.031140,0.000000
  4,-0.012150,0.029330,0.000000
  5,0.012150,0.029330,0.000000
  6,-0.017640,0.026400,0.000000
  7,-0.010530,0.025420,0.000000
  8,0.000000,0.027520,0.000000
  9,0.010530,0.025420,0.000000
  10,0.017640,0.026400,0.000000
  11,-0.022450,0.022450,0.000000
  12,-0.019460,0.019460,0.000000
  13,-0.011760,0.017600,0.000000
  14,-0.008100,0.019550,0.000000
  15,-0.004130,0.020760,0.000000
  16,0.000000,0.021170,0.000000
  17,0.004130,0.020760,0.000000
  18,0.008100,0.019550,0.000000
  19,0.011760,0.017600,0.000000
  20,0.019460,0.019460,0.000000
  21,0.022450,0.022450,0.000000
  22,-0.026400,0.017640,0.000000
  23,-0.014970,0.014970,0.000000
  24,-0.009340,0.015070,0.000000
  25,0.000000,0.016930,0.000000
  26,0.009340,0.015070,0.000000
  27,0.014970,0.014970,0.000000
  28,0.026400,0.017640,0.000000
  29,-0.029330,0.012150,0.000000
  30,-0.025420,0.010530,0.000000
  31,-0.019550,0.008100,0.000000
  32,-0.017600,0.011760,0.000000
  33,-0.015070,0.009340,0.000000
  34,-0.010580,0.010580,0.000000
```

35,-0.005290,0.010580,0.000000
36,0.000000,0.010580,0.000000
37,0.005290,0.010580,0.000000
38,0.010580,0.010580,0.000000
39,0.015070,0.009340,0.000000
40,0.017600,0.011760,0.000000
41,0.019550,0.008100,0.000000
42,0.025420,0.010530,0.000000
43,0.029330,0.012150,0.000000
44,-0.031140,0.006190,0.000000
45,-0.020760,0.004130,0.000000
46,-0.010580,0.005290,0.000000
47,0.000000,0.005290,0.000000
48,0.010580,0.005290,0.000000
49,0.020760,0.004130,0.000000
50,0.031140,0.006190,0.000000
51,-0.031750,0.000000,0.000000
52,-0.027520,0.000000,0.000000
53,-0.021170,0.000000,0.000000
54,-0.016930,0.000000,0.000000
55,-0.010580,0.000000,0.000000
56,-0.005290,0.000000,0.000000
57,0.000000,0.000000,0.000000
58,0.005290,0.000000,0.000000
59,0.010580,0.000000,0.000000
60,0.016930,0.000000,0.000000
61,0.021170,0.000000,0.000000
62,0.027520,0.000000,0.000000
63,0.031750,0.000000,0.000000
64,-0.031140,-0.006190,0.000000
65,-0.020760,-0.004130,0.000000
66,-0.010580,-0.005290,0.000000
67,0.000000,-0.005290,0.000000
68,0.010580,-0.005290,0.000000
69,0.020760,-0.004130,0.000000
70,0.031140,-0.006190,0.000000
71,-0.029330,-0.012150,0.000000
72,-0.025420,-0.010530,0.000000
73,-0.019550,-0.008100,0.000000
74,-0.017600,-0.011760,0.000000
75,-0.015070,-0.009340,0.000000
76,-0.010580,-0.010580,0.000000
77,-0.005290,-0.010580,0.000000
78,0.000000,-0.010580,0.000000
79,0.005290,-0.010580,0.000000
80,0.010580,-0.010580,0.000000
81,0.015070,-0.009340,0.000000
82,0.017600,-0.011760,0.000000
83,0.019550,-0.008100,0.000000
84,0.025420,-0.010530,0.000000
85,0.029330,-0.012150,0.000000
86,-0.026400,-0.017640,0.000000
87,-0.014970,-0.014970,0.000000
88,-0.009340,-0.015070,0.000000
89,0.000000,-0.016930,0.000000

```
90,0.009340,-0.015070,0.000000
91,0.014970,-0.014970,0.000000
92,0.026400,-0.017640,0.000000
93,-0.022450,-0.022450,0.000000
94,-0.019460,-0.019460,0.000000
95,-0.011760,-0.017600,0.000000
96,-0.008100,-0.019550,0.000000
97,-0.004130,-0.020760,0.000000
98,0.000000,-0.021170,0.000000
99,0.004130,-0.020760,0.000000
100,0.008100,-0.019550,0.000000
101,0.011760,-0.017600,0.000000
102,0.019460,-0.019460,0.000000
103,0.022450,-0.022450,0.000000
104,-0.017640,-0.026400,0.000000
105,-0.010530,-0.025420,0.000000
106,0.000000,-0.027520,0.000000
107,0.010530,-0.025420,0.000000
108,0.017640,-0.026400,0.000000
109,-0.012150,-0.029330,0.000000
110,0.012150,-0.029330,0.000000
111,-0.006190,-0.031140,0.000000
112,0.006190,-0.031140,0.000000
113,0.000000,-0.031750,0.000000
201,0.000000,0.028380,0.020000
204,-0.010860,0.026220,0.020000
205,0.010860,0.026220,0.020000
211,-0.020060,0.020060,0.020000
214,-0.007240,0.017480,0.020000
216,0.000000,0.018920,0.020000
218,0.007240,0.017480,0.020000
221,0.020060,0.020060,0.020000
223,-0.013380,0.013380,0.020000
227,0.013380,0.013380,0.020000
229,-0.026220,0.010860,0.020000
231,-0.017480,0.007240,0.020000
234,-0.009460,0.009460,0.020000
236,0.000000,0.009460,0.020000
238,0.009460,0.009460,0.020000
241,0.017480,0.007240,0.020000
243,0.026220,0.010860,0.020000
251,-0.028380,0.000000,0.020000
253,-0.018920,0.000000,0.020000
255,-0.009460,0.000000,0.020000
257,0.000000,0.000000,0.020000
259,0.009460,0.000000,0.020000
261,0.018920,0.000000,0.020000
263,0.028380,0.000000,0.020000
271,-0.026220,-0.010860,0.020000
273,-0.017480,-0.007240,0.020000
276,-0.009460,-0.009460,0.020000
278,0.000000,-0.009460,0.020000
280,0.009460,-0.009460,0.020000
283,0.017480,-0.007240,0.020000
285,0.026220,-0.010860,0.020000
```

287,-0.013380,-0.013380,0.020000
291,0.013380,-0.013380,0.020000
293,-0.020060,-0.020060,0.020000
296,-0.007240,-0.017480,0.020000
298,0.000000,-0.018920,0.020000
300,0.007240,-0.017480,0.020000
303,0.020060,-0.020060,0.020000
309,-0.010860,-0.026220,0.020000
310,0.010860,-0.026220,0.020000
313,0.000000,-0.028370,0.020000
401,0.000000,0.025000,0.040000
402,-0.004880,0.024520,0.040000
403,0.004880,0.024520,0.040000
404,-0.009570,0.023100,0.040000
405,0.009570,0.023100,0.040000
406,-0.013890,0.020790,0.040000
407,-0.008290,0.020020,0.040000
408,0.000000,0.021670,0.040000
409,0.008290,0.020020,0.040000
410,0.013890,0.020790,0.040000
411,-0.017680,0.017680,0.040000
412,-0.015320,0.015320,0.040000
413,-0.009260,0.013860,0.040000
414,-0.006380,0.015400,0.040000
415,-0.003250,0.016350,0.040000
416,0.000000,0.016670,0.040000
417,0.003250,0.016350,0.040000
418,0.006380,0.015400,0.040000
419,0.009260,0.013860,0.040000
420,0.015320,0.015320,0.040000
421,0.017680,0.017680,0.040000
422,-0.020790,0.013890,0.040000
423,-0.011780,0.011790,0.040000
424,-0.007350,0.011870,0.040000
425,0.000000,0.013330,0.040000
426,0.007360,0.011870,0.040000
427,0.011790,0.011790,0.040000
428,0.020790,0.013890,0.040000
429,-0.023100,0.009570,0.040000
430,-0.020020,0.008290,0.040000
431,-0.015400,0.006380,0.040000
432,-0.013860,0.009260,0.040000
433,-0.011860,0.007360,0.040000
434,-0.008330,0.008330,0.040000
435,-0.004170,0.008330,0.040000
436,0.000000,0.008330,0.040000
437,0.004170,0.008330,0.040000
438,0.008330,0.008330,0.040000
439,0.011870,0.007360,0.040000
440,0.013860,0.009260,0.040000
441,0.015400,0.006380,0.040000
442,0.020020,0.008290,0.040000
443,0.023100,0.009570,0.040000
444,-0.024520,0.004880,0.040000
445,-0.016350,0.003250,0.040000

446,-0.008330,0.004170,0.040000
447,0.000000,0.004170,0.040000
448,0.008330,0.004170,0.040000
449,0.016350,0.003250,0.040000
450,0.024520,0.004880,0.040000
451,-0.025000,0.000000,0.040000
452,-0.021670,0.000000,0.040000
453,-0.016670,0.000000,0.040000
454,-0.013330,0.000000,0.040000
455,-0.008330,0.000000,0.040000
456,-0.004170,0.000000,0.040000
457,0.000000,0.000000,0.040000
458,0.004170,0.000000,0.040000
459,0.008330,0.000000,0.040000
460,0.013330,0.000000,0.040000
461,0.016670,0.000000,0.040000
462,0.021670,0.000000,0.040000
463,0.025000,0.000000,0.040000
464,-0.024520,-0.004880,0.040000
465,-0.016350,-0.003250,0.040000
466,-0.008330,-0.004170,0.040000
467,0.000000,-0.004170,0.040000
468,0.008330,-0.004170,0.040000
469,0.016350,-0.003250,0.040000
470,0.024520,-0.004880,0.040000
471,-0.023100,-0.009570,0.040000
472,-0.020020,-0.008290,0.040000
473,-0.015400,-0.006380,0.040000
474,-0.013860,-0.009260,0.040000
475,-0.011860,-0.007350,0.040000
476,-0.008330,-0.008330,0.040000
477,-0.004170,-0.008330,0.040000
478,0.000000,-0.008330,0.040000
479,0.004170,-0.008330,0.040000
480,0.008330,-0.008330,0.040000
481,0.011870,-0.007350,0.040000
482,0.013860,-0.009260,0.040000
483,0.015400,-0.006380,0.040000
484,0.020020,-0.008290,0.040000
485,0.023100,-0.009570,0.040000
486,-0.020790,-0.013890,0.040000
487,-0.011790,-0.011790,0.040000
488,-0.007350,-0.011860,0.040000
489,0.000000,-0.013330,0.040000
490,0.007360,-0.011860,0.040000
491,0.011790,-0.011790,0.040000
492,0.020790,-0.013890,0.040000
493,-0.017680,-0.017680,0.040000
494,-0.015320,-0.015320,0.040000
495,-0.009260,-0.013860,0.040000
496,-0.006380,-0.015400,0.040000
497,-0.003250,-0.016350,0.040000
498,0.000000,-0.016670,0.040000
499,0.003250,-0.016350,0.040000
500,0.006380,-0.015400,0.040000

501,0.009260,-0.013860,0.040000
502,0.015320,-0.015320,0.040000
503,0.017680,-0.017680,0.040000
504,-0.013890,-0.020790,0.040000
505,-0.008290,-0.020020,0.040000
506,0.000000,-0.021670,0.040000
507,0.008290,-0.020020,0.040000
508,0.013890,-0.020790,0.040000
509,-0.009570,-0.023100,0.040000
510,0.009570,-0.023100,0.040000
511,-0.004880,-0.024520,0.040000
512,0.004880,-0.024520,0.040000
513,0.000000,-0.025000,0.040000
601,0.000000,0.020730,0.041460
604,-0.007930,0.019150,0.041460
605,0.007930,0.019150,0.041460
611,-0.014660,0.014660,0.041460
614,-0.005290,0.012770,0.041460
616,0.000000,0.013820,0.041460
618,0.005290,0.012770,0.041460
621,0.014660,0.014660,0.041460
623,-0.009770,0.009770,0.041460
627,0.009770,0.009780,0.041460
629,-0.019150,0.007930,0.041460
631,-0.012770,0.005290,0.041460
634,-0.006910,0.006910,0.041460
636,0.000000,0.006910,0.041460
638,0.006910,0.006910,0.041460
641,0.012770,0.005290,0.041460
643,0.019150,0.007930,0.041460
651,-0.020730,0.000000,0.041460
653,-0.013820,0.000000,0.041460
655,-0.006910,0.000000,0.041460
657,0.000000,0.000000,0.041460
659,0.006910,0.000000,0.041460
661,0.013820,0.000000,0.041460
663,0.020730,0.000000,0.041460
671,-0.019150,-0.007930,0.041460
673,-0.012770,-0.005290,0.041460
676,-0.006910,-0.006910,0.041460
678,0.000000,-0.006910,0.041460
680,0.006910,-0.006910,0.041460
683,0.012770,-0.005290,0.041460
685,0.019150,-0.007930,0.041460
687,-0.009780,-0.009780,0.041460
691,0.009780,-0.009780,0.041460
693,-0.014660,-0.014660,0.041460
696,-0.005290,-0.012770,0.041460
698,0.000000,-0.013820,0.041460
700,0.005290,-0.012770,0.041460
703,0.014660,-0.014660,0.041460
709,-0.007930,-0.019150,0.041460
710,0.007930,-0.019150,0.041460
713,0.000000,-0.020730,0.041460
801,0.000000,0.020000,0.045000

802,-0.003900,0.019620,0.045000
803,0.003900,0.019620,0.045000
804,-0.007650,0.018480,0.045000
805,0.007650,0.018480,0.045000
806,-0.011110,0.016630,0.045000
807,-0.006630,0.016010,0.045000
808,0.000000,0.017330,0.045000
809,0.006630,0.016010,0.045000
810,0.011110,0.016630,0.045000
811,-0.014140,0.014140,0.045000
812,-0.012260,0.012260,0.045000
813,-0.007410,0.011090,0.045000
814,-0.005100,0.012320,0.045000
815,-0.002600,0.013080,0.045000
816,0.000000,0.013330,0.045000
817,0.002600,0.013080,0.045000
818,0.005100,0.012320,0.045000
819,0.007410,0.011090,0.045000
820,0.012260,0.012260,0.045000
821,0.014140,0.014140,0.045000
822,-0.016630,0.011110,0.045000
823,-0.009430,0.009430,0.045000
824,-0.005880,0.009490,0.045000
825,0.000000,0.010670,0.045000
826,0.005880,0.009490,0.045000
827,0.009430,0.009430,0.045000
828,0.016630,0.011110,0.045000
829,-0.018480,0.007650,0.045000
830,-0.016010,0.006630,0.045000
831,-0.012320,0.005100,0.045000
832,-0.011090,0.007410,0.045000
833,-0.009490,0.005880,0.045000
834,-0.006670,0.006670,0.045000
835,-0.003330,0.006670,0.045000
836,0.000000,0.006670,0.045000
837,0.003330,0.006670,0.045000
838,0.006670,0.006670,0.045000
839,0.009490,0.005880,0.045000
840,0.011090,0.007410,0.045000
841,0.012320,0.005100,0.045000
842,0.016010,0.006630,0.045000
843,0.018480,0.007650,0.045000
844,-0.019620,0.003900,0.045000
845,-0.013080,0.002600,0.045000
846,-0.006670,0.003330,0.045000
847,0.000000,0.003330,0.045000
848,0.006670,0.003330,0.045000
849,0.013080,0.002600,0.045000
850,0.019620,0.003900,0.045000
851,-0.020000,0.000000,0.045000
852,-0.017330,0.000000,0.045000
853,-0.013330,0.000000,0.045000
854,-0.010670,0.000000,0.045000
855,-0.006670,0.000000,0.045000
856,-0.003330,0.000000,0.045000

857,0.000000,0.000000,0.045000
858,0.003330,0.000000,0.045000
859,0.006670,0.000000,0.045000
860,0.010670,0.000000,0.045000
861,0.013330,0.000000,0.045000
862,0.017330,0.000000,0.045000
863,0.020000,0.000000,0.045000
864,-0.019620,-0.003900,0.045000
865,-0.013080,-0.002600,0.045000
866,-0.006670,-0.003330,0.045000
867,0.000000,-0.003330,0.045000
868,0.006670,-0.003330,0.045000
869,0.013080,-0.002600,0.045000
870,0.019620,-0.003900,0.045000
871,-0.018480,-0.007650,0.045000
872,-0.016010,-0.006630,0.045000
873,-0.012320,-0.005100,0.045000
874,-0.011090,-0.007410,0.045000
875,-0.009490,-0.005880,0.045000
876,-0.006670,-0.006670,0.045000
877,-0.003330,-0.006670,0.045000
878,0.000000,-0.006670,0.045000
879,0.003330,-0.006670,0.045000
880,0.006670,-0.006670,0.045000
881,0.009490,-0.005880,0.045000
882,0.011090,-0.007410,0.045000
883,0.012320,-0.005100,0.045000
884,0.016010,-0.006630,0.045000
885,0.018480,-0.007650,0.045000
886,-0.016630,-0.011110,0.045000
887,-0.009430,-0.009430,0.045000
888,-0.005880,-0.009490,0.045000
889,0.000000,-0.010670,0.045000
890,0.005880,-0.009490,0.045000
891,0.009430,-0.009430,0.045000
892,0.016630,-0.011110,0.045000
893,-0.014140,-0.014140,0.045000
894,-0.012260,-0.012260,0.045000
895,-0.007410,-0.011090,0.045000
896,-0.005100,-0.012320,0.045000
897,-0.002600,-0.013080,0.045000
898,0.000000,-0.013330,0.045000
899,0.002600,-0.013080,0.045000
900,0.005100,-0.012320,0.045000
901,0.007410,-0.011090,0.045000
902,0.012260,-0.012260,0.045000
903,0.014140,-0.014140,0.045000
904,-0.011110,-0.016630,0.045000
905,-0.006630,-0.016010,0.045000
906,0.000000,-0.017330,0.045000
907,0.006630,-0.016010,0.045000
908,0.011110,-0.016630,0.045000
909,-0.007650,-0.018480,0.045000
910,0.007650,-0.018480,0.045000
911,-0.003900,-0.019620,0.045000

912,0.003900,-0.019620,0.045000
913,0.000000,-0.020000,0.045000
1001,0.000000,0.020000,0.047500
1004,-0.007650,0.018480,0.047500
1005,0.007650,0.018480,0.047500
1011,-0.014140,0.014140,0.047500
1014,-0.005100,0.012320,0.047500
1016,0.000000,0.013330,0.047500
1018,0.005100,0.012320,0.047500
1021,0.014140,0.014140,0.047500
1023,-0.009430,0.009430,0.047500
1027,0.009430,0.009430,0.047500
1029,-0.018480,0.007650,0.047500
1031,-0.012320,0.005100,0.047500
1034,-0.006670,0.006670,0.047500
1036,0.000000,0.006670,0.047500
1038,0.006670,0.006670,0.047500
1041,0.012320,0.005100,0.047500
1043,0.018480,0.007650,0.047500
1051,-0.020050,0.000000,0.047500
1053,-0.013330,0.000000,0.047500
1055,-0.006670,0.000000,0.047500
1057,0.000000,0.000000,0.047500
1059,0.006670,0.000000,0.047500
1061,0.013330,0.000000,0.047500
1063,0.020000,0.000000,0.047500
1071,-0.018480,-0.007650,0.047500
1073,-0.012320,-0.005100,0.047500
1076,-0.006670,-0.006670,0.047500
1078,0.000000,-0.006670,0.047500
1080,0.006670,-0.006670,0.047500
1083,0.012320,-0.005100,0.047500
1085,0.018480,-0.007650,0.047500
1087,-0.009430,-0.009430,0.047500
1091,0.009430,-0.009430,0.047500
1093,-0.014140,-0.014140,0.047500
1096,-0.005100,-0.012320,0.047500
1098,0.000000,-0.013330,0.047500
1100,0.005100,-0.012320,0.047500
1103,0.014140,-0.014140,0.047500
1109,-0.007650,-0.018480,0.047500
1110,0.007650,-0.018480,0.047500
1113,0.000000,-0.020000,0.047500
1201,0.000000,0.020000,0.050000
1202,-0.003900,0.019620,0.050000
1203,0.003900,0.019620,0.050000
1204,-0.007650,0.018480,0.050000
1205,0.007650,0.018480,0.050000
1206,-0.011110,0.016630,0.050000
1207,-0.006630,0.016010,0.050000
1208,0.000000,0.017330,0.050000
1209,0.006630,0.016010,0.050000
1210,0.011110,0.016630,0.050000
1211,-0.014140,0.014140,0.050000
1212,-0.012260,0.012260,0.050000

1213,-0.007410,0.011090,0.050000
1214,-0.005100,0.012320,0.050000
1215,-0.002600,0.013080,0.050000
1216,0.000000,0.013330,0.050000
1217,0.002600,0.013080,0.050000
1218,0.005100,0.012320,0.050000
1219,0.007410,0.011090,0.050000
1220,0.012260,0.012260,0.050000
1221,0.014140,0.014140,0.050000
1222,-0.016630,0.011110,0.050000
1223,-0.009430,0.009430,0.050000
1224,-0.005880,0.009490,0.050000
1225,0.000000,0.010670,0.050000
1226,0.005880,0.009490,0.050000
1227,0.009430,0.009430,0.050000
1228,0.016630,0.011110,0.050000
1229,-0.018480,0.007650,0.050000
1230,-0.016010,0.006630,0.050000
1231,-0.012320,0.005100,0.050000
1232,-0.011090,0.007410,0.050000
1233,-0.009490,0.005880,0.050000
1234,-0.006670,0.006670,0.050000
1235,-0.003330,0.006670,0.050000
1236,0.000000,0.006670,0.050000
1237,0.003330,0.006670,0.050000
1238,0.006670,0.006670,0.050000
1239,0.009490,0.005880,0.050000
1240,0.011090,0.007410,0.050000
1241,0.012320,0.005100,0.050000
1242,0.016010,0.006630,0.050000
1243,0.018480,0.007650,0.050000
1244,-0.019620,0.003900,0.050000
1245,-0.013080,0.002600,0.050000
1246,-0.006670,0.003330,0.050000
1247,0.000000,0.003330,0.050000
1248,0.006670,0.003330,0.050000
1249,0.013080,0.002600,0.050000
1250,0.019620,0.003900,0.050000
1251,-0.020050,0.000000,0.050000
1252,-0.017330,0.000000,0.050000
1253,-0.013330,0.000000,0.050000
1254,-0.010670,0.000000,0.050000
1255,-0.006670,0.000000,0.050000
1256,-0.003330,0.000000,0.050000
1257,0.000000,0.000000,0.050000
1258,0.003330,0.000000,0.050000
1259,0.006670,0.000000,0.050000
1260,0.010670,0.000000,0.050000
1261,0.013330,0.000000,0.050000
1262,0.017330,0.000000,0.050000
1263,0.020000,0.000000,0.050000
1264,-0.019620,-0.003900,0.050000
1265,-0.013080,-0.002600,0.050000
1266,-0.006670,-0.003330,0.050000
1267,0.000000,-0.003330,0.050000

```
1268,0.006670,-0.003330,0.050000
1269,0.013080,-0.002600,0.050000
1270,0.019620,-0.003900,0.050000
1271,-0.018480,-0.007650,0.050000
1272,-0.016010,-0.006630,0.050000
1273,-0.012320,-0.005100,0.050000
1274,-0.011090,-0.007410,0.050000
1275,-0.009490,-0.005880,0.050000
1276,-0.006670,-0.006670,0.050000
1277,-0.003330,-0.006670,0.050000
1278,0.000000,-0.006670,0.050000
1279,0.003330,-0.006670,0.050000
1280,0.006670,-0.006670,0.050000
1281,0.009490,-0.005880,0.050000
1282,0.011090,-0.007410,0.050000
1283,0.012320,-0.005100,0.050000
1284,0.016010,-0.006630,0.050000
1285,0.018480,-0.007650,0.050000
1286,-0.016630,-0.011110,0.050000
1287,-0.009430,-0.009430,0.050000
1288,-0.005880,-0.009490,0.050000
1289,0.000000,-0.010670,0.050000
1290,0.005880,-0.009490,0.050000
1291,0.009430,-0.009430,0.050000
1292,0.016630,-0.011110,0.050000
1293,-0.014140,-0.014140,0.050000
1294,-0.012260,-0.012260,0.050000
1295,-0.007410,-0.011090,0.050000
1296,-0.005100,-0.012320,0.050000
1297,-0.002600,-0.013080,0.050000
1298,0.000000,-0.013330,0.050000
1299,0.002600,-0.013080,0.050000
1300,0.005100,-0.012320,0.050000
1301,0.007410,-0.011090,0.050000
1302,0.012260,-0.012260,0.050000
1303,0.014140,-0.014140,0.050000
1304,-0.011110,-0.016630,0.050000
1305,-0.006630,-0.016010,0.050000
1306,0.000000,-0.017330,0.050000
1307,0.006630,-0.016010,0.050000
1308,0.011110,-0.016630,0.050000
1309,-0.007650,-0.018480,0.050000
1310,0.007650,-0.018480,0.050000
1311,-0.003900,-0.019620,0.050000
1312,0.003900,-0.019620,0.050000
1313,0.000000,-0.020000,0.050000
1401,0.000000,0.020000,0.072500
1404,-0.007650,0.018480,0.072500
1405,0.007650,0.018480,0.072500
1411,-0.014140,0.014140,0.072500
1414,-0.005100,0.012320,0.072500
1416,0.000000,0.013330,0.072500
1418,0.005100,0.012320,0.072500
1421,0.014140,0.014140,0.072500
1423,-0.009430,0.009430,0.072500
```

1427,0.009430,0.009430,0.072500
1429,-0.018480,0.007650,0.072500
1431,-0.012320,0.005100,0.072500
1434,-0.006670,0.006670,0.072500
1436,0.000000,0.006670,0.072500
1438,0.006670,0.006670,0.072500
1441,0.012320,0.005100,0.072500
1443,0.018480,0.007650,0.072500
1451,-0.020050,0.000000,0.072500
1453,-0.013330,0.000000,0.072500
1455,-0.006670,0.000000,0.072500
1457,0.000000,0.000000,0.072500
1459,0.006670,0.000000,0.072500
1461,0.013330,0.000000,0.072500
1463,0.020000,0.000000,0.072500
1471,-0.018480,-0.007650,0.072500
1473,-0.012320,-0.005100,0.072500
1476,-0.006670,-0.006670,0.072500
1478,0.000000,-0.006670,0.072500
1480,0.006670,-0.006670,0.072500
1483,0.012320,-0.005100,0.072500
1485,0.018480,-0.007650,0.072500
1487,-0.009430,-0.009430,0.072500
1491,0.009430,-0.009430,0.072500
1493,-0.014140,-0.014140,0.072500
1496,-0.005100,-0.012320,0.072500
1498,0.000000,-0.013330,0.072500
1500,0.005100,-0.012320,0.072500
1503,0.014140,-0.014140,0.072500
1509,-0.007650,-0.018480,0.072500
1510,0.007650,-0.018480,0.072500
1513,0.000000,-0.020000,0.072500
1601,0.000000,0.020000,0.095000
1602,-0.003900,0.019620,0.095000
1603,0.003900,0.019620,0.095000
1604,-0.007650,0.018480,0.095000
1605,0.007650,0.018480,0.095000
1606,-0.011110,0.016630,0.095000
1607,-0.006630,0.016010,0.095000
1608,0.000000,0.017330,0.095000
1609,0.006630,0.016010,0.095000
1610,0.011110,0.016630,0.095000
1611,-0.014140,0.014140,0.095000
1612,-0.012260,0.012260,0.095000
1613,-0.007410,0.011090,0.095000
1614,-0.005100,0.012320,0.095000
1615,-0.002600,0.013080,0.095000
1616,0.000000,0.013330,0.095000
1617,0.002600,0.013080,0.095000
1618,0.005100,0.012320,0.095000
1619,0.007410,0.011090,0.095000
1620,0.012260,0.012260,0.095000
1621,0.014140,0.014140,0.095000
1622,-0.016630,0.011110,0.095000
1623,-0.009430,0.009430,0.095000

1624,-0.005880,0.009490,0.095000
1625,0.000000,0.010670,0.095000
1626,0.005880,0.009490,0.095000
1627,0.009430,0.009430,0.095000
1628,0.016630,0.011110,0.095000
1629,-0.018480,0.007650,0.095000
1630,-0.016010,0.006630,0.095000
1631,-0.012320,0.005100,0.095000
1632,-0.011090,0.007410,0.095000
1633,-0.009490,0.005880,0.095000
1634,-0.006670,0.006670,0.095000
1635,-0.003330,0.006670,0.095000
1636,0.000000,0.006670,0.095000
1637,0.003330,0.006670,0.095000
1638,0.006670,0.006670,0.095000
1639,0.009490,0.005880,0.095000
1640,0.011090,0.007410,0.095000
1641,0.012320,0.005100,0.095000
1642,0.016010,0.006630,0.095000
1643,0.018480,0.007650,0.095000
1644,-0.019620,0.003900,0.095000
1645,-0.013080,0.002600,0.095000
1646,-0.006670,0.003330,0.095000
1647,0.000000,0.003330,0.095000
1648,0.006670,0.003330,0.095000
1649,0.013080,0.002600,0.095000
1650,0.019620,0.003900,0.095000
1651,-0.020050,0.000000,0.095000
1652,-0.017330,0.000000,0.095000
1653,-0.013330,0.000000,0.095000
1654,-0.010670,0.000000,0.095000
1655,-0.006670,0.000000,0.095000
1656,-0.003330,0.000000,0.095000
1657,0.000000,0.000000,0.095000
1658,0.003330,0.000000,0.095000
1659,0.006670,0.000000,0.095000
1660,0.010670,0.000000,0.095000
1661,0.013330,0.000000,0.095000
1662,0.017330,0.000000,0.095000
1663,0.020000,0.000000,0.095000
1664,-0.019620,-0.003900,0.095000
1665,-0.013080,-0.002600,0.095000
1666,-0.006670,-0.003330,0.095000
1667,0.000000,-0.003330,0.095000
1668,0.006670,-0.003330,0.095000
1669,0.013080,-0.002600,0.095000
1670,0.019620,-0.003900,0.095000
1671,-0.018480,-0.007650,0.095000
1672,-0.016010,-0.006630,0.095000
1673,-0.012320,-0.005100,0.095000
1674,-0.011090,-0.007410,0.095000
1675,-0.009490,-0.005880,0.095000
1676,-0.006670,-0.006670,0.095000
1677,-0.003330,-0.006670,0.095000
1678,0.000000,-0.006670,0.095000

```
1679,0.003330,-0.006670,0.095000
1680,0.006670,-0.006670,0.095000
1681,0.009490,-0.005880,0.095000
1682,0.011090,-0.007410,0.095000
1683,0.012320,-0.005100,0.095000
1684,0.016010,-0.006630,0.095000
1685,0.018480,-0.007650,0.095000
1686,-0.016630,-0.011110,0.095000
1687,-0.009430,-0.009430,0.095000
1688,-0.005880,-0.009490,0.095000
1689,0.000000,-0.010670,0.095000
1690,0.005880,-0.009490,0.095000
1691,0.009430,-0.009430,0.095000
1692,0.016630,-0.011110,0.095000
1693,-0.014140,-0.014140,0.095000
1694,-0.012260,-0.012260,0.095000
1695,-0.007410,-0.011090,0.095000
1696,-0.005100,-0.012320,0.095000
1697,-0.002600,-0.013080,0.095000
1698,0.000000,-0.013330,0.095000
1699,0.002600,-0.013080,0.095000
1700,0.005100,-0.012320,0.095000
1701,0.007410,-0.011090,0.095000
1702,0.012260,-0.012260,0.095000
1703,0.014140,-0.014140,0.095000
1704,-0.011110,-0.016630,0.095000
1705,-0.006630,-0.016010,0.095000
1706,0.000000,-0.017330,0.095000
1707,0.006630,-0.016010,0.095000
1708,0.011110,-0.016630,0.095000
1709,-0.007650,-0.018480,0.095000
1710,0.007650,-0.018480,0.095000
1711,-0.003900,-0.019620,0.095000
1712,0.003900,-0.019620,0.095000
1713,0.000000,-0.020000,0.095000
**
**************************************************************
**
**        NODE SETS DEFINED FOR FIXED NODES (BOTT)
**        AND LOADED NODES (TOPP).
**
**************************************************************
**
*NSET,NSET=BOTT,GENERATE
1,113
*NSET,NSET=TOPP,GENERATE
1601,1713
**
**************************************************************
**
**        TWENTY NODED BRICK ELEMENTS ARE DEFINED
**        BY NUMBER AND THE NODES THAT
**        COMPRISE THE ELEMENT.
**
**************************************************************
```

```
**
*ELEMENT,TYPE=C3D20R
1,  4,14,16,1, 404,414,416,401, 7,15,8,2, 407,415,408
   402, 204,214,216,201
5,  1,16,18,5, 401,416,418,405, 8,17,9,3, 408,417,409
   403, 201,216,218,205
9,  11,23,14,4, 411,423,414,404, 12,13,7,6, 412,413,407
   406, 211,223,214,204
13,  5,18,27,21, 405,418,427,421, 9,19,20,10, 409,419,420
   410, 205,218,227,221
17,  29,31,23,11, 429,431,423,411, 30,32,12,22, 430,432,412
   422, 229,231,223,211
21,  23,31,34,14, 423,431,434,414, 32,33,24,13, 432,433,424
   413, 223,231,234,214
25,  14,34,36,16, 414,434,436,416, 24,35,25,15, 424,435,425
   415, 214,234,236,216
29,  16,36,38,18, 416,436,438,418, 25,37,26,17, 425,437,426
   417, 216,236,238,218
33,  18,38,41,27, 418,438,441,427, 26,39,40,19, 426,439,440
   419, 218,238,241,227
37,  21,27,41,43, 421,427,441,443, 20,40,42,28, 420,440,442
   428, 221,227,241,243
41,  29,51,53,31, 429,451,453,431, 44,52,45,30, 444,452,445
   430, 229,251,253,231
45,  31,53,55,34, 431,453,455,434, 45,54,46,33, 445,454,446
   433, 231,253,255,234
49,  34,55,57,36, 434,455,457,436, 46,56,47,35, 446,456,447
   435, 234,255,257,236
53,  36,57,59,38, 436,457,459,438, 47,58,48,37, 447,458,448
   437, 236,257,259,238
57,  38,59,61,41, 438,459,461,441, 48,60,49,39, 448,460,449
   439, 238,259,261,241
61,  41,61,63,43, 441,461,463,443, 49,62,50,42, 449,462,450
   442, 241,261,263,243
65,  51,71,73,53, 451,471,473,453, 64,72,65,52, 464,472,465
   452, 251,271,273,253
69,  53,73,76,55, 453,473,476,455, 65,75,66,54, 465,475,466
   454, 253,273,276,255
73, 55,76,78,57, 455,476,478,457, 66,77,67,56, 466,477,467
   456, 255,276,278,257
77,  57,78,80,59, 457,478,480,459, 67,79,68,58, 467,479,468
   458, 257,278,280,259
81, 59,80,83,61, 459,480,483,461, 68,81,69,60, 468,481,469
   460, 259,280,283,261
85,  61,83,85,63, 461,483,485,463, 69,84,70,62, 469,484,470
   462, 261,283,285,263
89, 71,93,87,73, 471,493,487,473, 86,94,74,72, 486,494,474
   472, 271,293,287,273
93, 73,87,96,76, 473,487,496,476, 74,95,88,75, 474,495,488
   475, 273,287,296,276
97, 76,96,98,78, 476,496,498,478, 88,97,89,77, 488,497,489
   477, 276,296,298,278
101,78,98,100,80,478,498,500,480,89,99,90,79,489,499,490
   479,278,298,300,280
105,80,100,91,83,480,500,491,483,90,101,82,81,490,501,482
```

```
   481,280,300,291,283
109,83,91,103,85,483,491,503,485,82,102,92,84,482,502,492
   484,283,291,303,285
113,93,109,96,87,493,509,496,487,104,105,95,94,504,505,495
   494,293,309,296,287
117,100,110,103,91,500,510,503,491,107,108,102,101,507,508,502
   501,300,310,303,291
121,96,109,113,98,496,509,513,498,105,111,106,97,505,511,506
   497,296,309,313,298
125,98,113,110,100,498,513,510,500,106,112,107,99,506,512,507
   499,298,313,310,300
**
**
*ELGEN,ELSET=ALL
1,4,400
5,4,400
9,4,400
13,4,400
17,4,400
21,4,400
25,4,400
29,4,400
33,4,400
37,4,400
41,4,400
45,4,400
49,4,400
53,4,400
57,4,400
61,4,400
65,4,400
69,4,400
73,4,400
77,4,400
81,4,400
85,4,400
89,4,400
93,4,400
97,4,400
101,4,400
105,4,400
109,4,400
113,4,400
117,4,400
121,4,400
125,4,400
**
************************************************************
**
**        ELEMENT SET DEFINITION FOR NOTCH ELEMENTS.
**
************************************************************
**
*ELSET,ELSET=ONE
2,6,10,14,18,38,42,62,
```

```
66,86,90,110,114,118,122,126
26,30,50,54,74,78,98,102
3,7,11,15,19,39,43,63,
67,87,91,111,115,119,123,127
27,31,51,55,75,79,99,103
**
************************************************************
**
**       DEFINITION OF MATERIALS PROPERTIES
**       FOR ISOTROPIC HARDING MODEL. THE CYCLIC
**       STRESS-STRAIN CURVE IS IMPLIMENTED.
**
************************************************************
**
*MATERIAL,ELSET=ALL
*ELASTIC
2.02375E11,.3
*PLASTIC
2.06844E8
255.919E6,5.0E-4
296.511E6,1.0E-3
323.179E6,1.5E-3
343.542E6,2.0E-3
360.216E6,2.5E-3
374.439E6,3.0E-3
386.902E6,3.5E-3
398.033E6,4.0E-3
408.116E6,4.5E-3
417.352E6,5.0E-3
425.887E6,5.5E-3
433.831E6,6.0E-3
441.269E6,6.5E-3
448.270E6,7.0E-3
454.887E6,7.5E-3
461.166E6,8.0E-3
467.143E6,8.5E-3
472.849E6,9.0E-3
478.310E6,9.5E-3
483.55E6,0.01
488.587E6,0.0105
493.438E6,0.011
498.119E6,0.0115
502.642E6,0.012
507.020E6,0.0125
511.261E6,0.013
515.376E6,0.0135
519.372E6,0.014
523.258E6,0.0145
527.039E6,0.015
530.722E6,0.0155
534.313E6,0.016
537.817E6,0.0165
541.238E6,0.017
544.581E6,0.0175
547.849E6,0.018
```

```
551.047E6,0.0185
554.177E6,0.019
557.243E6,0.0195
560.247E6,0.02
587.440E6,0.025
610.635E6,0.03
630.959E6,0.035
649.110E6,0.04
665.554E6,0.045
680.616E6,0.05
694.535E6,0.055
707.490E6,0.06
*DENSITY
7780.
**
**************************************************************
**
**        BOUNDARY CONDITIONS.
**
**************************************************************
**
*BOUNDARY
BOTT,1,3
**
**************************************************************
**
**        DEFINE LOAD AMPLITUDES FOR THE ANALYSIS.
**        BENDING MOMENTS ARE SCALED TO 1000NM LOAD FILE.
**        TORSION MOMENTS ARE SCALED TO 2000NM LOAD FILE.
**
**************************************************************
**
*AMPLITUDE,NAME=B1
0.001,0.005,1.0,0.990
**
*AMPLITUDE,NAME=T1
0.001,0.005,1.0,0.695
**
**************************************************************
**
**        DEFINE LOAD STEP AND OUTPUT DATA.
**
**************************************************************
**
**
*STEP,MONOTONIC,INC=14,CYC=10
*STATIC,PTOL=1500.
**
*CLOAD,AMP=B1
*CLOAD,AMP=T1
**
**************************************************************
**
**        LOAD FILE FOR 1000NM BENDING MOMENT
**
```

```
TOPP,2,58.997
1601,3,-1047
1602,3,-1027
1603,3,-1027
1604,3,-967
1605,3,-967
1606,3,-870
1607,3,-838
1608,3,-907
1609,3,-838
1610,3,-870
1611,3,-740
1612,3,-642
1613,3,-580
1614,3,-645
1615,3,-685
1616,3,-698
1617,3,-685
1618,3,-645
1619,3,-580
1620,3,-642
1621,3,-740
1622,3,-582
1623,3,-494
1624,3,-497
1625,3,-558
1626,3,-497
1627,3,-494
1628,3,-582
1629,3,-400
1630,3,-347
1631,3,-267
1632,3,-388
1633,3,-308
1634,3,-349
1635,3,-349
1636,3,-349
1637,3,-349
1638,3,-349
1639,3,-308
1640,3,-388
1641,3,-267
1642,3,-347
1643,3,-400
1671,3,400
1672,3,347
1673,3,267
1674,3,388
1675,3,308
1676,3,349
1677,3,349
1678,3,349
1679,3,349
1680,3,349
1681,3,308
```

```
1682,3,388
1683,3,267
1684,3,347
1685,3,400
1686,3,582
1687,3,494
1688,3,497
1689,3,558
1690,3,497
1691,3,494
1692,3,582
1693,3,740
1694,3,642
1695,3,580
1696,3,645
1697,3,685
1698,3,698
1699,3,685
1700,3,645
1701,3,580
1702,3,642
1703,3,740
1704,3,870
1705,3,838
1706,3,907
1707,3,838
1708,3,870
1709,3,967
1710,3,967
1711,3,1027
1712,3,1027
1713,3,1047
**
**        END OF 1000NM BENDING MOMENT FILE.
**
************************************************************
**
************************************************************
**
**        FILE FOR 2000NM TORSION MOMENT
**
**
 1601 1 1488.27
 1602 1 1459.7
 1602 2 290.35
 1603 2 -290.35
 1603 1 1459.7
 1604 2 569.5
 1604 1 1374.9
 1605 1 1374.9
 1605 2 -569.5
 1606 1 1237.4
 1606 2 826.8
 1607 1 1374.9
 1607 2 569.5
```

```
1608 1 1488.27
1609 1 1374.9
1609 2 -569.5
1610 1 1237.4
1610 2 -826.8
1611 1 1052.4
1611 2 1052.4
1612 2 1052.4
1612 1 1052.4
1613 1 1237.4
1613 2 826.8
1614 2 569.5
1614 1 1374.9
1615 1 1459.7
1615 2 290.35
1616 1 1488.27
1617 1 1459.7
1617 2 -290.35
1618 1 1374.9
1618 2 -569.5
1619 2 -826.8
1619 1 1237.4
1620 2 -1052.4
1620 1 1052.4
1621 1 1052.4
1621 2 -1052.4
1622 2 1237.5
1622 1 826.8
1623 2 1052.4
1623 1 1052.4
1627 2 -1052.4
1627 1 1052.4
1628 2 -1237.5
1628 1 826.8
1629 2 1374.98
1629 1 569.5
1630 1 569.5
1630 2 1374.98
1631 2 1374.98
1631 1 569.5
1632 2 1237.5
1632 1 826.8
1640 2 -1237.5
1640 1 826.8
1641 2 -1374.98
1641 1 569.5
1642 1 569.5
1642 2 -1374.98
1643 2 -1374.98
1643 1 569.5
1644 2 1459.7
1644 1 290.4
1645 1 290.4
1645 2 1459.7
1649 2 -1459.7
```

```
1649 1 290.4
1650 1 290.4
1650 2 -1459.7
1651 2 1488.3
1652 2 1488.3
1653 2 1488.3
1661 2 -1488.3
1662 2 -1488.3
1663 2 -1488.3
1664 1 -290.4
1664 2 1459.7
1665 1 -290.4
1665 2 1459.7
1669 2 -1459.7
1669 1 -290.4
1670 2 -1459.7
1670 1 -290.4
1671 2 1374.98
1671 1 -569.5
1672 1 -569.5
1672 2 1374.98
1673 1 -569.5
1673 2 1374.98
1674 2 1237.5
1674 1 -826.8
1682 1 -826.8
1682 2 -1237.5
1683 2 -1374.98
1683 1 -569.5
1684 2 -1374.98
1684 1 -569.5
1685 2 -1374.98
1685 1 -569.5
1686 1 -826.8
1686 2 1237.5
1687 2 1052.4
1687 1 -1052.4
1691 1 -1052.4
1691 2 -1052.4
1692 2 -1237.5
1692 1 -826.8
1693 1 -1052.4
1693 2 1052.4
1694 1 -1052.4
1694 2 1052.4
1695 1 -1237.4
1695 2 826.8
1696 2 569.5
1696 1 -1374.9
1697 1 -1459.7
1697 2 290.35
1698 1 -1488.3
1699 2 -290.35
1699 1 -1459.7
1700 1 -1374.9
```

```
 1700 2 -569.5
 1701 2 -826.8
 1701 1 -1237.4
 1702 1 -1052.4
 1702 2 -1052.4
 1703 1 -1052.4
 1703 2 -1052.4
 1704 2 826.8
 1704 1 -1237.4
 1705 2 569.5
 1705 1 -1374.9
 1706 1 -1488.3
 1707 1 -1374.9
 1707 2 -569.5
 1708 1 -1237.4
 1708 2 -826.8
 1709 1 -1374.9
 1709 2 569.5
 1710 2 -569.5
 1710 1 -1374.9
 1711 1 -1459.7
 1711 2 290.35
 1712 2 -290.35
 1712 1 -1459.7
 1713 1 -1488.3
**
**       END FOR TORSION MOMENT FILE
************************************************************
**
************************************************************
**
**       OUTPUT REQUEST.
**
************************************************************
**
IPRINT,FREQ=20
*NODE PRINT
1,1,1,1
1,1,1,1
*EL PRINT,ELSET=ALL
1,1
1,1,1,1
1,1,1,1,1
*EL PRINT,ELSET=ONE
2,2
2,2,2,2
2,2,2,2,2
*END STEP
```

APPENDIX C SIMILITUDE IN CRACK DEVELOPMENT FOR SMOOTH AND NOTCHED SPECIMENS SUBJECTED TO UNIAXIAL LOADING

Initiation of the first crack during fatigue loading is a weakest link statistical problem. In the smooth specimen, a crack will initiate first at the most probable location. Two situations can then exist. First, if the bulk stress level and local metallurgical structure are favorable for further growth, this crack will continue to develop, and since growth is in a uniform stress-strain field the crack can rapidly grow to a catistrophic size. If this occurs very few other crack systems will develop. The second case is one where the local stress-strain and metallurgical structure are not favorable for growth of the first most probable crack that initiates. The second crack, which is slightly less favorable, than has time to initiate and if the local conditions are favorable will grow and result in failure. This is similar to the first situation except that the second or third, etc. most favorable initiation site is the one that has favorable growth conditions. In either case, once an initiated crack achieves favorable growth conditions, the probability of subsequent initiation and growth of other cracks is reduced since the local stress field at the developing crack becomes dominant, relieving the surrounding stress-strain field and resulting in relatively rapid growth to failure.

In the case of notched members the situation is different. In the first place, the local critical area over which to consider the statistical probability of critical initiation sites is usually much smaller than the surface area of the smooth specimen, particularly in the case of the thin-wall tube and notched shaft. This is a size effect consideration. Initiation of the first crack then occurs at the first

consideration. Initiation of the first crack then occurs at the first most probable location in the notch region. If the local stress-strain and metallurgical conditions are favorable for microgrowth, this crack will begin to develop. Its growth rate decreases rapidly however, since growth is still controlled by the local notch stress-strain field that is decreasing rapidly in the direction of growth. Rather than becoming a dominant crack, this first crack to initiate slows or stop growing. In this scenario, the second most probable crack initiation site has an opportunity to develop a crack, which then has a similar period of decreasing growth rate. Similar behavior will occur at other probable initiation sites in the notch until there are several microcracks present. This has been shown for several multiaxial loading conditions in this thesis and was shown for axial loading of an edge notched plate [C1]. At some point, (again a consideration of the statistical distribution) the developing cracks will begin to interact with one another. Eventually, a single dominant crack develops from linking of the many small cracks and the crack tip stress field rather than the notch stress-strain field, begins to dominate the growth behavior. It is sometime after this point that an "engineering size" crack (0.5 - 5.0 mm) will become visible on the surface of the specimen at the root of the notch. This linking process, to form a "engineering size" crack on the surface, may, in part, be responsible for the anomalous short crack behavior often reported [C2].

Similitude between the smooth and notched specimen is likely to exist in the initiation of the first most probable crack if the local strains are similar. The microgrowth behavior, however, is very

different. A single crack dominates very soon in the smooth specimen. In the notch problem several cracks form before a single dominant crack forms. The question of macrocrack growth does not enter into the consideration of these two specimen geometries, since little or no macrogrowth exists in the smooth specimen.

Crack initiation and growth in a notched member subjected to multiaxial fatigue differs from the uniaxial case. Similar to the uniaxial notch problem, multiple cracks form in the notch of the SAE shaft. At low and medium amplitudes though, the stress state causes these cracks to grow out of the notch at an angle when the growth switches to stage II. This results in the growth of individual cracks parallel to one another rather than the crack linking process described above for the uniaxial notch case. Only at high amplitudes is crack nucleation so extensive that a linking process plays a role in the rate and development of the failure crack in the notched shaft.

Reference

C.1 Nowack, H., Hanschmann, D., Foth, J., Lütjering, G. and Jacoby, G., "Prediction Capability and Improvements of the Numerical Notch Analysis for Fatigue Loaded Aircraft and Automotive Components," Low-Cycle Fatigue and Life Prediction, ASTM STP 770, American Society for Testing and Materials, (1982), pp. 269-295.

C.2 Leis, B. N., and Forte, T. P., "Fatigue Growth of Initially Physically Short Cracks in Notched Aluminum and Steel Plates," Fracture Mechanics: Thirteenth Conference, ASTM STP 743, American Society for Testing and Materials, (1981), pp. 100-124.

REFERENCES

1. Ewing, J. A. and Humfrey, J. C. W. "The Fracture of Metals under Repeated Alternations of Stress," Phil. Trans. Royal Soc., Vol. 200, (1903), pp. 241-253.

2. Wood, W. A., "Recent Observations on Fatigue Fracture in Metals," ASTM STP 237, Symposium on Basic Mechanisms of Fatigue, American Society for Testing and Materials, (1958), pp. 110-121.

3. Peterson, R. E., "Fatigue Cracks and Fracture Surfaces - Mechanics of Development and Visual Appearance," in Metal Fatigue. Edited by George Sines and J. L. Waisman, McGraw Hill Book Company, (1959), pp. 68-86.

4. Forsyth, P. J. E., "Two Stage Process of Fatigue Crack Growth," Proceedings Crack Propagation Symposium, Cranfield, England, (1961), pp. 76-94.

5. Neumann, P., "Coarse Slip Model of Fatigue," Acta Metallurgica, Vol. 17, (1969), pp. 1219-1225.

6. Laird, C., "The Influence of Metallurgical Structure on the Mechanisms of Fatigue Crack Propagation," Fatigue Crack Propagation, ASTM STP 415, American Society for Testing and Materials, (1967), pp. 131-180.

7. Broek, D., Elementary Engineering Fracture Mechanics, Sijthoff and Noordhoff publishers, The Netherlands, (1978).

8. Edited by R. M. Wetzel, Fatigue Under Complex Loading: Analysis and Experiments, Advances in Engineering, Vol. 6, Society of Automotive Engineers, (1977).

9. Edited by R. M. Wetzel, Manual on Low Cycle Fatigue Testing, ASTM STP 465, American Society for Testing and Materials, (1969).

10. Watson, P. and Hill, S. J., "Fatigue Life Assessment of Ground Vehicle Components," Design of Fatigue and Fracture Resistant Structures, ASTM STP 761, American Society for Testing and Materials, (1982), pp. 5-27.

11. Dowling, N. E., "Crack Growth During Low-Cycle Fatigue of Smooth Axial Specimens," Cyclic Stress-Strain and Plastic Deformation Aspects of Fatigue Crack Growth, ASTM STP 637, American Society for Testing and Materials, (1977), pp. 97-121.

12. Fash, J. W., Socie, D. F., Russell, E. S., "Fatigue Crack Initiation and Growth in Gray Cast Iron," Materials, Experimentation and Design in Fatigue. Proceedings of Fatigue '81, Society of Environmental Engineers, Fatigue Group Conference, Warwick University, England, Westbury House, (1981), pp. 40-51.

13. Hua, C. T. and Socie, D. F., "Fatigue Damage in 1045 Steel Under Constant Amplitude Biaxial Loading," Fatigue of Engineering Materials and Structures, Vol. 7, No. 3, (1984), pp. 165-179.

14. Krempl, E., "The Influence of State of Stress on Low Cycle Fatigue of Structural Materials: A Literature Survey and Interpretive Report," ASTM STP 549, American Society for Materials and Testing, (1974).

15. Garud, Y. S., "Multiaxial Fatigue: A Survey of the State of the Art," Journal of Testing and Evaluation, JTEVA, Vol. 9, No. 3, (1981), pp. 165-178.

16. Miller, K. J. and Brown, M. W., "Multiaxial Fatigue: A Brief Review," Proceedings of the 6th ICF, New Delhi, India. To be published by Pergamon Press, (1984).

17. Tipton, S. M., "Fatigue Behavior Under Multiaxial Loading in the Presence of a Notch: Methodologies for the Prediction of Life to Crack Initiation and Life Spent in Crack Propagation," Ph.D. Thesis, Stanford University, Stanford, California (1984).

18. Libertiny, G. F., "Short Life Fatigue Under Combined Stresses," Journal of Strain Analysis, Vol. 2, No. 1, (1967), pp. 91-95.

19. Yokobori, T., Yamanouchi, H. and Yamamoto, S., "Low Cycle Fatigue of Thin-Walled Cylindrical Specimens of Mild Steel in Uni-axial and Torsional Tests at Constant Strain Amplitude," International Journal of Fracture, Vol. 1-2, (1966) pp. 3-13.

20. Nadia, A., Plasticity: A Mechanics of the Plastic State of Matter, McGraw-Hill Book Company, Inc., (1931).

21. Findley, W. N., "Combined-Stress Fatigue Strength of 76S-T61 Aluminum Alloy with Superimposed Mean Stresses and Corrections for Yielding," Natural Advisory Committee for Aeronautics Technical Note #2924 (1953).

22. Stullen, F. B. and Cummings, H. N., "A Failure Criterion for Multiaxial Fatigue Stresses," Proceedings ASTM, Vol. 54, American Society for Testing and Materials, (1954), p. 822-836.

23. Brown, M. W. and Miller, K. J. "A Theory for Fatigue Failure Under Multiaxial Stress-Strain Conditions," Proceedings of the Institute of Mechanical Engineers, Vol. 187, No. 65, (1973), pp. 745-755.

24. Brown, M. W., and Miller, K. J., "Initiation and Growth of Cracks in Biaxial Fatigue," Fatigue of Engineering Materials and Structures, Vol. 1, (1979), pp. 231-246.

25. Lohr, R. D. and Ellison, E. G., "A Simple Theory for Low Cycle Multiaxial Fatigue," Fatigue of Engineering Materials and Structures, Vol. 3, (1980), pp. 1-17.

26. Socie, D. F., Waill, L. E. and Dittmer, D. F. "Biaxial Fatigue of Inconel 718 Including Mean Stress Effects," Multiaxial Fatigue, ASTM STP 853, American Society for Testing and Materials, (1982). To be published.

27. Fash, J. W., Socie, D. F. and McDowell, D. L., "Fatigue Life Estimates for a Simple Notched Component Under Biaxial Loading," Multiaxial Fatigue, ASTM STP 853, American Society for Testing and Materials, (1982). To be published.

28. Nishihara, Y. and Kawamoto, M., "The Strength of Metals under Combined Alternating Bending and Torsion," Memoirs of the College of Engineering, Kyota Imperial Univerity, Vol. X, No. 6, (1941), pp. 177-201.

29. Taira, S., Inoue, T. and Yoshida, T., "Low Cycle Fatigue under Multiaxial Stresses (In the case of Combined Cyclic Tension - Compression and Cyclic Torsion at Room Temperature," Proceedings of the Twelfth Japanese Congress on Materials Research, (1969), pp. 50-55.

30. Taira, S., Inoue, T. and Takahashi, M., "Low Cycle Fatigue under Multiaxial Stresses (in the case of Combined Cyclic Tension - Compression and Cyclic Torsion in the Same Phase at Elevated Temperatures)," Proceedings of the Tenth Japanese Congress on Materials Research, (1967), pp. 18-23.

31. Pascoe, K. J. and deVilliers, J. W. R., "Low Cycle Fatigue of Steels Under Biaxial Straining, "Journal of Strain Analysis, Vol. 2, No. 2, (1967), pp. 117-126.

32. Parsons, M. W. and Pascoe, K. J., "Observations of Surface Deformation, Crack Initiation and Crack Growth in Low Cycle Fatigue under Biaxial Stress," Materials Science and Engineering, Vol. 22, (1976), pp. 31-56.

33. Kanazawa, K., Miller, K. J. and Brown, M. W., "Low Cycle Fatigue under Out-of-Phase Loading Conditions," Journal of Engineering Materials and Technology, Vol. 99H, (1977), pp. 222-228.

34. Socie, D. F., and T. W. Shield, "Mean Stress Effects in Biaxial Fatigue of Inconel 718," Journal of Engineering Materials and Technology, Vol. 106H, (1984), pp. 227-232.

35. Waill, L. E., "Crack Observations in Biaxial Fatigue," Design and Materials Division Report No. 108, Department of Mechanical and Industrial Engineering, University of Illinois at Urbana-Champaign, Il., (1983).

36. Beer, T. A., "Crack Shapes During Biaxial Fatigue," Material Engineering-Mechanical Behavior Report No. 106, College of Engineering, University of Illinois at Urbana-Champaign, Urbana, IL, (1984).

37. Hua, C. T., "Fatigue Damage and Small Crack Growth During Biaxial Loading," Materials Engineering Report No. 109, University of Illinois at Urbana-Champaign, Urbana, IL., (1984). See also Ph. D. Thesis, Department of Mechanical Engineering, University of Illinois, Urbana, Il., (1984).

38. Tucker, L. E., and Galliart, D. R. "A Fatigue Test Program for a Notched Round Component," Multiaxial Fatigue, ASTM STP 853, American Society of Testing and Materials, (1982), to be published.

39. Conle, F. A., Report to the Society of Automotive Engineers Fatigue Design and Evaluation Committee.

40. Leese, G. E. and Morrow, J., "Low Cycle Torsional Fatigue of 1045 Steel in Shear Strain Control," Multiaxial Fatigue, ASTM STP 853, American Society of Testing and Materials, (1982), to be published.

41. Fash, J. W., "Fatigue Crack Initiation and Growth in Gray Cast Iron," FCP Report No. 35, College of Engineering, University of Illinois at Urbana-Champaign, Urbana, IL, (1980).

42. Downing, S. D., and Galliart, D. R., "A Fatigue Test System for a Notched Shaft in Combined Bending and Torsion," Multiaxial Fatigue, ASTM STP 853, American Society for Testing and Materials, (1985). To be published.

43. Coffin, L. F., Jr., "A Study of Cyclic Thermal Stresses on a Ductile Metal," Transactions of the American Society of Mechanical Engineers, Vol. 76, (1954), pp. 931-950.

44. Manson, S. S., "Behavior of Materials Under Conditions of Thermal Stress," Heat Transfer Symposium, University of Michigan Engineering Research Institute (1953), pp. 9-75.

45. Morrow, J., "Cyclic Plastic Strain Energy and Fatigue of Metals," Internal Friction Dampening and Cyclic Plasticity, ASTM STP 378, American Society for Testing and Materials, (1965), pp. 45-87.

46. Leis, B. N., and Laflen, J. H., "Problems in Damage Analysis Under Nonproportional Cycling," Journal of Engineering Materials and Technology, Vol. 102, (1980), pp. 127-134.

47. Kandil, F. A., Brown, M. W., and Miller, K. J., "Biaxial Low Cycle Fatigue Fracture of 316 Stainless Steel at Elevated Temperatures," Book 280, The Metals Society, London, (1982), pp. 203-210.

48. Abaques Finite Element Code, Version 4.4, Hibbitt, Karlson, and Sorenson, Inc., Providence, RI, (1980).

49. Hartman, J. B., and Leven, M. M., "Factors of Stress Concentration for the Bending Case of Fillets in Flat Bars and Shafts with Central Enlarged Section," Proceedings, Society of Experimental Stress Analysis, Vol. IX, No. 1, (1951), pp. 53-62.

50. Peterson, R. E., Stress Concentration Factors, John Wiley and Sons, New York, (1974).

51. Hurd, N. J., private communication.

52. Brose, W. R., Dowling, N. E. and Morrow, J., "Effect of Periodic Large Strain Cycles on the Fatigue Behavior of Steels," Society of Automotive Engineers, Paper No. 740221, (1974).

53. Mann, J. Y., Fatigue of Materials, Melbourne University Press, (1967).

54. Miller, K. J., and Chandler, D. C., "High Strain Torsion Fatigue of Solid and Tubular Specimens," discussion by D. J. Hatter, Proceedings of the Institute of Mechanical Engineers, Vol. 184, (1969-70), pp. 433-448.

55. Frost, N. E., Marsh, K. J., and Pook, L. P., Metal Fatigue, Oxford University Press, (1974).

56. Fatami, A., private communication.

57. Fash, J. W., Minter, G. L., and Conle, F. A., "Analysis of Irregular Loading Histories for the SAE Biaxial Fatigue Program," to be published by the SAE, (1985).